Titre: Title:	Evaluating the coolant void reactivity for assemblies of CANDU lattices
Auteur: Author:	Farshad Talebi
Date:	2006
Type:	Mémoire ou thèse / Dissertation or Thesis
Référence: Citation:	Talebi, F. (2006). Evaluating the coolant void reactivity for assemblies of CANDU lattices [Master's thesis, École Polytechnique de Montréal]. PolyPublie. https://publications.polymtl.ca/7685/

UNIVERSITÉ DE MONTRÉAL

EVALUATING THE COOLANT VOID REACTIVITY FOR ASSEMBLIES OF CANDU LATTICES

FARSHAD TALEBI
DÉPARTEMENT DE GÉNIE PHYSIQUE
ÉCOLE POLYTECHNIQUE DE MONTRÉAL

MÉMOIRE PRÉSENTÉ EN VUE DE L'OBTENTION
DU DIPLÔME DE MAÎTRISE ÈS SCIENCES APPLIQUÉES
(GÉNIE ÉNERGÉTIQUE)
MARCH 2006

Your file Votre référence
ISBN: 978-0-494-16858-5
Our file Notre référence
ISBN: 978-0-494-16858-5

UNIVERSITÉ DE MONTRÉAL

ÉCOLE POLYTECHNIQUE DE MONTRÉAL

Ce mémoire intitulé:

EVALUATING THE COOLANT VOID REACTIVITY FOR ASSEMBLIES OF CANDU LATTICES

présenté par: TALEBI Farshad

en vue de l'obtention du diplôme de: Maîtrise ès sciences appliquées

a été dûment accepté par le jury d'examen constitué de:

M. CONAN Jean, Ph.D., président

M. MARLEAU Guy, Ph.D., membre et directeur de recherche

M. KOCLAS Jean, Ph.D., membre et codirecteur de recherche

Mme. VARIN Elisabeth, D.Sc., membre

To

My Mother

My Father

ACKNOWLEDGMENTS

I wish to express my sincere and profound gratitude to those who helped me in the completion of my thesis. First of all, I am indebted to my supervisor and co-supervisor, Doctor Guy Marleau and Professor Jean Koclas for their kind guidance, insightful advice, helpful suggestions and encouragement on me.

I would like to thank all the member of my jury, for taking the time to read my thesis. It is pleasure to thank all the Professors at Institut de Génie Nucléaire, especially Professor Alberto Teyssedou for his support during the time that I was a student at École Polytechnique de Montréal.

I would like to extend my thanks to all my friends and colleagues for sharing with me their friendship and knowledge during my M.Sc at École Polytechnique. I am in particular thankful to Karthikeyan Ramamoorthy for his friendship and fruitful discussions we had during the research, conferences and courses.

I would like to acknowledge the Natural Sciences and Engineering Research Council of Canada for their grant that partially supported my thesis project.

ABSTRACT

Coolant Void Reactivity (CVR) is a very important safety parameter in reactor analysis. It is a mandatory safety requirement that an accurate estimation of CVR be available. It is often considered desirable that the CVR is negative so that the reactor is inherently safe when there is a Loss Of Coolant Accident (LOCA). For CANDU reactors, which employ the pressure tube technology that separates the hot coolant from the cold moderator, a LOCA can introduce positive reactivity as the moderator still continues to pump in thermal neutrons.

Canada is pursuing the Advanced CANDU Reactors (ACR), which are in the conceptual stage. It was found that one of the designs, the ACR-700, had a positive coolant void reactivity. Efforts are being pursued to modify the concept in such away as to design a fuel assembly with a negative CVR under LOCA conditions.

The main objective for the current study is to establish a model to evaluate the CVR for a 2×2 heterogeneous assembly of CANDU lattices (CANDU-6 and ACR-700 type lattices) using DRAGON. The DRAGON code solves the integral neutron transport equation using 2-D and 3-D collision probability techniques. With the current version of DRAGON, one can only compute the CVR for a single CANDU cluster cell. Because the existing version of DRAGON has inherent geometry limitations, CANDU assembly calculations cannot be performed in the exact geometry. Accordingly, an approximate model for each geometry must be considered. The model we propose consists of replacing the annular fuel pins (fuel plus its sheathing) by equivalent square fuel pins. The equivalence between annular fuel pins and square fuel pins is brought about by homogenizing the fuel and clad and subsequently conserving the reaction rates between the two geometries. In order to achieve these purposes, the superhomogenization (SPH) technique is used to create such equivalent square pins along with generating cross section libraries. The approximate CANDU lattices constructed using square pins were used to perform the transport calculations in the 2×2 assembly pattern. The cross section

libraries used here are those generated using a single cell model. The model was applied on CANDU-6 lattice and several studies were performed to estimate the CVR. The lattice pitch was subsequently reduced, but maintaining the same configuration of pressure tube and calandria tube of that of CANDU-6. Subsequently the calandria tube diameter was increased in order to almost match that of ACR-700. The coolant and moderator were heavy water. It was followed by increasing the number of pins from 37 to 43, changing natural uranium to enriched uranium and changing the coolant from heavy water to light water, thereby obtaining an ACR-700 type lattice. A study was performed to evaluate the effect of different boundary conditions for the assembly calculation in 2×2 pattern. The boundary conditions considered were translational and reflective. The CVR for CANDU-6 lattice was found to be positive. When assembly calculation in a 2×2 pattern was performed, with diagonal cells completely voided (called checkerboard voiding pattern), the CVR was found to be nearly half of that of CVR when all cells are 100% voided. The behavior is linear as expected, because the CANDU-6 is a well moderated system. For ACR-700 lattices, the CVR was found to be positive, but lower than that of CANDU-6. Interestingly, when diagonal cells were completely voided, the CVR was found to be more than that of CVR when all cells are 100% voided. This non linear behavior is mainly due to coupling of neutrons born in one lattice to those in neighboring lattices, and due to highly absorptive behavior of light water coolant as compared to heavy water coolant.

CONDENSÉ EN FRANÇAIS

Le changement de réactivité due à la vidange du caloporteur (RVC) est un paramètre très important à considérer pour les analyses de sûreté dans des réacteurs nucléaires. L'évaluation précise de RVC est une condition de sûreté primordiale avant la construction d'un réacteur. Il est généralement souhaitable que le résultat obtenu pour le RVC soit négatif de telle sorte que le réacteur soit sécuritaire dans le cas d'une perte accidentelle du caloporteur (PERCA). Les réacteurs CANDU utilisent des tubes de force qui séparent le caloporteur chaud du modérateur froid, la PERCA peut avoir comme conséquence l'insertion d'une réactivité positive puisque le modérateur continue à interagir avec les neutrons thermiques.

Le Canada poursuit la voie des réacteurs avancés de type CANDU (ACR), qui sont pour l'instant à l'étape de conception. On a constaté lors de la conception initiale du modèle ACR-700 qu'on avait une réactivité positive lors d'une perte du caloporteur. On poursuit les efforts de recherche afin de modifier la conception du combustible pour obtenir un RVC négatif dans le cas d'une PERCA.

L'objectif principal de cette étude est d'établir un modèle pour évaluer le RVC pour un assemblage hétérogène 2×2 des cellules de CANDU (les modèles CANDU-6 et ACR-700) en utilisant le programme de modélisation DRAGON. Ce programme résout l'équation de transport des neutrons en utilisant des techniques d'évaluation de probabilité de collision en 2-D et 3-D. Avec la version courante de DRAGON, on peut seulement calculer le RVC pour une cellule simple de CANDU à cause de limites géométriques. Ainsi les calculs des assemblages de CANDU ne peuvent pas être exécutés sur une géométrie exacte. En conséquence, une approximation pour chaque géométrie doit être faite. Le modèle que nous proposons consiste à remplacer les barres de combustible annulaires (combustible plus la gaine) par des barres de combustible carrées équivalentes. L'équivalence entre les barres de combustible annulaires et carrées est obtenue en homogénéisant le combustible et la gaine et en assurant la conservation des

taux de réaction entre les deux géométries. Afin d'atteindre ce but, la technique de super-homogénéisation (SPH) est employée pour créer ces barres carrées équivalentes et générer une banque de données de sections efficaces. Ces cellules approximatives ont été utilisées pour les calculs de transport sur les assemblages 2×2. La banque de données employée ici est celle produite en utilisant le modèle à une cellule. Le modèle a été appliqué sur le cellule CANDU-6 et plusieurs études ont été réalisées pour estimer le RVC. La distance entre les cellules a été réduite à celle de l'ACR-700, mais en gardant la même configuration de tubes de force et de calandre et en conservant l'eau lourde pour le caloporteur et le modérateur. Par la suite le diamètre du tube de calandre a été augmenté au niveau du ACR-700. Ensuite, on a augmenté le nombre de barres de 37 à 43, remplacé l'uranium naturel par de l'uranium enrichi et enfin changé l'eau lourde par de l'eau légère pour le caloporteur. Une étude a été réalisée pour évaluer les effets des conditions aux frontières pour le calcul d'un assemblage 2×2. Des conditions aux frontières de translation et réflexion ont été étudiées. Le RVC pour la cellule CANDU-6 s'est avéré positif. Pour le calcul d'un assemblage 2×2 avec les cellules diagonales complètement vidées (appelé aussi modèle de vidange en échiquier), le RVC s'est avéré être environ la moitié du RVC quand toutes les cellules sont à 100% vidées. Le comportement est linéaire comme prévu, parce que le CANDU-6 est un système bien modéré. Pour la cellule ACR-700, le RVC s'est avéré positif, mais moins que celui du CANDU-6. Ce qui est intéressant, c'est que si les cellules diagonales sont complètement vidées, le RVC est plus élevé que lorsque toutes les cellules sont à 100% vidées. Ce comportement non linéaire est principalement dû au fait que les neutrons générés dans un assemblage sont fortement couplés aux assemblages voisins, et également dû au comportement très absorbant de l'eau légère comparativement à l'eau lourde.

TABLE OF CONTENTS

LIST OF FIGURES

LIST OF TABLES

LIST OF APPENDICES

INTRODUCTION

In this thesis, we investigate CANDU reactor response to the Loss of Coolant Accident (LOCA) [Glasstone, 1981], and estimate a very important safety related parameter, the Coolant Void Reactivity (CVR) [Whitlock, 1995].

In this introductory chapter, we comment the reasons to establish this investigation. Included in the first section is the concept of fission, followed by the physical aspects of coolant voiding inside the core for different types of thermal reactors especially CANDU reactor [Rozon, 1992]. Subsequently a brief description on the chain of calculation, including cell and finite core calculation, required to perform a reactor simulation are introduced. Then the importance of assembly calculation in a 2×2 pattern using DRAGON is presented. Introduction of an approximate model to circumvent the limitation in DRAGON is briefly described [Marleau, 1992, Hébert, 1995]. Later on, the literature pertinent to the phenomena of coolant voiding is reviewed.

The Concept of Fission

Nuclear fission is the most likely reaction when a thermal neutron is absorbed by a fissionable nucleus (such as ^{235}U). These nuclei become highly unstable when the total energy of the compound nucleus, i.e., binding energy of neutron plus kinetic energy of incident neutron, exceeds the critical energy needed for fissioning the nucleus. Consequently, the nucleus splits into a pair of lighter nuclei and the potential energy of the system is quickly converted to kinetic energy. This event generates about 200 MeV of energy along with two or three fast neutrons (with an average energy of 2 Mev) which can initiate the next fission.

Based on the kinetic energy (or speed) of the neutrons causing most of the fissions,

the nuclear reactors can be classified into thermal reactors or fast reactors. Here, we will focus our discussion on thermal reactors where the average energy of the neutron initiating the fission is of the order of 0.0253 eV.

Different types of thermal reactors have been constructed worldwide. Neutron slowing down from 2 MeV to 0.0253 eV (also called moderation) is achieved in these reactors by the choice of a variety of coolant and moderator materials. The coolant essentially removes heat from the fuel assemblies and also contributes towards moderation of neutrons. In Pressurized Water Reactors (or PWRs) and Boiling Water Reactors (or BWRs), light water acts as coolant and moderator. The fuel and coolant are enclosed within a pressure vessel. In reactors like that of CANDU, hot pressurized heavy water coolant is separated from cold moderator, which is also heavy water. In new generation reactors like the ACR, light water is the coolant while heavy water acts as moderator. There are other type of reactors like the gas cooled reactors, where graphite acts as moderator of neutrons and helium is used as coolant.

As we noted above, the neutrons born at high energies of the order of 2.0 MeV, must be slowed down to thermal energies, which is below 1.0 eV, where the probability of fission of nuclides like ^{233}U, ^{235}U, ^{239}Pu and ^{241}Pu is enhanced. The loss in energy for the neutrons is made possible by the use of moderating materials like light water, heavy water or graphite. Neutrons lose most of their energy by undergoing elastic scattering collisions with the moderating and coolant nuclides. Also a smaller part of their energy is lost by inelastic scattering collisions with heavy nuclides. The neutrons, while slowing down to thermal energies, are likely to undergo absorption or leakage from the system. It is very important to understand the behavior of the system in order to accurately establish the neutron population as a function of space, energy, angle and time. In PWR and BWR, neutrons slow down to thermal energies after undergoing scattering collisions with hydrogen bound in light water while in CANDU reactors, deuterium bound in heavy water is mainly responsible for slowing down the neutrons. It is a well known fact that

light water has a very good capacity to slow down the neutrons. A neutron can lose all its energy in one head-on collision with hydrogen. However light water has a relatively high probability of absorption of thermal neutrons, in comparison to any other moderating material. In contrast neutron has to undergo larger number of collisions in heavy water medium, before it gets thermalized. But heavy water has a low probability of absorption of thermal neutrons in comparison to light water. Heavy water reactors are thus big in size in comparison with light water reactors for the same electrical power.

The fission reaction is considered to be self-sustaining, when there is a perfect balance between neutron production and removal of neutrons. In reactor physics language, this is represented by multiplication factor. The multiplication factor (k) is related to the number of neutrons born in one generation to the number of neutrons being absorbed in the previous generation. Several safety related parameters like the fuel temperature coefficient, coolant void reactivity, moderator and coolant temperature coefficients can be estimated using the multiplication factor for the reference and perturbed state [Glasstone, 1981]. In the following section we will be focussing mainly on coolant voiding, which is a very important reactor safety related parameter.

Physics Aspects of Coolant Voiding

In fission reactors, energy production is mainly due to the kinetic energy of fission products that are stopped within the fuel lattice. The kinetic energy is converted to heat and is subsequently removed by the coolant. The coolant is generally under pressure so that the boiling point can be increased from a value that corresponds to atmospheric pressure. The inlet temperature of the coolant is typically of the order of 270 ° C and the outlet temperature is of the order of 310 ° C [Glasstone, 1981]. The coolant at this high temperature helps to increase the thermodynamic cycle efficiency. The heat energy of the coolant is subsequently converted to steam and is used to run the turbine and generate

electricity. It is very important for a smooth functioning power reactor to have a stable coolant circuit. But during some accidents like break in feedwater line of PWR, or main steamline break in BWR or header pipe break in CANDU, there is a possibility of loss of coolant from the system. This is referred to as Loss of Coolant Accident (LOCA).

The loss of coolant from a system can be partial or total. The effect of a LOCA scenario is different for different types of reactors. In PWRs the LOCA is accompanied with loss of moderation. In these reactors the coolant voiding has always an adverse effect on the multiplication factor and results in a negative void reactivity that in absolute value increases with burnup [Asahi, 1989]. In PWRs, boron is generally added to the moderator in order to suppress initial excess reactivity and also help in keeping the control rods fully out to avoid loss of regulation accident. When there is a loss of borated coolant, the effect is a combination of loss of absorption due to boron and loss of moderation. In general, this effect is globally negative.

In pressure tube reactors, the coolant and moderator are located in two separate systems (see Appendix-I). Accordingly, the loss of coolant does not necessarily mean loss of moderation. For CANDU reactors, which employ the pressure tube technology that separates the hot coolant from the cold moderator, a LOCA can introduce positive reactivity as the moderator still continues to produce thermal neutrons. This leads to a rapid increase in power and temperature of the fuel. If this condition goes unchecked, there could be fuel failures and release of fission products into the coolant circuit, which is quite undesirable.

In this thesis we will be focussing on the LOCA in CANDU type reactors only. In all the subsequent discussions reference will be made to CANDU type reactors. For more detailed physics explanation on LOCA, let us look into the four factors that constitute the infinite multiplication factor [Rozon, 1992]. The four factors are fast fission factor (ϵ), resonance escape probability (p), thermal utilization factor (f) and thermal reproduction

factor (η). The fast fission factor increases when there is a LOCA. This is mainly due to increase in probability of fast fission in ^{238}U due to large fraction of first collision neutrons having an energy greater than the fission threshold. This ϵ effect is responsible for 31% of the void coefficient for a fresh bundle. The resonance escape probability increases when there is a LOCA. In the absence of coolant there is a greater probability of the neutrons to escape into the moderator and get thermalized before it re-enters the fuel. They thus escape the probability of getting absorbed in the resonances of nuclides like ^{238}U. The contribution due to resonance escape probability is 37% of the void coefficient in the initial core without boron. There is a slight increase in the thermal utilization factor. This is due to the absence of small amount of absorption by heavy water. The component of the void coefficient is of the order of 18% in the initial core without boron. The thermal reproduction factor increases slightly in fresh fuel. The neutrons, slowed down in moderator, re-enters the pressure tube where there is no coolant to re-thermalize it. Re-thermalization essentially means the change in energy of the neutron to higher/lower value in presence/absence of coolant, than it was when it is slowed down in moderator. Therefore there is a contribution of 14% to the void coefficient when the fuel is fresh. So it is clear that when there is a LOCA in CANDU type reactors there is a net positive effect in reactivity.

The next generation pressure tube reactor concept that is being envisaged in Canada is the Advanced CANDU Reactor (ACR) [Love, 2002,Ovanes, 2002]. This reactor will use CANFLEX fuel type, which is 43 element cluster with enriched uranium. The fuel composition is under constant development with the intention of obtaining negative coolant void reactivity as a function of burnup. The coolant is light water and moderator is heavy water. Again, the coolant and moderator are separate entities like that in CANDU. As discussed earlier the light water is a very good moderator but has a high absorption cross section for thermal neutrons in comparison to that of heavy water.

Description of Calculation Methodology

Several codes have been developed all around the world in order to study the behavior of a nuclear reactor system. Reactor calculations can be broadly classified into two main levels, i.e., lattice level and core level. Most of the intricate details of the reactor geometry are treated at the lattice level. The homogenized cross sections thus generated at the lattice level are subsequently used at the core level to understand the behavior of reactor system. In the present study, we will be focussing mainly on the lattice level.

Lattice level calculations involve intricate geometry details, including presence and absence of control rods, burnable absorber rods along with that of the fuel pins. Reflective and translational boundary conditions are applied to the lattice in order to estimate global reactor related parameters like the infinite multiplication factor, flux distribution at various locations, spectral indices like ρ^{28}, δ^{28}, δ^{25}, conversion ratio etc [Aldama, 2003].

The factor that is estimated by lattice level calculations pertaining to LOCA scenario, is the coolant void reactivity (CVR). In order to estimate the CVR, one needs to perform assembly calculation in a 2×2 pattern as compared to single lattice calculation. In case of single lattice, one can only perform eigenvalue calculation for either fully cooled or fully voided condition using reflective boundary condition. The difference between these two conditions will give the CVR corresponding to full voiding, and is representative of infinitely similar lattices. But there is a possibility that coolant is not lost uniformly from all the pressure tubes. When there is a single pump failure or break in only one header pipe, thereby leading to a checkerboard voiding pattern. Therefore an assembly calculation in a 2×2 pattern with translational boundary condition must be modelled to study such a state.

The main objective of the current study is to establish a model to evaluate the CVR for a 2×2 heterogeneous assembly of CANDU lattices (CANDU-6 and ACR-700 type

lattices) using DRAGON [Marleau, 1992, Hébert, 1995]. DRAGON has been developed at the École Polytechnique and is considered as one of the recommended codes by nuclear industry in Canada. The DRAGON code solves the integral neutron transport equation using 2-D and 3-D collision probability techniques. With the current version of DRAGON, one can only compute the CVR for a single CANDU cluster cell. Because the existing version of DRAGON has inherent geometry limitations, CANDU assembly calculations cannot be performed in the exact geometry. Accordingly, an approximate model for each geometry must be considered.

The model we propose consists of replacing the annular fuel pins (fuel plus its sheathing) by equivalent square fuel pins. The equivalence between annular fuel pins and square fuel pins is brought about by homogenizing the fuel and clad and subsequently conserving the reaction rates between the reference and homogenized geometries. In order to achieve this goal, the superhomogenization (SPH) technique is used to associate with each equivalent square pin, an adequately homogenized cross section library [Hébert, 1993a, Hébert, 1993b]. The approximate CANDU lattices constructed using square pins is then used to perform the transport calculations in a 2×2 assembly pattern.

Using the proposed model, DRAGON can perform assembly calculation in a 2×2 pattern for different combinations of voiding and fuel state. One can consider fuel assemblies with different exposures, which would represent equilibrium core pattern in a typical CANDU reactor. However, in the present study we have considered only fresh fuel and coolant state corresponding to 25% void, 50% void, 75% void and 100% void. The 2×2 pattern can also include reflector cells along with fuel cells. This would give the effect of reflector on neutron flux distribution during coolant voiding. Another interesting possibility of using this model is to estimate the reactivity effect due to heterogeneous draining. It is essentially the loss of coolant from top to bottom of the lattice.

Such a calculation is currently not possible in DRAGON. This can be taken up for future

studies. In regular lattice calculations, the outermost boundary is annularized, so that one can consider annular regions for tracking and estimating the collision probability matrix. But when the outermost boundary is square or hexagonal, the consideration of annular regions is limited to the boundary of lattice, thus leaving a large region in the corner without discretization. This problem is resolved by using the square pin model, whereby there is a possibility of corner discretization and estimating the effects thereof.

Literature Review

In this section, a chronological detail of earlier work on estimation of CVR is presented. The coolant void reactivity was simulated for current operating CANDU reactors with several nuclear codes. Atomic Energy of Canada is developing the Advanced CANDU Reactors (ACR) which is also called CANDU-NG (CANDU New Generation).

The CVR was calculated by J.J. Whitlock and J. Garland [Whitlock, 1995] with the WIMS-AECL code [Donnelly, 1986] in a single CANDU-6 cell. They used nominal geometric bucklings and 69 neutron energy groups based on ENDF/B-IV. The CVR was estimated for instantaneous draining of the coolant. The authors have reasoned out that the absence of upscattering and an increase in streaming upon voiding results in a redistribution of thermal flux across the lattice. They have also pointed out that at mid-burnup the overall positive contribution from ^{235}U equals the negative contribution from ^{239}Pu leaving the decrease in resonance absorption in ^{238}U as the significant source of positive void effect. They have estimated the CVR to be +16.3 mk for fresh fuel and +13 mk for mid-burnup fuel.

J. Valkó et al., [Valkó, 1995] obtained the reactivity effect due to coolant voiding in a CANDU-6 cell using SCALE code system [Nureg, 1990] and JEF-1.1 basic nuclear data source. SCALE-3 uses 219 group cross section library while SCALE-4 uses 172

group cross section library. They used three different models in their analysis. First was the ring model, second was the pin model and third was the cluster model. They compared the results obtained using the three models with that of multigroup Monte Carlo code, MCNP [Briesmeister, 1986]. The Monte Carlo calculations were performed using 219 group cross section library. The flux calculation in ring model and pin model is performed using Sn transport code. The flux calculation for cluster model uses the module implemented in WIMSD4. They have estimated the CVR for CANDU-6 cell for fresh fuel and end of life fuel. They have quoted values for CVR from +15.5 mk to +17.9 mk using various models. The MCNP value quoted is +16.9 $\pm$ 0.1 mk. They have also studied a modified bundle containing dysprosium and slightly enriched uranium in order to eliminate the positive reactivity effect. The CVR estimate obtained using ring and pin model was found to be between +0.8 and +1.1 mk. But the cluster model gave a result of -7.4 mk. The MCNP quoted value was -7.9 mk. They thus found that one dimensional cylindrical calculation (Sn method) was inadequate for increased heterogeneity of the modified fuel.

Void reactivity calculations for a CANDU-6 lattice were also performed by F. Rahnema et al., [Rahnema, 1998]. They used two different codes, HELIOS [Villarino, 1992] and MCNP4B [Briesmeister, 1997]. The study was essentially to benchmark the HELIOS calculations and assess the accuracy of void reactivities computed with this code. HELIOS calculations were performed using 190 group library based on ENDF/B-VI. Current Coupled Collision Probability (CCCP) is implemented in HELIOS to perform the flux calculation. A total number of 155 unique nuclides were chosen as part of the library. In both simulation reflected boundary condition was used. Eigenvalues were computed with HELIOS in five coolant densities (0.8623, 0.6, 0.3, 0.1 and 0.001 g/cc) and three burnup points of 0.0, 4000 and 13000 MWd/T. For MCNP4B, reactivity calculations were estimated in two coolant densities (0.8623 and 0.001 g/cc) and the same three burnup points and using continuous neutron energy. They observed that k_∞ shows

a linear dependence on coolant density. It was also noted that the reactivity worth of each coolant density change decreased with burnup. HELIOS was found to under-estimate k_∞ at zero and 4000 MWD/T and over-estimate it at 13000 MWD/T for both coolant states. The uncertainty associated with void reactivity calculation performed with HELIOS in a typical CANDU cell for large changes in coolant density are small at exposures from zero to 4000 MWD/T and of the order of 10% at high burnups of 13000 MWD/T. The CVR estimated using HELIOS for fresh fuel was +17.43 mk against +17.37 $\pm$ 0.18 mk using MCNP4B for change in density from 0.80623 g/cc to 0.001 g/cc.

Void reactivity coefficient in a CANDU-6 lattice was computed with the transport codes HELIOS and CP-2D by M. Constantin [Constantin, 2002]. Collision Probability (CP) technique is implemented in CP-2D to perform the flux calculation. The authors have proposed a new model called the heterogeneous two-stratified coolant model. The coolant is treated as a two phase (liquid and vapour) medium, gravitationally separated. The results were compared with the classical homogeneous model. Eigenvalues were computed with code CP-2D for five coolant densities (0.8623, 0.6, 0.3, 0.1 and 0.001 g/cc) and three burnup points of 0.0, 4000 and 13000 MWd/T. The results were compared with HELIOS which use nuclear data in 190 neutron energy groups generated from ENDF/B-VI. For the calculations using CP-2D code, WIMSD-5B library in 69 neutron energy groups was used. HELIOS code uses the homogeneous model to estimate the CVR. The authors have estimated a value of +16.32 mk for homogeneous model and +16.35 mk for the heterogeneous two-stratified coolant model for CVR. They have thus concluded that the heterogeneous two-stratified coolant model is not necessary to estimate the CVR and a homogeneous model is sufficient. However for power and flux distributions during LOCA, one needs to apply the heterogeneous two-stratified coolant model. This model was found to be capable of calculating the asymmetries of the fluxes and power distributions in a fuel assembly during LOCA. In another study by the authors [Constantin, 2003], the model was applied to estimate the CVR for a Slightly Enriched Uranium

SEU-43 bundle (0.96 wt%). The results were compared with those obtained using Monte Carlo code MCNP4C. Cross section libraries based on ENDF/B-V and ENDL85 were used. The neutron cross sections were selected from those libraries which had the evaluation years corresponding to that of the WIMSD-5B library. A CVR of +14.87 mk was estimated with the CP-2D code against +15.63 mk obtained using MCNP4C [Briesmeister, 2000]. The authors have observed that there is a systematic slight under-estimation of the void reactivity by CP-2D code when compared to MCNP4C. The results were compared only for the fresh fuel. The authors observed that the void reactivity showed an approximate linear dependence with the void fraction. They also observe that the void reactivity remained approximately constant with the burnup, with a slight decrease at high burnup.

The Coolant void reactivity was computed in the CANDU-6 and ACR-700 by C. A. Cotton et al., [Cotton, 2004]. The HELIOS code [Stammler, 2003] was chosen for both geometries. The results were obtained using data in 45 neutron energy groups. For the ACR calculation the authors considered 43 element CANFLEX bundle with 7 wt% dysprosium in the central natural pin. The other pins were enriched up to 2.1 wt%. They have compared the individual components that contribute towards the CVR. All the results pertain to lattice level. They have obtained a CVR of +16.7 mk for fresh CANDU fuel and +17.1 mk for fuel with equilibrium xenon. Similarly they obtained -0.93 mk and -1.23 mk for the respective fuel states for ACR-700 fuel.

The coolant voiding studies were performed on a CANDU-NG core by P. S. W. Chan [Chan, 2001]. In this paper, the author has attempted to obtain an optimum configuration for the futuristic reactor. He has varied the lattice pitch, enrichment and calandria tube diameter in order to obtain a CVR value of less than one beta of reactivity for full core. Some of the design requirements that were taken into account in order to obtain an optimum design were, to have a moderator-to-fuel volume ratio of about 7.1 and to achieve a burnup of about 20 GWD/T. The lattice calculations were performed using

WIMS-AECL code and burnup calculations were performed with the fuel management code RFSP version IST-REL-300HP [Rouben, 1995]. For optimum CANDU-NG lattice configuration, the authors have proposed a square lattice pitch of 22 cm, a fuel enrichment of 1.65 wt%, with a 5.17 cm inner radius of pressure tube and a 7.8 cm outer radius of calandria tube. They obtained a full core void reactivity of +5.0 mk, which is less than one beta for a ^{235}U fuelled reactor. Another related work for designing next generation fuel with negative CVR was performed by M. Ovanes [Ovanes, 2002]. In this study 43 element CANFLEX bundle was used with 4.6 wt% dysprosium in the central natural pin. The other pins were enriched up to 2%. WIMS-IST (which is WIMS-AECL version 2-5d) was used to achieve the optimum moderator to fuel ratio for negative coolant void reactivity. The LOCA simulations were performed using 3-D DONJON [Varin, 2000] with WIMS-IST generated cross section library using ENDF/B-VI. They obtained a CVR of -3.0 mk for full core voiding. This work also shows that when LOCA is introduced into the CANDU-NG system, the reactor power begins to reduce spontaneously and it could shut down the reactor automatically.

A very interesting study was performed in a 2×2 pattern for ACR-700 by C.A. Cotton et al. [Cotton, 2005]. In this paper CVR was estimated using code HELIOS using 47 neutron energy group structure. Several voiding scenarios were examined. They were checkerboard voiding of two diagonal channels, 50% reduction in coolant density in all four channels, and a complete voiding in all channels. The authors have discussed the CVR phenomena using the four factor formula and neutron non-leakage probabilities. It was observed that each of the four factors play a significant role in affecting the multiplication factor. The authors have found that the CVR is positive in the checkerboard voiding pattern in opposition with the negative values obtained for fully voided and 50% homogeneously voided scenarios.

With the previous study by C.A. Cotton et al. [Cotton, 2005], the worst LOCA scenario is not total coolant voiding for ACR-700 type lattice but is the checkerboard kind of

voiding. This was thus the starting point of the present research, where we have attempted to estimate CVR for a 2×2 pattern of ACR-700 type lattice using DRAGON. An assembly calculation in a 2×2 pattern with translational boundary condition must be modelled to study such a state, since the neutrons born in one cell are coupled to those in neighboring lattices. However, the existing version of DRAGON has inherent geometry limitations and hence CANDU assembly calculations cannot be performed in the exact geometry. Accordingly, an approximate model is being proposed to perform such an analysis within the present framework of the code DRAGON.

With the proposed model, we have also attempted to ascertain the fact that total coolant voiding is a much more serious scenario than checkerboard voiding for the present CANDU-6 lattice.

CHAPTER 1

DRAGON CODE

The lattice code DRAGON has been developed at the École Polytechnique and is considered as one of the recommended codes by nuclear industry in Canada and is used for our lattice calculations. The DRAGON code solves the integral neutron transport equation using 2-D and 3-D Collision Probability techniques or 2-D Characteristic method. The computer code DRAGON is an ensemble of models which can simulate the neutron behavior in a pincell or fuel assembly in 2-D and 3-D. The code is capable of handling nuclear data in various formats that include WIMSD (both 69 and 172 group), WIMS-AECL (89 group) and MATXS. Each level of lattice calculation is divided into a variety of modules. They include modules to read the geometry, read the microscopic cross section libraries from various sources, perform self shielding calculation, track the geometry, obtain the collision probabilities, and solve for the flux. There are also modules to perform the burnup of the fuel under consideration, merging the fluxes in certain regions and generating new cross section libraries. Since the code is in a modular structure, one could implement new ideas in the form of modules. A detailed description of each of the modules can be obtained from the DRAGON manual [Marleau, 2000].

In this chapter we introduce the transport equation that is solved using DRAGON, followed by the collision probability technique. This will be followed by description of reactivity formula and homogenization technique.

1.1 Neutron Transport Equation

Transport equation was formulated by Boltzmann in the context of explaining the kinetic theory of gases. Since the neutrons in a reactor behave like free gases, the transport theory can be extended to describe their behavior in a reactor system. The neutrons once born, continuously undergo collisions with resident nuclides, till they are absorbed, or leak away from the system. Neutron conservation equation is thus built on these interactions. It is then used to establish the neutron flux distribution in the reactor as a function of space, angle, energy and time.

The purpose of this equation is to explain the behavior of the system in which the neutrons move through space in all directions and with a full spectrum of energies. In this equation, seven independent variables are required to characterize the distribution of neutrons: the three spatial coordinate vectors ($\vec{r}$), the two angles ($\hat{\Omega}$) that specify the neutron direction of travel, the energy (E), and time (t). The neutron transport equation is written as [Lewis , 1984]:

$$\frac{1}{v} \cdot \frac{\partial \psi(\vec{r}, \hat{\Omega}, E, t)}{\partial t} + \hat{\Omega} \cdot \vec{\nabla} \psi(\vec{r}, \hat{\Omega}, E, t) + \Sigma(\vec{r}, E) \psi(\vec{r}, \hat{\Omega}, E, t) = Q(\vec{r}, \hat{\Omega}, E, t) \quad (1.1)$$

where ψ, Σ, Q and v are the angular flux, total macroscopic cross section, emission density and speed of neutrons, respectively. The angular flux is defined as:

$$\psi(\vec{r}, \hat{\Omega}, E, t) \equiv vN(\vec{r}, \hat{\Omega}, E, t) \quad (1.2)$$

where N is the number of neutrons per unit volume ($N \frac{neutrons}{cm^3}$), $v = \sqrt{2E/m}$ is the neutron velocity and m is its mass. The time independent neutron transport equation can

be expressed as:

$$\hat{\Omega} \cdot \vec{\nabla}\psi(\vec{r}, \hat{\Omega}, E) + \Sigma(\vec{r}, E)\psi(\vec{r}, \hat{\Omega}, E) = Q(\vec{r}, \hat{\Omega}, E) \tag{1.3}$$

and emission density can be described as a contribution from the three terms i.e., external source (Q_{ex}), scattered particles (Q_s) and fission source (Q_f):

$$Q(\vec{r}, \hat{\Omega}, E) = Q_{ex}(\vec{r}, \hat{\Omega}, E) + Q_s(\vec{r}, \hat{\Omega}, E) + Q_f(\vec{r}, \hat{\Omega}, E) \tag{1.4}$$

The scattering contribution is expressed by:

$$Q_s(\vec{r}, \hat{\Omega}, E) = \int_{\hat{\Omega}'} \int_0^{\infty} \Sigma_s(\vec{r}, E' \rightarrow E, \hat{\Omega}' \rightarrow \hat{\Omega})\psi(\vec{r}, \hat{\Omega}', E')dE'd^2\Omega' \tag{1.5}$$

where, Σ_s is the macroscopic scattering cross section and fission source is:

$$Q_f(\vec{r}, \hat{\Omega}, E) = \frac{\chi(E)}{k} \int_{\hat{\Omega}'} \int_0^{\infty} \nu\Sigma_f(\vec{r}, E')\psi(\vec{r}, \hat{\Omega}', E')dE'd^2\Omega' \tag{1.6}$$

that χ, ν and Σ_f are the fission energy spectrum, the average number of neutrons produced per fission and macroscopic fission cross section. k is the multiplication factor or eigenvalue that provides an idea of deviation of the system from equilibrium in the case where external source is equal to zero ($Q_{ex} = 0$). k for an infinite lattice calculation is represented as k_∞, and is represented as k_{eff} for finite lattice calculation. The total

number of interactions (per unit volume and second) between the neutron and nuclides is given by reaction rate $R(\vec{r})$:

$$R(\vec{r}) = \int_E \Sigma(\vec{r}, E)\phi(\vec{r}, E)dE \tag{1.7}$$

where ϕ is the scalar flux and can be expressed as:

$$\phi(\vec{r}, E) = \int_{\hat{\Omega}} \psi(\vec{r}, \hat{\Omega}, E)d^2\Omega \tag{1.8}$$

In order to solve the neutron transport equation in the volume V surrounded by a surface Γ, the incoming flux distribution on the boundaries must be known. Therefore, if $\hat{n}$ is considered as an outward normal vector of Γ, the neutron flux distribution is estimated for $\hat{\Omega} \cdot \hat{n} < 0$, $\vec{r} \in \Gamma$ as a boundary condition. For a known surface source $\tilde{\Psi}$, the incoming flux on the boundary is:

$$\psi(\vec{r}, \hat{\Omega}, E) = \tilde{\Psi}(\vec{r}, \hat{\Omega}, E), \qquad \hat{\Omega} \cdot \hat{n} < 0, \vec{r} \in \Gamma \tag{1.9}$$

For example for $\tilde{\Psi} = 0$ we have void boundary condition. For the implicit boundary condition, a relation between incoming ($\psi(\vec{r}, \hat{\Omega}, E)$) and outgoing ($\psi(\vec{r}, \hat{\Omega}', E)$) fluxes is defined. They can be either albedo, translational (or periodic) or white boundary conditions. For example for albedo boundary condition with outgoing ($\hat{\Omega}'$) and incoming ($\hat{\Omega}$) angles we have:

$$\psi(\vec{r},\hat{\Omega},E)=\beta(E)\psi(\vec{r},\hat{\Omega}',E),\qquad \hat{\Omega}\cdot\hat{n}<0,\vec{r}\in\Gamma \tag{1.10}$$

$$\hat{n}\cdot\hat{\Omega}=-\hat{n}\cdot\hat{\Omega}' \quad \text{and} \quad (\hat{\Omega}\times\hat{\Omega}')\cdot\hat{n}=0 \tag{1.11}$$

where β is the reflection coefficient and by selecting $\beta = 1$ at a surface, the outgoing fluxes will be reflected back into the volume. It is thus referred to as reflective boundary condition. In the periodic (or translational) boundary condition we should specify that the flux distribution on the surface under consideration is linked to the opposite surface in a periodic pattern with distance, $\vec{r_l}$ and thus:

$$\psi(\vec{r},\hat{\Omega},E)=\psi(\vec{r}+\vec{r_l},\hat{\Omega},E),\qquad \hat{\Omega}\cdot\hat{n}<0,\vec{r}\in\Gamma \tag{1.12}$$

Both reflective and translational boundary conditions are used for our assembly calculation in a 2×2 pattern of CANDU lattices (which will be explained in Chapter 3).

1.2 Collision Probability Method

Collision probability (CP) method is one of the methods for solving the integral transport equation. In this method, after creating the integral form of transport equation by integrating out the angular dependency, the scalar flux is estimated. Another simplification to continuous energy transport equation (1.3) is done by discretizing the energy variable in multigroup form. It is done so to avoid the complicated energy dependence of the cross sections. The cross sections are discretized (such as Σ^g, $\Sigma_s^{g'\to g}$ for each energy group g) using various codes like NJOY [Macfarlane, 2000], which collapses continuous energy into multigroup format, for use in deterministic codes like DRAGON.

DRAGON code solves the multigroup integral transport equation using 2-D and 3-D collision probability techniques [Marleau, 2001]. DRAGON evaluates the CP matrix associated with the various type of geometries. In order to explain the CP method of solution for the transport equation, we rewrite the time independent transport equation (1.3) for the energy group g as:

$$\left[\hat{\Omega}\cdot\vec{\nabla}+\Sigma^g(\vec{r})\right]\psi^g(\vec{r},\hat{\Omega})=Q^g(\vec{r},\hat{\Omega}) \tag{1.13}$$

where emission density without external sources become:

$$\begin{aligned} Q^g(\vec{r},\hat{\Omega}) &= \frac{\chi^g}{k_{eff}}\int_{\hat{\Omega}'}\sum_{g'}\nu\Sigma_f^{g'}(\vec{r})\psi^{g'}(\vec{r},\hat{\Omega}')d^2\Omega' \\ &+ \int_{\hat{\Omega}'}\sum_{g'}\Sigma_s^{g'\to g}(\vec{r},\hat{\Omega}'\to\hat{\Omega})\psi^{g'}(\vec{r},\hat{\Omega}')d^2\Omega' \end{aligned} \tag{1.14}$$

where angular flux in the energy group g is:

$$\psi^g(\vec{r},\hat{\Omega}) = \int_{E_g}^{E_{g-1}} \psi(\vec{r},\hat{\Omega},E)dE \tag{1.15}$$

By considering the source to be isotropic and defining $q^g(\vec{r})$ as a scalar source in group g and at point $\vec{r}$, we have:

$$q^g(\vec{r}) = \int_{\hat{\Omega}} Q^g(\vec{r},\hat{\Omega})d^2\Omega \tag{1.16}$$

where $Q^g(\vec{r},\hat{\Omega}) = \frac{1}{4\pi}q^g(\vec{r})$. The integral transport equation thus becomes:

$$\left[\hat{\Omega}\cdot\vec{\nabla} + \Sigma^g(\vec{r})\right]\psi^g(\vec{r},\hat{\Omega}) = \frac{1}{4\pi}q^g(\vec{r}) \tag{1.17}$$

The neutron flux $\psi^g(\vec{r},\hat{\Omega})$ is estimated at a point $\vec{r}$ due to neutrons generated at any point $\vec{r'}$ surrounding it. Since the neutron flux $\psi^g(\vec{r'},\hat{\Omega})$ at any point $\vec{r'}$ satisfies the transport equation, we can represent the leakage term as $\hat{\Omega}\cdot\vec{\nabla} = -d/dR$ for each point $\vec{r'} = \vec{r} - R\hat{\Omega}$ with $R = |\vec{r} - \vec{r'}|$, and the local transport equation can be written as:

$$\left[\frac{-d}{dR} + \Sigma^g(\vec{r} - R\hat{\Omega})\right]\psi^g(\vec{r} - R\hat{\Omega},\hat{\Omega}) = \frac{1}{4\pi}q^g(\vec{r} - R\hat{\Omega}) \tag{1.18}$$

Using integrating factor ($e^{-\tau^g(R)} \equiv e^{-\int_0^R \Sigma^g(\vec{r}-R'\hat{\Omega})dR'}$) and multiplying both sides of the equation, we obtain:

$$\frac{-d}{dR}\left[e^{-\tau^g(R)}\psi^g(\vec{r} - R\hat{\Omega},\hat{\Omega})\right] = \frac{1}{4\pi}e^{-\tau^g(R)}q^g(\vec{r} - R\hat{\Omega}) \tag{1.19}$$

where the optical path τ^g is defined as:

$$\tau^g(R) = \int_0^R \Sigma^g(\vec{r} - R'\hat{\Omega})dR' \tag{1.20}$$

Therefore, the solution to the integral transport equation (1.19) with respect to the boundary conditions becomes:

$$\psi^g(\vec{r}, \hat{\Omega}) = e^{-\tau^g(R_s)}\psi_-^g(\vec{r}_s, \hat{\Omega}) + \frac{1}{4\pi}\int_0^R e^{-\tau^g(R')}q^g(\vec{r'})dR' \tag{1.21}$$

where $\psi_-^g(\vec{r}_s, \hat{\Omega})$ represents the incoming flux at a point $\vec{r_s}$ on the boundary surface S surrounding V and we express:

$$\vec{r}_s = \vec{r} - R_s\hat{\Omega} \quad \text{and} \quad R_s = |\vec{r} - \vec{r}_s|$$

The scalar flux (ϕ^g) is obtained by integrating angular flux over all angles, therefore:

$$\phi^g(\vec{r}) = \int_S \frac{e^{-\tau^g(R_s)}}{4\pi R_s^2}(\hat{\Omega} \cdot \vec{N}_-)\psi_-^g(\vec{r}_s, \hat{\Omega}')d^2r' + \int_V \frac{e^{-\tau^g(R')}}{4\pi R'^2}q^g(\vec{r'})d^3r' \tag{1.22}$$

where the relations considered are:

$$d^3r = R^2d^2\Omega dR, \quad \text{and} \quad (\hat{\Omega} \cdot \vec{N}_-)d^2r = R_s^2d^2\Omega$$

Similarly, one can obtain an equation for outgoing angular flux $\psi_+^g(\vec{r}_s, \hat{\Omega}')$ at surface S by taking the limit $\vec{r} = \vec{r}_s$ in equation (1.21):

$$\psi_+^g(\vec{r_s}, \hat{\Omega}) = e^{-\tau^g(R_s)}\psi_-^g(\vec{r}_s, \hat{\Omega}) + \frac{1}{4\pi}\int_0^R e^{-\tau^g(R')}q^g(\vec{r'})dR' \tag{1.23}$$

The outgoing and incoming angular fluxes can be linked at the surface S by a boundary condition. For example, the albedo condition can be obtained by:

$$\psi_-^g(\vec{r}_s) = \beta^g(\vec{r}_s)\psi_+^g(\vec{r}_s) \tag{1.24}$$

where β^g is the albedo coefficient. In order to obtain the discretized flux equations, the problem is divided into N_v regions of volume V_i and the external boundary, Γ, is divided into N_s surfaces of area S_α. It will be assumed that all the properties (i.e., cross sections, atomic density, source etc.) are constant within each region. The average scalar flux (ϕ_i^g) inside each volume and average angular flux ($\psi_{\pm,\alpha}^g$) on each surface can be obtained as:

$$\begin{aligned} \phi_i^g &= \frac{1}{V_i}\int_{V_i}\phi^g(\vec{r})d^3r \\ \psi_{\pm,\alpha}^g &= \frac{4}{S_\alpha}\int_{S_\alpha} d^2r(\hat{\Omega}\cdot\vec{N}_\pm)\psi_\pm^g(\vec{r}_s) \end{aligned}$$

By integrating over each volume V_i of equation (1.22) and using previous equations, the average flux in region i becomes:

$$V_i\phi_i^g = \sum_{\alpha=1}^{N_S} \int_{V_i}\int_{S_\alpha} \frac{e^{-\tau^g(R_s)}}{4\pi R_s^2}(\hat{\Omega}\cdot\vec{N}_-)\psi^g_{-,\alpha}d^3r d^2r' + \sum_{j=1}^{N_V}\int_{V_i}\int_{V_j}\frac{e^{-\tau^g(R)}}{4\pi R^2}q_j^g d^3r' d^3r \tag{1.25}$$

where q_j^g is the constant source inside volume j. Using equation (1.23) the average outgoing angular flux $(\psi^g_{+,\alpha})$ on the surface α becomes:

$$\frac{S_\alpha}{4}\psi^g_{+,\alpha} = \sum_{\beta=1}^{N_S}\int_{S_\alpha}\int_{S_\beta}\frac{e^{-\tau^g(R_s)}}{4\pi R_s^2}(\hat{\Omega}\cdot\vec{N}_+)(\hat{\Omega}\cdot\vec{N}_-)\psi^g_{-,\beta}d^2r d^2r' + \sum_{j=1}^{N_V}\int_{S_\alpha}\int_{V_j}\frac{e^{-\tau^g(R)}}{4\pi R^2}(\hat{\Omega}\cdot\vec{N}_+)q_j^g d^3r' d^2r \tag{1.26}$$

The relation between the outgoing flux on a given surface and the incoming flux on various surfaces is represented by an albedo boundary condition matrix (A^g) which connects the surface S_α to the surface S_β:

$$\psi^g_{-,\alpha} = \sum_{\beta=1}^{N_S} A^g_{\alpha\beta}\psi^g_{+,\beta} \tag{1.27}$$

Using the equations (1.25) and (1.26) the general form of collision probabilities are defined:

$$\tilde{p}_{ij}^{g} = V_i p_{ij}^{g} = \int_{V_i}\int_{V_j} \frac{e^{-\tau^g(R)}}{4\pi R^2} d^3r' d^3r \tag{1.28}$$

$$\tilde{p}_{i\alpha}^{g} = V_i p_{i\alpha}^{g} = \int_{V_i}\int_{S_\alpha} \frac{e^{-\tau^g(R_s)}}{4\pi R_s^2} (\vec{\Omega}\cdot\vec{N}_-) d^3r d^2r' \tag{1.29}$$

$$\tilde{p}_{\alpha i}^{g} = \frac{S_\alpha}{4} p_{\alpha i}^{g} = \int_{S_\alpha}\int_{V_i} \frac{e^{-\tau^g(R)}}{4\pi R^2} (\vec{\Omega}\cdot\vec{N}_+) d^3r' d^2r \tag{1.30}$$

$$\tilde{p}_{\alpha\beta}^{g} = \frac{S_\alpha}{4} p_{\alpha\beta}^{g} = \int_{S_\alpha}\int_{S_\beta} \frac{e^{-\tau^g(R_s)}}{4\pi R_s^2} (\vec{\Omega}\cdot\vec{N}_-)(\vec{\Omega}\cdot\vec{N}_+) d^2r d^2r' \tag{1.31}$$

and collision probability equations with respect to the transport equation are written:

$$\phi_i^g = \sum_{\alpha=1}^{N_S} p_{i\alpha}^g \psi_{-,\alpha}^g + \sum_{j=1}^{N_V} p_{ij}^g q_j^g \tag{1.32}$$

$$\psi_{+,\alpha}^g = \sum_{\beta=1}^{N_S} p_{\alpha\beta}^g \psi_{-,\beta}^g + \sum_{j=1}^{N_V} p_{\alpha j}^g q_j^g \tag{1.33}$$

The matrix form of the collision probability equations are derived:

$$\vec{\phi}^g = \mathbf{P}_{vs}^g \vec{J}_-^g + \mathbf{P}_{vv}^g \vec{q}^g \tag{1.34}$$

$$\vec{J}_+^g = \mathbf{P}_{ss}^g \vec{J}_-^g + \mathbf{P}_{sv}^g \vec{q}^g \tag{1.35}$$

$$\vec{J}_-^g = \mathbf{A}^g \vec{J}_+^g \tag{1.36}$$

where $\vec{\phi}^g$, $\vec{J}_\pm^g$ and $\vec{q}^g$ are vectors containing ϕ_i^g, ψ_α^g and q_i^g, respectively. The matrices $\mathbf{P}_{vs}^g$, $\mathbf{P}_{vv}^g$, $\mathbf{P}_{ss}^g$ and $\mathbf{P}_{sv}^g$ consist of the elements p_{ij}^g, $p_{i\alpha}^g$, $p_{\alpha i}^g$ and $p_{\alpha\beta}^g$, respectively, and $\mathbf{A}^g$ is the albedo matrix.

By substituting the equation (1.35) in (1.36) one obtains:

$$\vec{J}_{-}^{g} = \left(\mathbf{I} - \mathbf{A}^{g}\mathbf{P}_{ss}^{g}\right)^{-1} \mathbf{A}^{g}\mathbf{P}_{sv}^{g}\vec{q}^{g} \tag{1.37}$$

and again substituting the equation (1.37) in (1.35), we obtain

$$\vec{J}_{+}^{g} = \left\{\mathbf{P}_{ss}^{g}\left(\mathbf{I} - \mathbf{A}^{g}\mathbf{P}_{ss}^{g}\right)^{-1} \mathbf{A}^{g}\mathbf{P}_{sv}^{g} + \mathbf{P}_{sv}^{g}\right\}\vec{q}^{g} \tag{1.38}$$

and on substituting the equation (1.37) in (1.34) the flux becomes:

$$\vec{\phi}^{g} = \left\{\mathbf{P}_{vs}^{g}\left(\mathbf{I} - \mathbf{A}^{g}\mathbf{P}_{ss}^{g}\right)^{-1} \mathbf{A}^{g}\mathbf{P}_{sv}^{g} + \mathbf{P}_{vv}^{g}\right\}\vec{q}^{g} \tag{1.39}$$

In order to define complete collision probability matrices we have:

$$[\mathbf{P}_{sv}^{C}]^{g} \equiv \mathbf{P}_{ss}^{g}\left(\mathbf{I} - \mathbf{A}^{g}\mathbf{P}_{ss}^{g}\right)^{-1} \mathbf{A}^{g}\mathbf{P}_{sv}^{g} + \mathbf{P}_{sv}^{g} \tag{1.40}$$

$$[\mathbf{P}_{vv}^{C}]^{g} \equiv \mathbf{P}_{vs}^{g}\left(\mathbf{I} - \mathbf{A}^{g}\mathbf{P}_{ss}^{g}\right)^{-1} \mathbf{A}^{g}\mathbf{P}_{sv}^{g} + \mathbf{P}_{vv}^{g} \tag{1.41}$$

and therefore the equations (1.38) and (1.39) become:

$$\vec{J}_{+}^{g} = [\mathbf{P}_{sv}^{C}]^{g}\vec{q}^{g} \tag{1.42}$$

$$\vec{\phi}^{g} = [\mathbf{P}_{vv}^{C}]^{g}\vec{q}^{g} \tag{1.43}$$

Finally, with obtained expressions, using the source term $\vec{q^g}$ and the complete collision probability matrices i.e., $[\mathbf{P}_{sv}^C]^g$, $[\mathbf{P}_{vv}^C]^g$ and albedo matrix $\mathbf{A}^g$, the flux is evaluated in the volume and on the surface. It is to be noted that, the source term $\vec{q^g}$ has a dependency on the volume flux $\vec{\phi}^g$:

$$\vec{q^g} = \frac{\chi^g}{k_{eff}} \sum_{g'} [\nu \Sigma_f^{g'}] \vec{\phi}^{g'} + \sum_{g'} [\Sigma_s^{g' \to g}] \vec{\phi}^{g'} \tag{1.44}$$

DRAGON code solves the equations (1.42) and (1.43) using iterative methods and the source term defined in equation (1.44), to calculate the fluxes. In equation (1.44), $\Sigma_s^{g' \to g}$ is the cross section for scattering of neutrons from energy group g' to g. The effective multiplication factor (k_{eff}), in the absence of leakage, i.e. $(\hat{\Omega} \cdot \vec{\nabla} = 0)$ from the equation (1.17) and considering isotropic scattering, is computed by DRAGON, using the fluxes obtained earlier, according to equation (1.45):

$$k_{eff} = \frac{P_R}{D_R} \tag{1.45}$$

where the production rate (P_R) is defined as:

$$P_R = \sum_i \left[\sum_g \chi^g \sum_{g'} [\nu \Sigma_f^{g'}] \vec{\phi}^{g'} \right] V_i \tag{1.46}$$

and the destruction rate (D_R) without leakage is defined as:

$$D_R = \sum_i \left[\sum_g [\Sigma^g] \vec{\phi}^g - \sum_g \sum_{g'} [\Sigma_s^{g' \to g}] \vec{\phi}^{g'} \right] V_i \tag{1.47}$$

When one considers leakage, a homogenous buckling correction is to be applied on the

diffusion cross section ($\Sigma_s - dB^2$), where d is the diffusion coefficient and B is the buckling.

1.3 Reactivity Formula

The estimation of multiplication factor, which is the ratio of number of neutrons born in one generation (or production rate, P_R) to the number of neutrons in the previous generation being absorbed (or destruction rate, D_R without leakage), will help in understanding the behavior of the system. The system can be termed critical (the production and destruction rate are equal), subcritical (the production rate is smaller than destruction rate) or supercritical (the production rate is greater than destruction rate) based on the following definition:

$$k_{eff} \begin{cases} < 1: & \text{reactor sub critical} \\ = 1: & \text{reactor critical} \\ > 1: & \text{reactor super critical} \end{cases}$$

Another important quantity which needs to be defined to understand certain physical phenomena is - reactivity (ρ). It is defined as the fractional departure of a system from criticality, and is calculated as:

$$\rho = \frac{k_{eff} - 1}{k_{eff}} \tag{1.48}$$

Reactivity addition to the system can be positive or negative depending on the process involved. For example, addition of any form of poison, like boron in moderator or insertion

of control rod brings about an addition of negative reactivity, while removal of poison or addition of fuel can bring about an addition of positive reactivity. Certain reactor transients also change the reactivity. It is generally desired that when there is a transient, there is negative reactivity addition. Certain possible transients in reactors are increase in fuel temperature, loss of coolant, increase in temperature of moderator/coolant, increase in power etc. It is important from safety point of view that the reactivity estimation for these transients are done to the best of accuracy and all the shutdown systems are appropriately designed.

In this thesis we have focussed on the coolant void transient. The change in reactivity $\Delta\rho$, introduced due to total coolant voiding will be defined as:

$$\Delta\rho = \left(\frac{1}{k_{eff}^{cool}} - \frac{1}{k_{eff}^{void}} \right) \times 1000 \text{ mk} \tag{1.49}$$

1.4 Homogenization Technique

As mentioned earlier, the existing version of DRAGON has inherent geometry limitations to estimate coolant void reactivity (CVR) for 2×2 assembly pattern. A model must be developed in order to perform the calculation within the present constraints. This model is approximate and would involve replacing the annular fuel pins (fuel plus its sheathing) by equivalent square fuel pins. The equivalence between annular fuel pins and square fuel pins is brought about by homogenizing the fuel and clad and subsequently conserving the reaction rates between the two geometries. In order to ensure that the approximate model is equivalent with the original cluster, one will generally require to create a model dependent homogenized cross section library. We will describe the homogenization procedures presently available in the code DRAGON.

There are various ways to generate the cross section associated with homogenized regions. In the simplest technique, a new mixture can be formed by using a combination of earlier defined mixtures, using `LIB:` module. Therefore, the cross section for a homogeneous mixture I in group g is obtained as:

$$\Sigma_I^g = \frac{\sum_{i \in I} V_i \Sigma_i^g}{\sum_{i \in I} V_i} \tag{1.50}$$

The second technique is by using the flux/volume homogenization procedure of `EDI:` module. In this procedure, we use the fluxes obtained in each region to ensure the cross section for a homogeneous mixture. The fluxes are obtained by solving the transport equation. The cross section for a homogeneous mixture I in group g is thus obtained as:

$$\Sigma_I^g = \frac{\sum_{i \in I} \phi_i^g V_i \Sigma_i^g}{\sum_{i \in I} \phi_i^g V_i} \tag{1.51}$$

Both these techniques fail for partial cell homogenization, because the reaction rates obtained using the solution to the homogenized transport problem are different from the homogenized reaction rates for the heterogeneous problem. In order to remedy this problem, the SPH technique is used. In the present work, using the SPH procedure, equivalent square pins are created from annular pins and corresponding cross section libraries are generated.

The Superhomogenization (SPH) technique was developed by A. Hébert [Hébert, 1993a, Hébert, 1993b], for transport-transport and transport-diffusion equivalence with a series of SPH factors, for implementation in the code DRAGON. In this section we will briefly mention the importance of SPH technique in relation to the proposed approximate model.

The SPH algorithm proceeds in two steps. First the homogenized neutron flux (ϕ_I^g) in each energy group and mixture is determined by solving the transport equation. It is then followed by an iterative procedure, to create the SPH factors. Here in our calculations, the SPH factors (μ_I^g) are computed using a process that iterates between the partly homogenized (approximate) and heterogeneous (exact) problems to ensure that reaction rates are preserved. Therefore, by redefining the homogenized flux ($\tilde{\phi}_I^g$) and cross sections ($\tilde{\Sigma}_I^g$), as:

$$\tilde{\Sigma}_I^g = \mu_I^g \Sigma_I^g \tag{1.52}$$

$$\tilde{\phi}_I^g = (\mu_I^g)^{-1} \phi_I^g \tag{1.53}$$

using the iterative procedure, reaction rates will be preserved. The homogenized library will generally depend on the fuel burnup. In order to simplify our presentation, we will only consider the case where the fuel is fresh. Note that the SPH procedure must

also be applied when fewgroup condensation is considered. Here we have assumed that no condensation will take place and that all our calculations will be performed in the original (69) group structure.

Different cross section libraries for each voiding state are thus generated using the SPH module, and will be required for this approximate model. These libraries will subsequently be used to compute the CVR for 2×2 assemblies of cells.

Another important module that was utilized in the development of the approximate model is `MRG:` module [Marleau, 2000]. This module is used to pre-homogenize a geometry after it has been tracked using a tracking module. The module is used to combine the regions which have the same mixture. By doing so, one could reduce the number of surfaces and regions that needs to be tracked and the size of collision probability matrix can be drastically reduced. The combination of regions having the same mixture is left to the discretion of the experienced user. During the above procedure, the cross section however remains unchanged.

CHAPTER 2

CELL MODEL

With the current version of DRAGON, one can only compute the CVR for a single CANDU cluster cell. Because of the limitations in the tracking module, the DRAGON transport code cannot evaluate the effect of CVR on a heterogeneous 2×2 assembly of cells in the exact geometry. In addition, in regular cell calculations, the outermost boundary is annularized, so that one can consider annular regions for tracking and estimating the collision probability matrix. But when the outermost boundary is square or hexagonal, the discretization is limited to the annular regions, thus leaving a large region in the corner without discretization. In order to bypass these problems in the current version of DRAGON, we decided to simulate the standard CANDU geometry using an approximate model. In this work, the geometry is referred as the square pin model (SPM).

This chapter begins with a brief geometrical description of the CANDU-6 lattice and is followed by a description of the SPM for the standard CANDU-6 lattice. We will also consider variations in this geometry leading to ACR-700 type lattice. First, we will consider a reduction in lattice pitch. Then, we will increase the outer radius of the calandria tube along with a reduction in the lattice pitch. Finally, we will change the fuel assembly design by increasing the number of pins from 37 to 43, changing natural uranium to enriched uranium and changing the coolant from heavy water to light water.

2.1 Standard CANDU-6 Geometry

A lattice cell is a small repeatable structure in the reactor core, usually consisting of a fuel region surrounded by coolant and/or moderator and support material, with appropriate boundary conditions applied on the external surfaces. The typical CANDU-6 cell (Figure 2.1) is a 37 element rod cluster fuelled with natural uranium oxide and cladded with zircalloy. The fuel assemblies are located inside a pressure tube made of zirconium containing heavy water coolant. This pressure tube is separated by a helium cover gas from the zircalloy calandria tube which is immersed in a heavy water moderator. The square lattice pitch in a typical CANDU-6 core is 28.575 cm.

In this standard geometry, four fuel rings, containing respectively 1, 6, 12 and 18 fuel pins, are considered. The pitch circle radius of each ring are 0.0 cm, 1.4884 cm, 2.8755 cm and 4.3305 cm, respectively. The fuel pellet radius is 0.6122 cm and the thickness of its sheathing is 0.0418 cm. The effective density of the fuel is 10.44 g/cm^3 for all rings. The inner radius of the pressure tube is 5.168878 cm and its thickness is 0.4343 cm. The inner radius of the calandria tube is 6.4478 cm and its thickness is 0.1397 cm. The gap between the pressure and calandria tube is filled with a helium cover gas and the thickness of gap is 0.8446 cm. Heavy water moderator fills the region exterior to the calandria tube and within the square lattice pitch.

For transport calculations using the collision probability method, each fuel pin must be subdivided into three regions to ensure spatial convergence of the flux (see Figure 2.1) [Hébert, 1995]. The coolant region is also divided into three annular rings, the first ring containing the 7 central fuel pins while the second and third coolant region surround the rings containing respectively 12 and 18 fuel pins. Each coolant ring was further subdivided into three annular regions. Finally the moderator was divided into 9 regions, including 8 annular rings (with 0.9266 cm thickness) and a final annular/Cartesian re-

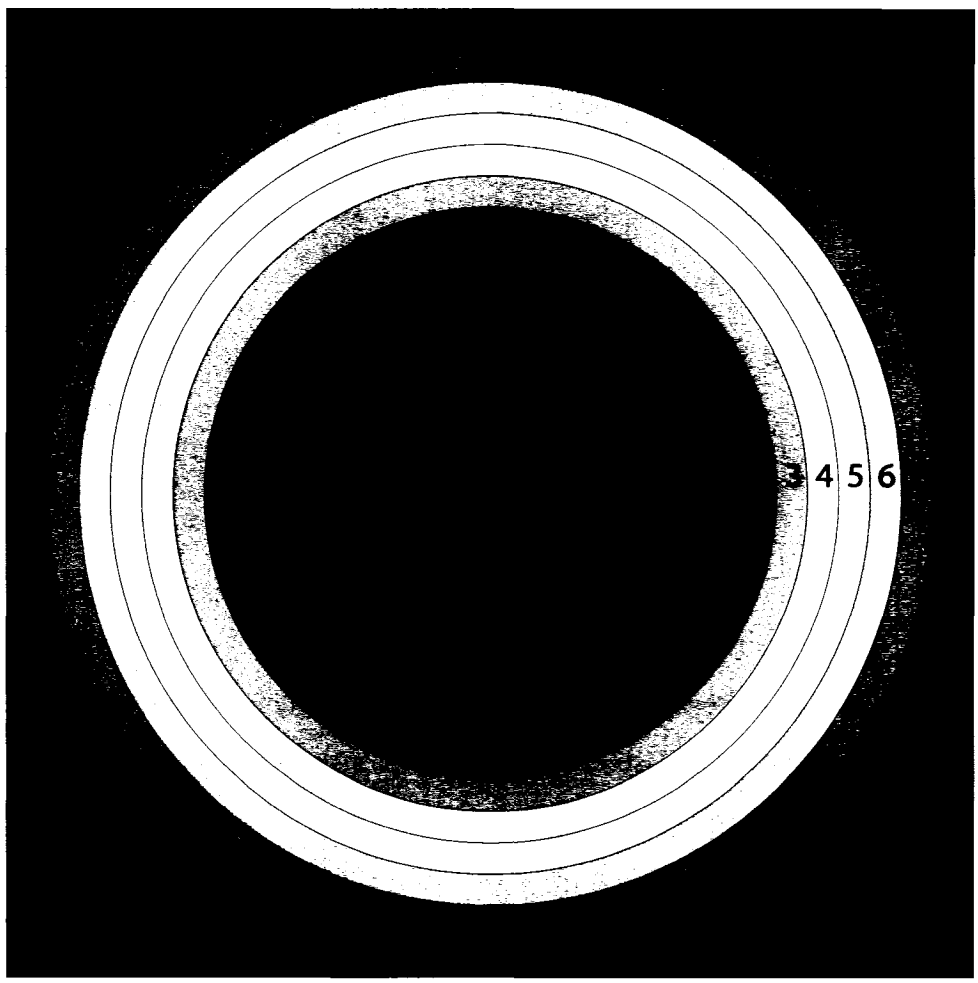

Figure 2.1 Exact CANDU-6 geometry.

gion. As a result, the number of flux regions and outer surfaces in a DRAGON treatment of the exact CANDU-6 geometry were 37 and 4 respectively.

The fuel in all rings is at a nominal temperature of 941.29 $^{\circ}K$ and the sheathing is at 560.66 $^{\circ}K$. The temperature of coolant and pressure tube is 560.66 $^{\circ}K$ while the temperature of helium gap, calandria tube and moderator is 345.66 $^{\circ}K$.

2.2 Square Pin Model for CANDU-6

In this section, an approximate geometry for a CANDU-6 cell will be designed. By creating such a model, a 2×2 assembly pattern of CANDU-6 can be analyzed with DRAGON. Using this model one can also finely discretize the Cartesian corner of a square lattice, an option which is not possible using the current cluster model in DRAGON. The Square Pin Model (SPM) that was considered for our simulations consists of replacing each annular fuel pin and its sheathing by a homogenized square pin. In this model, the total volume of each square pin (fuel plus sheathing) is selected to be identical to the volume of the original annular pins (see Figure 2.2 and Equation 2.1). The location of the center of each of the 37 pins in the SPM is identical to that found in the standard geometry. We will now briefly describe the steps that are to be followed to generate the SPM.

Figure 2.2 shows the conversion of an annular pin to a square pin for the model using MATLAB. Let us consider that the center of the annular pin in a Cartesian coordinates system is located at (X,Y). The side, a, of the square pin is estimated using the equation:

$$\mathrm{a}^2 = \pi \mathrm{r}^2 \longrightarrow \mathrm{a} = \sqrt{\pi \mathrm{r}^2} \tag{2.1}$$

where, r, is the outer radius of the sheathing surrounding the fuel pin. Using this value,

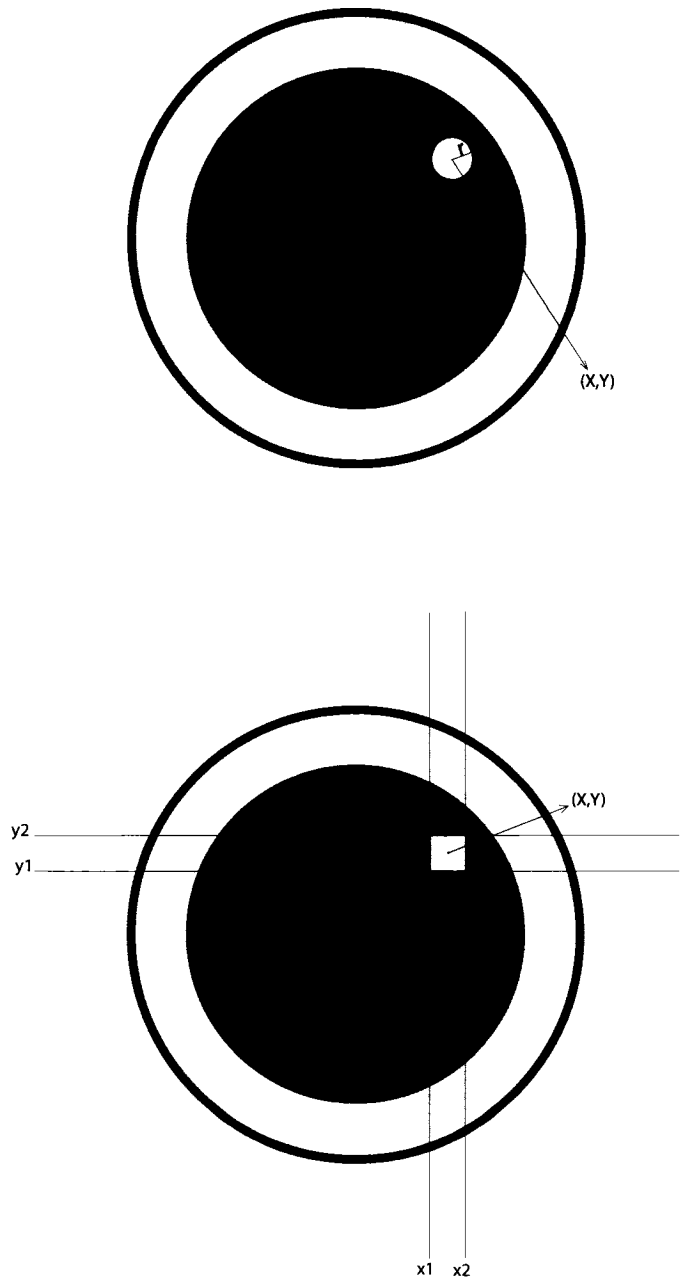

Figure 2.2 Square pin model.

the square pin is also placed at (X,Y), with the corners of square being (x1,y1), (x1,y2), (x2,y1) and (x2,y2), with the definitions:

$$x1 = X + a/2, \quad \text{and} \quad x2 = X - a/2$$
$$y1 = Y + a/2, \quad \text{and} \quad y2 = Y - a/2$$

The above procedure was followed for all the 37 pins of the CANDU-6 lattice. In order to perform DRAGON calculation, it is important to clearly define the regions and materials associated with each region. It was obtained as follows. One line was drawn along each side of every square till it intersects with the X-axis or Y-axis (see Figure 2.3). Each square was thus passed by four lines from the top, bottom, left and right side. For a 37 square pin CANDU-6 cluster, we had 35 and 31 intersections on X-axis and Y-axis, respectively. This means that for the Y-axis, there are 30 levels and in each level, 34 distinct regions were obtained. We thus have a total of $(30 \times 34 = 1020)$ regions without considering any annular region. But when one considers the pressure tube, calandria tube, helium gap and finely discretized coolant and moderator, the above procedure leads to generation of 3223 spatial regions and 132 outer surfaces, respectively (see Figure 2.4).

Each region that has been created for the SPM is subsequently associated with its corresponding mixture. The numbering of mixture is done from region 1 to region 34 in each level and from inner circle to outer circle. This procedure is followed for each level from bottom to top.

The mixtures considered for each region of SPM, except the fuel region, are the same as that of the standard CANDU-6 cell. The mixtures in the square fuel pins are made by merging the fuel and sheathing of the original CANDU-6 cell.

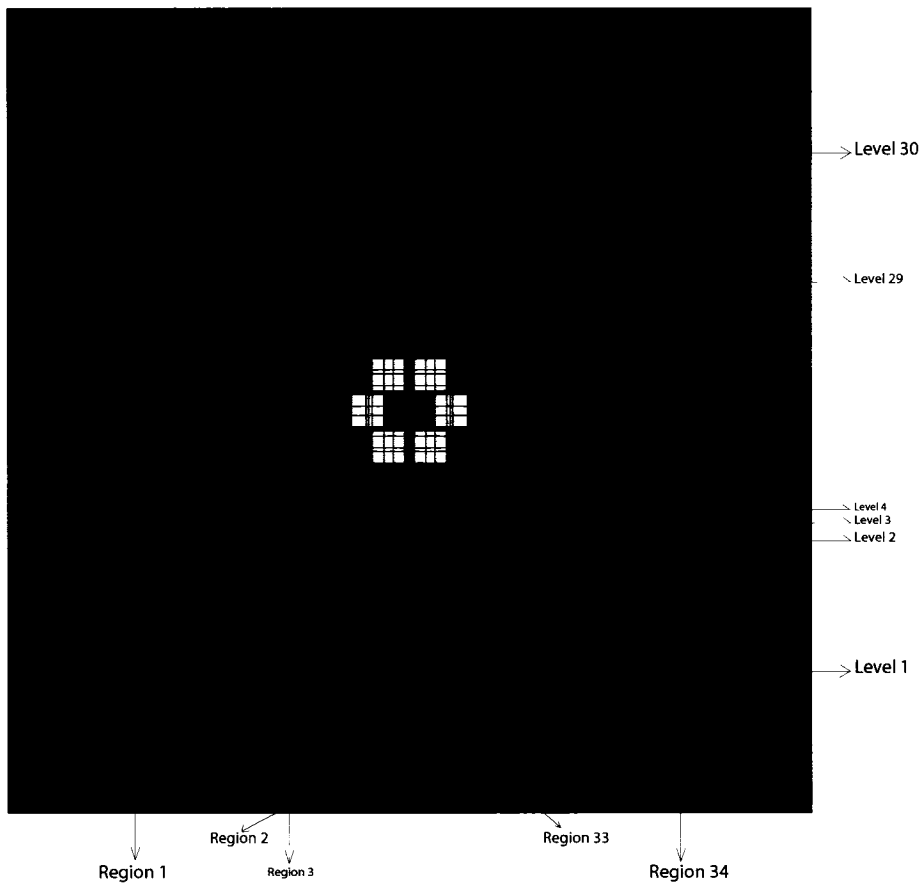

Figure 2.3 SPM for CANDU-6.

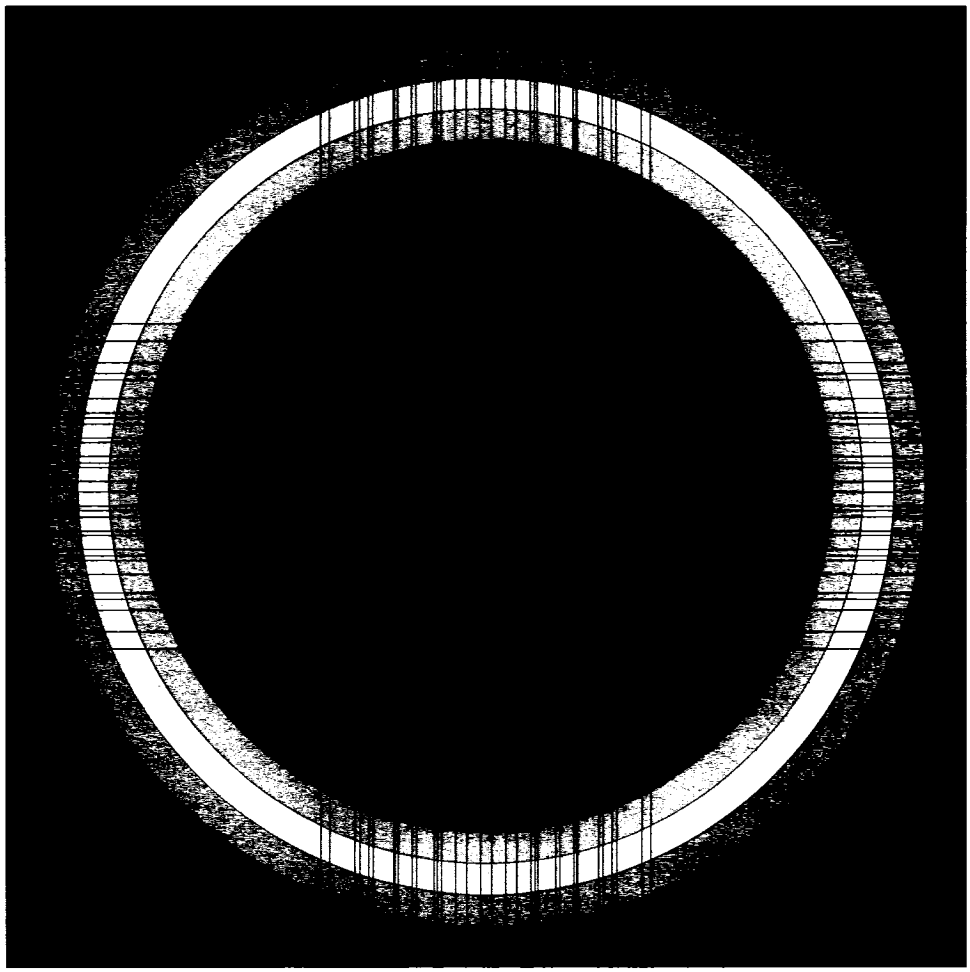

Figure 2.4 SPM for CANDU-6 with finely discretized coolant and moderator.

Hence, four different mixtures were considered for each square fuel pin in each ring respectively. Afterwards, all the information corresponding to each region was converted from MATLAB to a format that is subsequently utilized by the GEO: module of DRAGON. Because of the large number of regions involved, analyzing the square pin model is expensive from a computer resources point of view; therefore, we used quarter cell symmetry for this approximate geometry and the number of regions and outer surfaces was thus reduced to 843 and 34 respectively. In Figure 2.4, different colors illustrate different mixtures. We will now discuss the problem of generating the cross section library for this model that will ensure equivalence between the SPM and standard model for a CANDU-6 cell.

As we mentioned in Section 1.4, in order to perform reliable transport calculations for the proposed model, it is important to generate cross section libraries that can be utilized with the approximate geometry. This is made possible by SPH procedure where one performs transport calculations on the exact geometry and then generates the cross sections for the approximate geometry that satisfy conservation of the reaction rates. The generation of cross section libraries can be done in two different ways. They are the Multi-step Cell Simulation and Direct Cell Simulation. The steps involved in each of these simulation models will be explained in the following sections.

2.3 Multi-Step Cell Simulation

The multi-step cell simulation (MSCS) involves two distinct steps to generate the cross section libraries for SPM [Talebi, 2005]. In the first step, one solves the transport equation in the exact CANDU-6 geometry with annular fuel pins (Figure 2.5(a)) using a 2-D collision probability technique and estimates the fluxes in various regions of the lattice and the cell eigenvalue for various coolant conditions (coolant density). Subsequently, one uses the SPH technique to convert the annular fuel and clad region into a single

annular region and generate a library that can be used in the second step. The model will thus be referred to as HPM (Homogenized Pin Model). For the second step, one re-estimates the fluxes and the eigenvalue for the cell with the collapsed fuel-clad region (Figure 2.5(b)) using the library generated in the first calculation step. Then, using the SPH technique for a second time, the cylindrical fuel pins are converted into square pins (Figure 2.5(c)) and a new cross section library is generated.

These steps are repeated for different coolant density conditions and a series of coolant density dependent cross section libraries are generated. In fact, two different scenarios were considered for draining of the coolant. They were the heterogeneous and homogeneous draining conditions. Heterogeneous draining conditions were simulated by removing the coolant annularly for the three rings, first from the inside to the outside and then the other way around. A coolant density of 0.001 g/cm^3 was selected for the voided regions (because in eigenvalue calculation we need a value for those regions and further reduction, did not change the results). The cooled regions were at the reference coolant density of 0.81212 g/cm^3. Homogeneous draining conditions were simulated by reducing the heavy water density uniformly for all the rings in the coolant region. The density of the coolant is reduced uniformly in four discrete steps, i.e. 25% void (0.60909 g/cm^3), 50% void (0.4606 g/cm^3), 75% void (0.20303 g/cm^3) and 100% void (0.001 g/cm^3). The CPU time needed to perform such calculation for each coolant condition is about 122 minutes.

2.3.1 Validation of Multi-Step Cell Simulation

Here we will present our validation results by comparing the multiplication factor (k_{eff}) and the change in reactivity ($\Delta\rho$) resulting from total coolant voiding (see Section 1.3). All calculations were performed without considering any leakage.

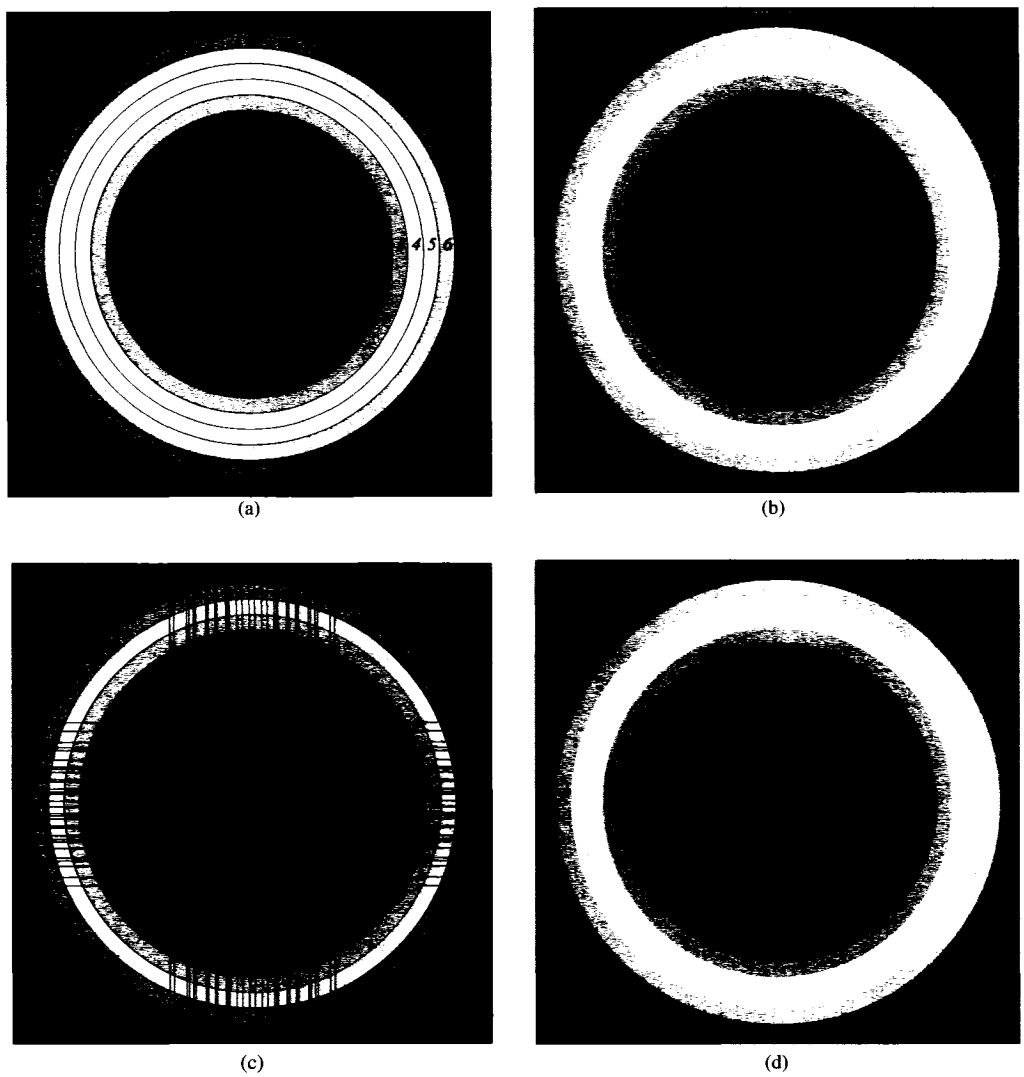

Figure 2.5 Exact CANDU-6 with 28.575 cm lattice pitch and eight annular regions in moderator (a), HPM (b), SPM fine mesh (c) and SPM coarse mesh (d).

Let us first consider the homogeneous draining effect and verify that the library generated for the SPM described before is adequate. Because we used the SPH technique to generate the library, the approximate solution to the neutron transport equation associated with this model should be identical with the reference solution. As one can see in Table 2.1 the three models (Exact, HPM and SPM fine mesh) give similar eigenvalues with deviations reaching a maximum of 0.1 mk, indicating our model is correctly programmed in DRAGON.

Table 2.1 Comparison of k_{eff} and $\Delta\rho$ for CANDU-6 lattice with homogeneous draining scenario using MSCS.

Coolant Density $\rightarrow$ (g/cm^3)	0.81212	0.60909	0.40606	0.20303	0.00100	$\Delta\rho$ (mk)
$k_{eff} \downarrow$	%100 Cooled	%25 Voided	%50 Voided	%75 Voided	%100 Voided	CVR
Exact Figure 2.5 (a)	1.1132	1.1180	1.1230	1.1281	1.1335	+16.0
HPM Figure 2.5 (b)	1.1133	1.1181	1.1231	1.1282	1.1335	+16.0
SPM (fine mesh) Figure 2.5 (c)	1.1133	1.1181	1.1230	1.1281	1.1335	+16.0
SPM (coarse mesh) Three coolant rings Figure 2.5 (d)	1.1142	1.1186	1.1232	1.1280	1.1332	+15.1
SPM (coarse mesh) Single coolant region	1.1153	1.1193	1.1234	1.1278	1.1327	+13.8
SPM (corners) Figure 2.8	1.1140	1.1185	1.1231	1.1279	1.1330	+15.1

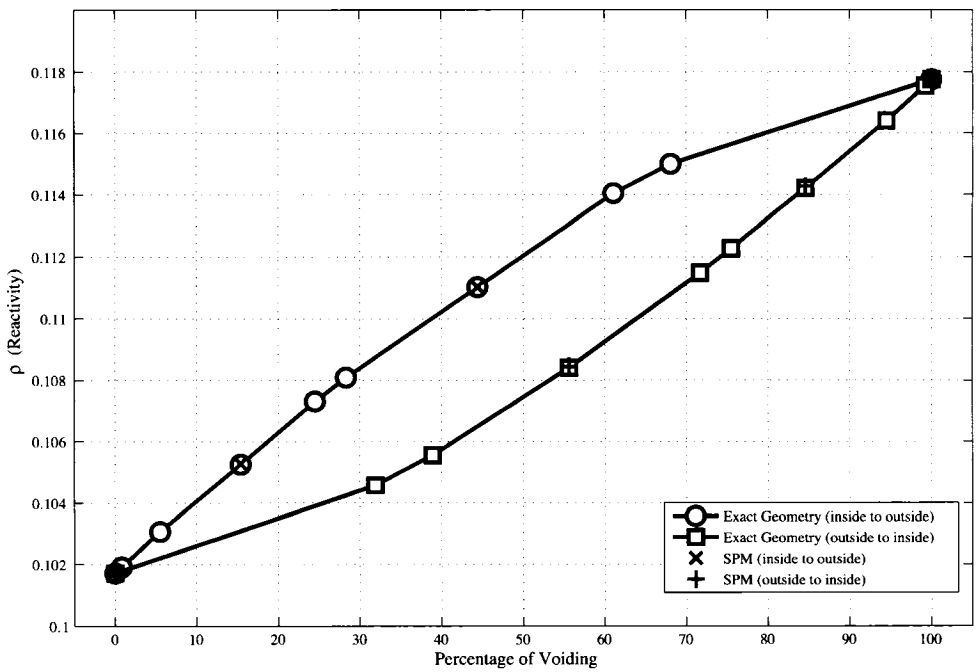

Figure 2.6 Heterogeneous draining in CANDU-6 cell.

We will now present the validation of SPM for heterogeneous draining scenario, with exact geometry. We considered various heterogeneous draining scenarios and observed the variation of reactivity as a function of voiding (Figure 2.6). As mentioned earlier, heterogeneous draining was performed in two ways, i.e., the coolant was drained from inside to outside and vice versa. One can first observe that, the results obtained using SPM match well with the exact model. A second observation is that the change in reactivity due to voiding of coolant from inside to outside is greater than from outside to inside. This can be explained by looking at the variation in the four factors due to draining. The factors that are most affected by draining are the thermal utilization factor f and the resonance escape probability p. The changes in p and f are in opposite directions with the change in p being the maximum contributing factor to reactivity. In fact, draining the coolant surrounding the interior fuel pins will increase the probability

of neutron escaping the resonance region as compared with a draining of the exterior fuel pins. This is because the slowing down of neutrons in the coolant region is less efficient due to the fact that the number of fuel pins surrounded by the coolant in the case is somewhat smaller.

2.3.2 Coarse Mesh Effect

In order to replace the annular pins by square pins in the SPM, a very fine mesh discretization is required (3223 regions). The problem is that for assembly calculations where we cannot use diagonal symmetry, one needs to perform calculation for the complete 2×2 assembly pattern, without any geometric simplification. Therefore, the total number of regions becomes larger than 10^4 which cannot be processed using the collision probability method in DRAGON. This problem can be resolved by using a coarser mesh instead of fine mesh. It is therefore important to assess the effect of using a coarser mesh in the solution of the transport equation. Here this coarser mesh will be generated using the `MRG:` module in DRAGON (see section 1.4). As mentioned earlier, the `MRG:` module merges the fine mesh regions having the same mixture, into a coarse mesh region, without altering the cross section.

Using the `MRG:` module for approximate geometry of CANDU-6 lattice, the fine regions were combined in such a way that there were nine coarse regions in the moderator and three coarse regions in the coolant. A single region was considered for pressure tube, calandria tube and air gap respectively, in addition to the four different square fuel regions. The Figure 2.5(d) shows the 19 coarse regions thus generated using the `MRG:` module.

We will now discuss the effect on the results due to merging of fine regions into coarse regions. It can be seen in Table 2.1, that the k_{eff} for SPM with fine mesh discretization is 1.1133 for cooled case and 1.1335 for voided case. The CVR thus estimated is +16

mk. As mentioned in Section 2.1, in the exact geometry we considered nine regions in coolant (3 regions in each of the three rings). When the fine regions in each ring were merged using the MRG: module, the k_{eff} obtained was 0.9 mk larger than the fine mesh results for a cooled case, while they remained almost identical for the fully voided case. As a result, the CVR for the coarse mesh SPM is under-predicted by about 1 mk (see the fourth line of Table 2.1). When the three rings in the coolant were merged, so as to obtain a single region in the coolant for the coarse mesh SPM, an increase of 2 mk in k_{eff} was observed with respect to the fine mesh SPM for cooled case and a loss of 0.8 mk for voided case, thus reducing the CVR estimated by about +2 mk (see the fifth line of Table 2.1). Even though finely discretizing the coolant region gives a better result, such a simulation is quite difficult from a modelling point of view. Hence, the rest of coarse mesh calculations for 37 rod cluster were performed by considering 3 rings in the coolant.

2.3.3 Effect of Corners with XS Libraries Generated Using MSCS

One restriction in the cluster model is that the code DRAGON is presently unable to discretize the corners of the Cartesian cell. This limitation can be overcome by using the model presented here. Accordingly, we can evaluate the effect of using a fine mesh in the Cartesian corners of the cell, on the eigenvalue and CVR. Therefore, a fine mesh discretization was performed, using the MRG: module (see section 1.4).

It can be seen from Figure 2.4, that there is a large region in the corner of the Cartesian cell representing the moderator. In order to discretize this region, we considered lines parallel to X-axis and Y-axis with a width almost equal to the annular regions already considered in the moderator (see Figure 2.7 (a)). We thus found that there are nine parallel lines that are to be drawn parallel to X-axis and Y-axis in order to discretize the corner completely.

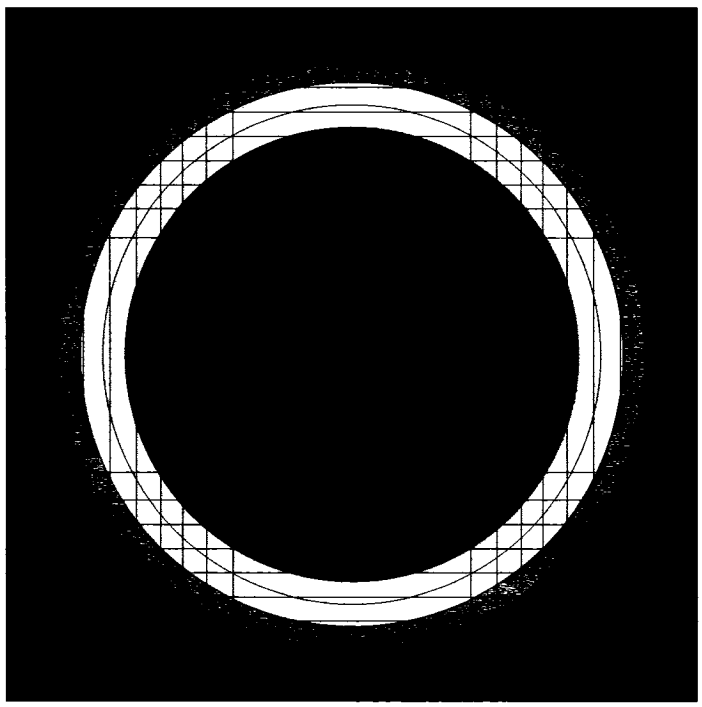

(a)

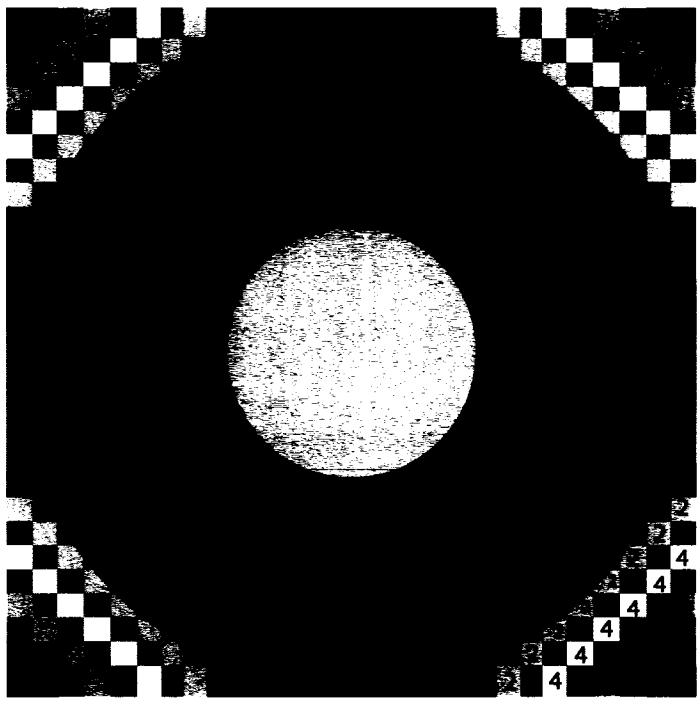

(b)

Figure 2.7 Creating nine levels (a) and generating nine annular-rectangular regions (b).

Therefore, we obtain nine levels in each corner of the CANDU-6 lattice having the same mixture. The rectangular annular regions thus obtained are merged with MRG: module so as to obtain nine different flux regions, as shown in Figure 2.7 (b).

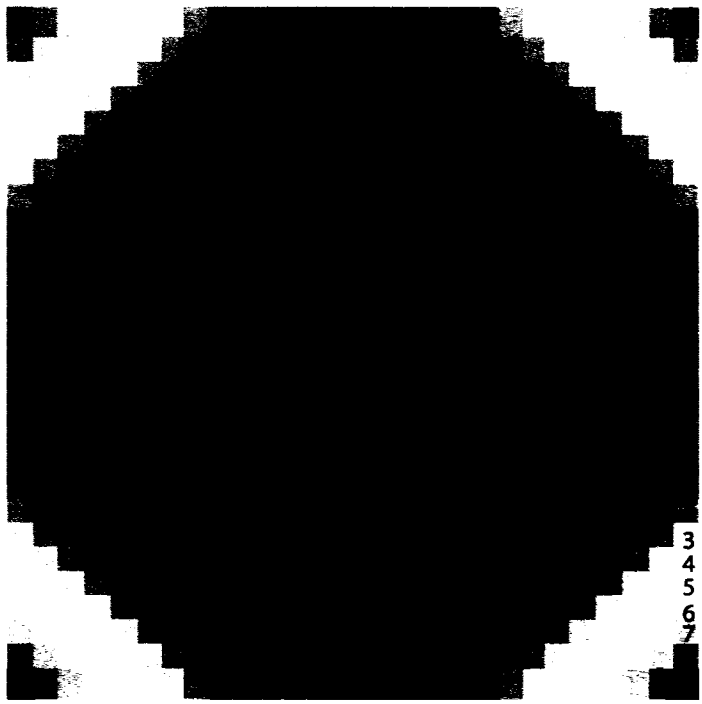

Figure 2.8 Fine mesh discretization in the Cartesian corners of CANDU-6 lattice

Fine mesh discretization for the whole lattice along with that of the corners was performed using MATLAB, along the same lines as mentioned before. We thus obtained 51 and 47 intersections on X-axis and Y-axis, respectively. It means that there are 46 levels for Y-axis and in each level we obtain 50 distinct regions. A format that is subsequently used in GEO: module of DRAGON is generated using MATLAB. The number of regions and outer surfaces increased to 4445 and 196, respectively. Finally, fine mesh regions that are assumed to possess identical fluxes were combined to obtain eight annular regions in the moderator, nine regions of annular-rectangular form in each corner and

three regions in the coolant. A single pressure tube, calandria tube and gap region was also generated in addition to four different square fuel regions. Finally 27 calculation regions were generated (Figure 2.8).

We observed that when one considers corner discretization, the reduction in eigenvalue reaches a maximum of 0.2 mk and the CVR is not changed, as shown in the last line of Table 2.1. It is interesting to note that these almost identical results indicate that the neutrons are sufficiently moderated and the results obtained using the fine mesh discretization in the Cartesian corners are almost identical to those obtained using a coarse mesh discretization.

2.4 Direct Cell Simulation

It was discussed earlier in Section 2.2 that the number of regions for SPM using fine mesh discretization was 3223. When one considers 69 energy group structure, the size of the collision probability matrix becomes too large to handle. Hence, a quarter cell calculation was performed with all 69 energy group structure, owing to symmetry in CANDU-6 type lattice. It would however still involve 843 regions and the computation time required for eigenvalue and flux convergence was found to be quite high. But in certain cases when there is no symmetry in lattice, one would have to perform calculations for the complete lattice in 69 energy group, which would be arduous as mentioned before. Moreover, in order to perform assembly calculations, one needs to perform full cell calculation. This is possible only when one considers coarse mesh. But as seen in Section 2.3.2, the k_{eff} and CVR estimation were affected when the calculations were performed using libraries generated for fine mesh regions with SPH procedure. This implies that a modification in the editing module of code DRAGON should be implemented, such that the tracking of structure created using the `MRG:` module is possible for SPH calculation. Considering all the above constraints, an alternative way for gener-

ation of homogenized cross sections was developed, which is the Direct Cell Simulation (DCS).

DCS involves one step to generate the cross section library for SPM. The SPH procedure is performed between standard geometry and SPM in the coarse mesh form. One solves the transport equation in the exact CANDU-6 geometry with annular fuel pins (Figure 2.5(a)) using a 2-D collision probability technique and evaluates the fluxes in various regions of the lattice and the cell eigenvalue for various coolant conditions. Consequently, one uses the SPH technique with modified tracking module, to convert the annular fuel and clad region into a single square pin region (Figure 2.5(d)) and generate a library. This step is repeated for different coolant density conditions and a series of coolant density dependent cross section libraries are generated. Only homogeneous draining condition was simulated with the DCS. The CPU time needed to perform this calculation is about 15 minutes which is 8 times faster than the CPU time required for MSCS.

2.4.1 Validation of Direct Cell Simulation

Here we will present our validation results by comparing the multiplication factor k_{eff} and the change in reactivity $\Delta\rho$ resulting from total coolant voiding (see Section 1.3). It can be observed from the Table 2.2 that the k_{eff} compares well with the results obtained for the exact geometry. As one can see in Table 2.2 the two models (Exact and SPM coarse mesh) give similar eigenvalues with deviations reaching a maximum of 0.1 mk in the cooled cases which is better than last simulation (MSCS). The results thus obtained confirm that the coarse mesh cross section libraries generated by single step DCS are better than the coarse mesh calculation using the fine mesh MSCS library.

Table 2.2 Comparison of k_{eff} and $\Delta\rho$ for CANDU-6 lattice using DCS.

Coolant Density → (g/cm^3)	0.81212	0.60909	0.40606	0.20303	0.00100	$\Delta\rho$ (mk)
k_{eff} ↓	%100 Cooled	%25 Voided	%50 Voided	%75 Voided	%100 Voided	CVR
Exact Figure 2.5 (a)	1.1132	1.1180	1.1230	1.1281	1.1335	+16.0
SPM (coarse mesh) Figure 2.5 (d)	1.1133	1.1181	1.1230	1.1281	1.1335	+16.0
SPM (corners) Figure 2.8	1.1131	1.1179	1.1229	1.1280	1.1334	+16.0

2.4.2 Effect of Corners with XS Libraries Generated Using DCS

The effect of using a fine mesh in the Cartesian corners of the cell on the eigenvalue and CVR is evaluated. We used the same SPM configuration with nine annular-rectangular regions shown in Figure 2.8. We observed that when one considers corner discretization, the reduction in eigenvalue is of the order of 0.2 mk and the CVR does not change, as shown in Table 2.2. It was noted in MSCS, that the CVR reduced by about 1 mk when one considers either SPM coarse mesh or SPM with corner discretization. But in DCS, it is interesting to note that we obtain results identical for the SPM coarse mesh to that of exact geometry, and we can directly compare the effect of using a fine mesh in the corners of SPM with exact geometry.

2.4.3 The Change in Production and Destruction Rate

The relation between eigenvalue and production and destruction rate was shown in equation (1.45). We will now define certain terms in order to explain the effect of corner discretization on the eigenvalue. The change in production rate ΔP_R is defined as:

$$\Delta P_R = \left(\frac{P_R(\text{SPM}) - P_R(\text{SPM with corner discretization})}{P_R(\text{SPM with corner discretization})} \right) \times 100\% \qquad (2.2)$$

Similarly the change in destruction rate ΔD_R is defined as:

$$\Delta D_R = \left(\frac{D_R(\text{SPM}) - D_R(\text{SPM with corner discretization})}{D_R(\text{SPM with corner discretization})} \right) \times 100\% \qquad (2.3)$$

ΔP_R for **fully cooled state** for a CANDU-6 lattice was found to be 0.0001%, while the ΔD_R was found to be -0.0718%. This means that with corner discretization, there is a relative decrease in production rate, while there is a relative increase in rate of destruction. However the changes are so small that it has a very insignificant effect on the eigenvalue (about 0.2 mk).

It can be seen in equations (1.46) and (1.47) that the production rate and destruction rate are dependent on the flux shape in the system under consideration. In the present context, we will mainly focus on the flux shape in the moderator region. As mentioned earlier the moderator is split into eight annular rings and nine annular-rectangular regions. Figure 2.9 shows the regions chosen in the moderator for flux calculation. The center of each of the 17 regions are named A to Q, from inside to corner. It corresponds to the radius of each of the 17 regions.

The 69 energy group that represent energies between 10 MeV and 0.00001 eV is con-

densed into two groups with the cutoff energy at 4.0 eV. The plots of variation of fast and thermal flux with respect to the radius of each region are shown in Figures 2.10 and 2.11. It can be seen in Figure 2.10 that the fast flux reduces from inside to corner. It is interesting to note that there is clear change in shape due to discretization of the corner. Similarly it can be seen in Figure 2.11 that there is an increase in thermal flux from inside to the corner, having a parabolic shape with corner discretization, against that of a straight line when a single region is considered in the corner.

Another interesting observation is change in slope of fast and thermal fluxes close to the corner of the lattice. It can be seen in Figure 2.10, that there is an increase of fast flux (or positive slope) in the regions near to the corner (with the center of O, P and Q) and a decrease of thermal fluxes (or negative slope) in the same regions (see Figure 2.11). This is mainly due to the use of approximate boundary conditions at the external surfaces. By approximate boundary conditions we mean that the reflection is isotropic and a uniform angular distribution of the reflected angular flux is considered on the outer surfaces, independent of the incoming neutron direction. The fast flux coming out of the fuel region are highly energetic and have a sense of direction when it reaches the surface. When such a neutron is distributed isotropically at the surface due to boundary condition, it represents a sort of fast flux source at the boundary. Therefore an increase in fast flux is observed near the corner. In the case of thermal neutrons, the scattering to slow the neutrons affects its sense of direction. Hence when these neutrons reach the surface, the isotropic distribution acts in such a way that there is a sink of thermal neutrons. Hence a reduction is observed. This effect will vanish when one considers a specular boundary condition or when one considers a 2×2 assembly of cells where there is no boundary condition applied on inner surfaces between lattices (we will observe this behavior in section 3.1.2).

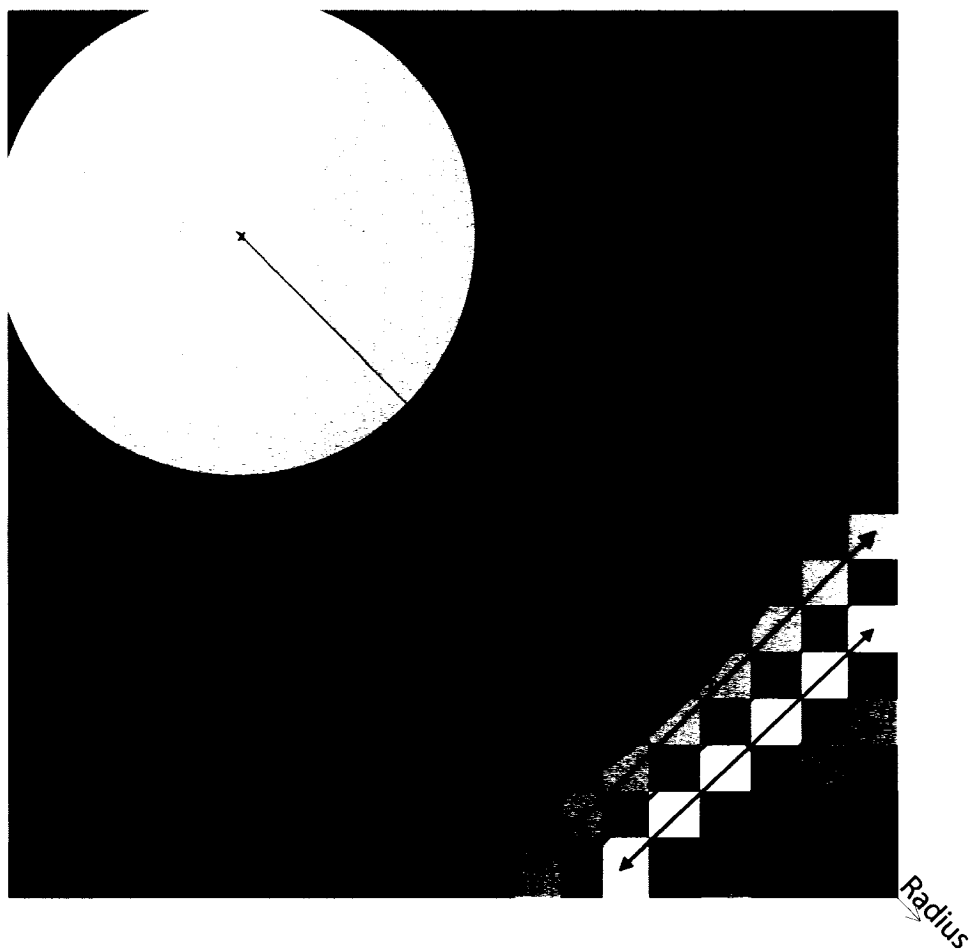

Figure 2.9 The center of regions in the moderator.

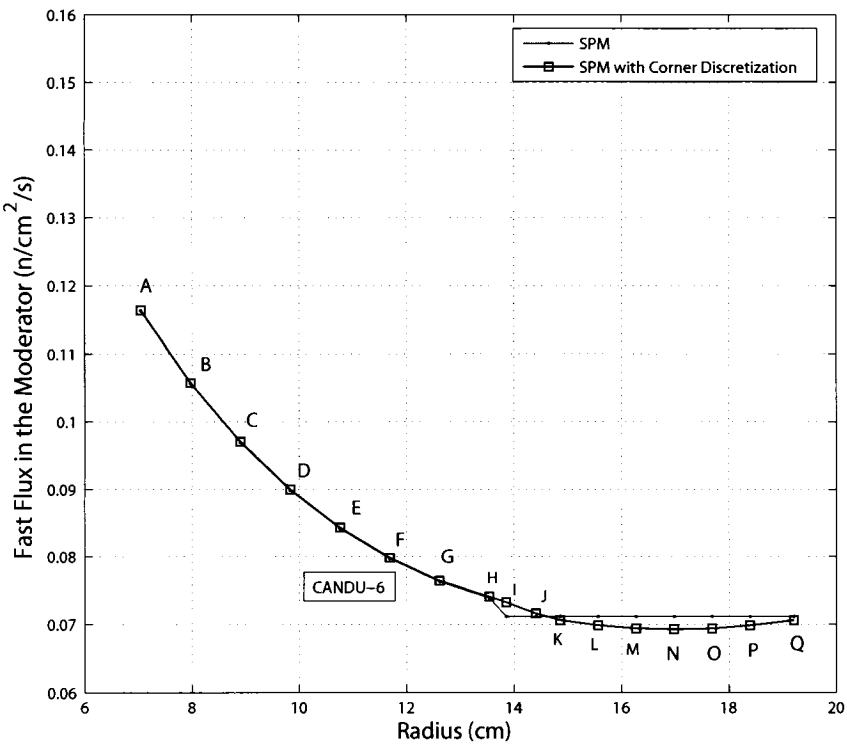

Figure 2.10 Fast flux in the moderator region of CANDU-6.

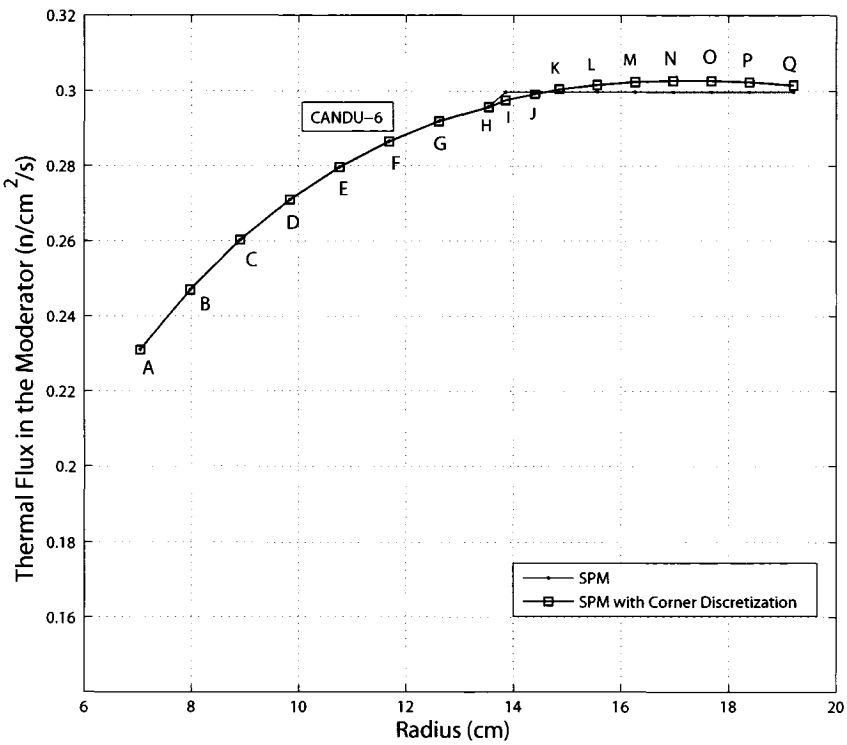

Figure 2.11 Thermal flux in the moderator region of CANDU-6.

2.4.4 Recommendations

For the DCS, the new SPH procedure generates better cross section library, when one directly considers coarse mesh from exact geometry. We would like to remind that, in the case of MSCS, the cross section libraries generated for fine mesh region was directly used for coarse mesh calculations without considering SPH procedure. Moreover, the time required for convergence for the DCS, was found to be drastically reduced due to reduction in number of regions. Also, coarse mesh results using DCS, matched well with that of the exact geometry. As we need to perform full cell calculations for lattices with no symmetry and for 2×2 assembly pattern, we will use the DCS to generate homogenized cross section library for the SPM for all future calculations.

2.5 Evolution of CANDU-6 Lattice Towards ACR-700

The following studies will focus on evaluation of CVR for ACR-700 type lattice using SPM. In order to achieve this goal, we will perform the evolution of CANDU-6 type of lattice to ACR-700 type in three steps. In the first step the lattice pitch will be reduced, maintaining the same configuration of pressure tube and calandria tube as that of CANDU-6. In the second step the calandria tube diameter will be increased. In the third step, the number of pins will be increased from 37 to 43, changing natural uranium to enriched uranium and changing the coolant from heavy water to light water, thereby obtaining an ACR-700 type lattice. For all the three steps, we estimated the CVR and have compared it with that obtained for the exact geometry.

2.5.1 The Effect of Reduction in Lattice Pitch

This section deals with the effect of reduction in the pitch of CANDU-6 type lattice on the eigenvalues and CVR. Lattice analysis was performed along the same lines as was done for original CANDU-6. The pitch is now reduced from 28.575 cm to 24.575 cm (see Figure 2.12(a)). Further reduction in lattice pitch showed that the system using CANDU-6 cluster becomes subcritical. By doing this study we can understand the impact of reduction in moderator volume on CVR. The moderator volume is reduced by 31.26% with respect to original CANDU-6 lattice. CANDU-6 lattice is designed such that it is well thermalized. But by reducing the lattice pitch, we are making the system slightly less moderated. As a result, there is hardening of the spectrum and the k_{eff} decreases. It would be interesting to estimate CVR for such a lattice. It was observed that (see the first line of Table 2.3 and Table 2.2) there is a reduction in k_{eff} of 38 mk from the original configuration of CANDU-6 lattice in the presence of coolant and a reduction of 40.5 mk in the absence of coolant. The CVR was estimated as +15 mk which is still positive but slightly lower than the CVR for the original CANDU-6 cluster.

SPM analysis was performed for the reduced lattice pitch along the same lines as was performed earlier for CANDU-6 lattice (see Section 2.2). The intersections along the X-axis and Y-axis remain the same as CANDU-6 lattice, as the number of fuel pins remain unchanged. We obtained a fine mesh with 2967 regions and 132 outer surfaces (see Figure 2.12 (b)). Quarter cell symmetry calculations could still be performed, as we have only reduced the lattice pitch without changing the fuel design. The number of regions and outer surfaces for this configuration was found to be 777 and 34, respectively. The SPH homogenization process thus generated 17 different mixtures in this case, as shown in Figure (2.12). As recommended earlier, we used the DCS method to generate the cross section library for the SPM analysis.

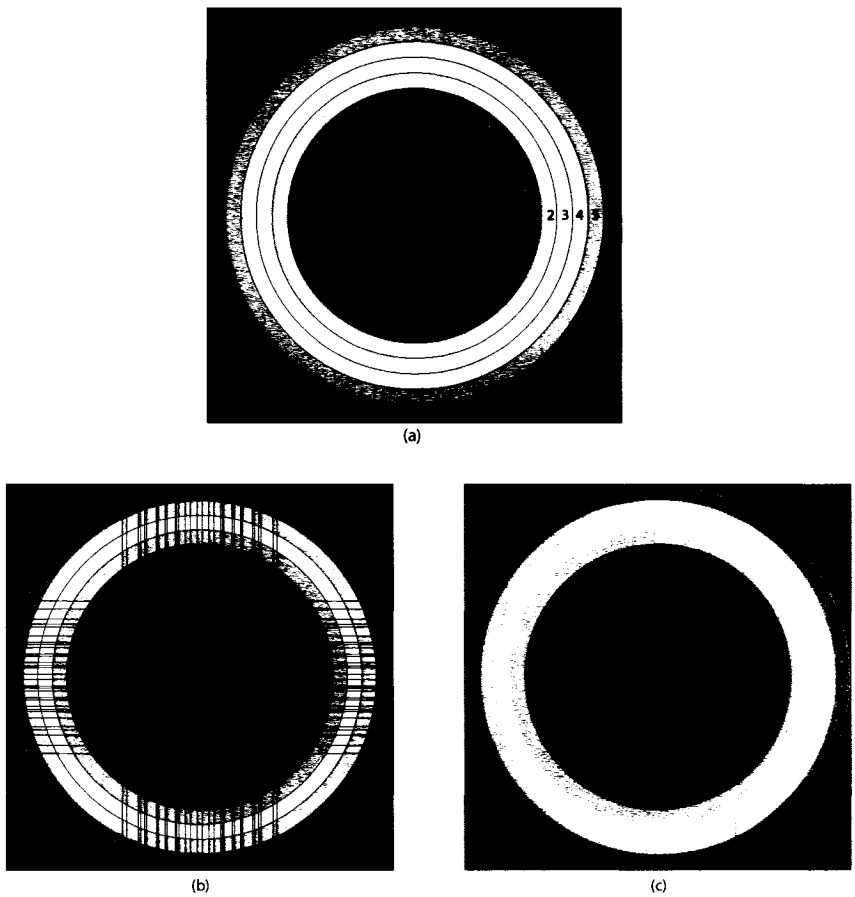

Figure 2.12 Reduced lattice pitch to 24.575 cm with six annular regions in moderator (a), SPM fine mesh (b) and SPM coarse mesh (c).

2.5.2 Direct Cell Simulation for Reduced Lattice Pitch

As explained earlier, DCS involves generation of cross section libraries in one step (see section 2.4). The SPH procedure is performed between standard geometry (Figure 2.12(a)) and SPM in the coarse mesh form (Figure 2.12(c)) and generate a library. This step is repeated for different coolant density conditions and a series of coolant density dependent cross section libraries are generated. Only CVR estimation under homogeneous draining conditions was considered. Here we will present our validation results by comparing the multiplication factor k_{eff} and the change in reactivity $\Delta\rho$ resulting from total coolant voiding (see Section 1.3). It can be observed from the Table 2.3 that the k_{eff} compares well with the results obtained for the exact geometry. As one can see in Table 2.3 the two models (Exact and SPM coarse mesh) give similar eigenvalues with deviations reaching a maximum of 0.1 mk in the cooled cases. The CVR estimated using Exact and SPM coarse mesh model match well as expected for SPH equivalence calculation.

MATLAB was used to create the geometry with corner discretization, in the same lines as mentioned earlier (see Section 2.3.3). We had 42 levels along Y-axis and in each level there were 46 distinct regions. As described earlier, the information corresponding to each region was converted from MATLAB to a form that is subsequently utilized by the `GEO:` module of DRAGON. The number of regions and outer surfaces was found to be 3685 and 180, respectively. Using the `MRG:` module, fine mesh regions were combined to obtain six annular regions in the moderator, seven regions of annular-rectangular form in each corner and three regions in the coolant. A total of 24 calculation regions were thus generated (Figure 2.13).

We observed that when one considers corner discretization, the reduction in eigenvalue is of the order of 0.1 mk and the CVR remains unchanged, as shown in Table 2.3. Thus there is no effect due to corner discretization for reduced lattice pitch, an observation

Table 2.3 Comparison of k_{eff} and $\Delta\rho$ for CANDU-6 with reduced lattice pitch (24.575 cm) using DCS.

Coolant Density → (g/cm^3)	0.81212	0.60909	0.40606	0.20303	0.00100	$\Delta\rho$ (mk)
k_{eff} ↓	%100 Cooled	%25 Voided	%50 Voided	%75 Voided	%100 Voided	CVR
Exact Figure 2.12 (a)	1.0753	1.0793	1.0836	1.0881	1.0930	+15.0
SPM (coarse mesh) Figure 2.12 (c)	1.0753	1.0793	1.0835	1.0881	1.0929	+15.0
SPM (corners) Figure 2.13	1.0752	1.0792	1.0835	1.0880	1.0929	+15.0

similar to that of CANDU-6 lattice.

As explained in Section 2.4.3, the effect of corner discretization can be explained in terms of the change in production and destruction rate. In the fully cooled state, the relative production rate reduced by 0.0011%, while the relative destruction rate increased by 0.0368%, when one considered corner discretization. When compared to that of CANDU-6, the relative destruction rate was found to be reduced almost by half. As a result, the eigenvalue is affected by only 0.1 mk against the value of 0.2 mk observed for the CANDU-6 lattice.

It can be seen in Figures 2.14 and 2.15, that the fast flux has a similar shape as that observed in CANDU-6. However the magnitude of fast flux is seen to increase and the thermal flux is slightly higher initially, but decreases towards the corner. This is due to flux normalization and spectral hardening due to reduced moderator volume. The flux normalization is done in such a way that one neutron is produced. The main con-

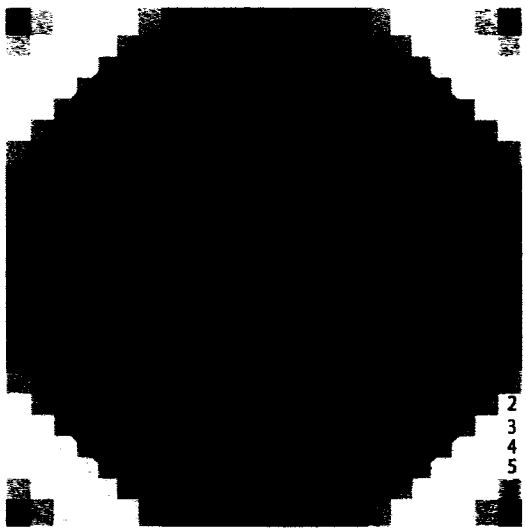

Figure 2.13 Seven annular-rectangular regions for each Cartesian corner of CANDU-6 with reduced lattice pitch (24.575 cm).

tribution comes from the thermal flux in the fuel because of high fission cross section at lower energies in comparison to that of high energies. Even though the fast neutron flux is increased in magnitude, it is the slight change in thermal flux which dictates the multiplication factor of the system and therefore the normalization.

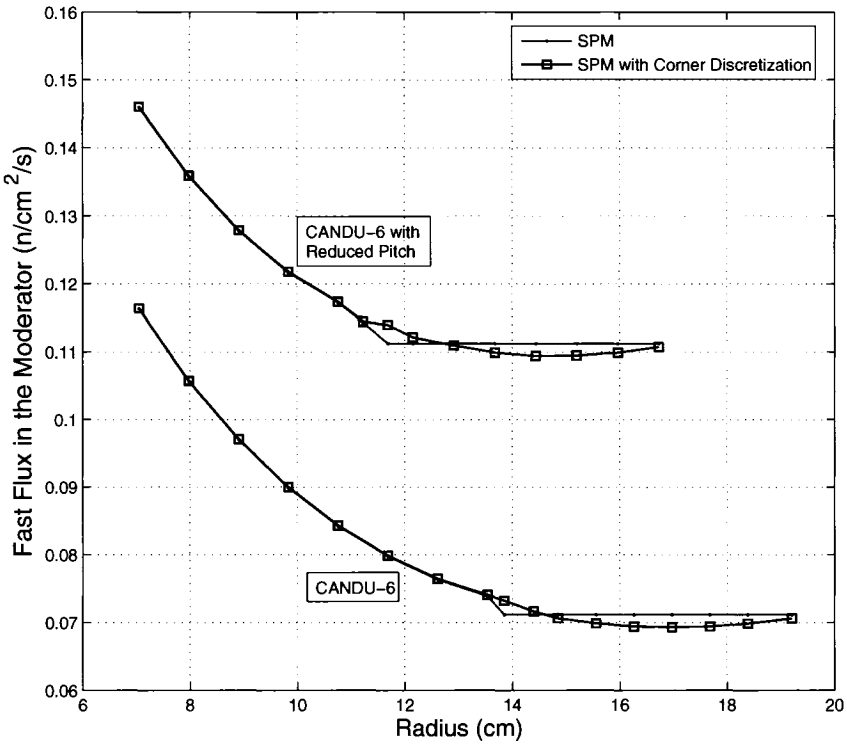

Figure 2.14 Fast flux in the moderator regions of CANDU-6 and CANDU-6 with reduced pitch.

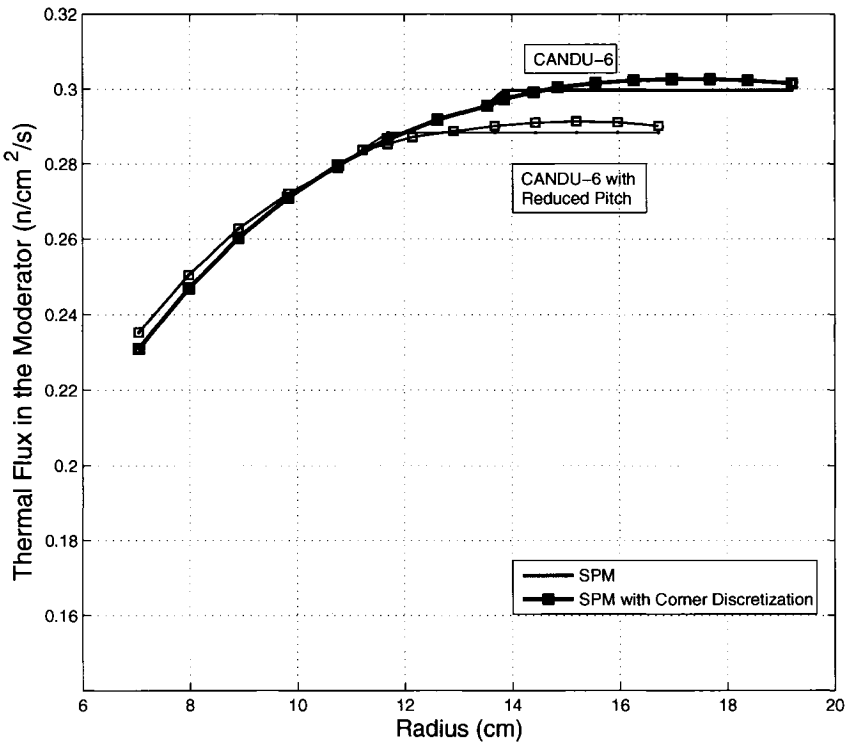

Figure 2.15 Thermal flux in the moderator regions of CANDU-6 and CANDU-6 with reduced pitch.

2.5.3 Effect of Increase in Calandria Tube Diameter

In the second step of evolution towards ACR-700 lattice, we will now consider the effect of increasing the calandria tube diameter along with reduced lattice pitch. In this study, the calandria tube inner/outer diameter is increased from 12.8956/13.175 to 14.8956/15.175 cm (Figure 2.16(a)) so as to almost match the calandria tube dimensions of the proposed ACR-700 lattice [Love, 2002, Ovanes, 2002]. The CANDU-6 configuration, including the fuel assembly and the pressure tube, remain unchanged.

By doing this analysis we can understand the impact of further reduction in moderator volume on CVR and eigenvalue. By reducing the lattice pitch and increasing the calandria tube diameter, the moderator volume is reduced by 37.87% with respect to that of original CANDU-6 lattice. We are thus making the system even less moderated in comparison to the situation of reduction in lattice pitch. As a result, there is a further hardening of the spectrum, and the k_{eff} reduces again (see the first line of Table 2.4 and Table 2.2). It was observed that there is a reduction in k_{eff} of 52.6 mk from the original configuration of CANDU-6 lattice in the presence of coolant and a reduction of 56.3 mk in the absence of coolant. The CVR was estimated as +14.5 mk which is still positive but lower than the CVR for original CANDU-6 cluster.

SPM was used to perform analysis for the present configuration of reduced lattice pitch plus increased calandria diameter along the same lines as was performed earlier for CANDU-6 lattice. We obtained fine mesh with 2839 regions and 132 outer surfaces (see Figure 2.16 (b)), that reduced to 744 and 34, respectively when quarter cell symmetry was used. Eventually, the SPH homogenization process generated 16 different mixtures in this case, as shown in Figure (2.16).

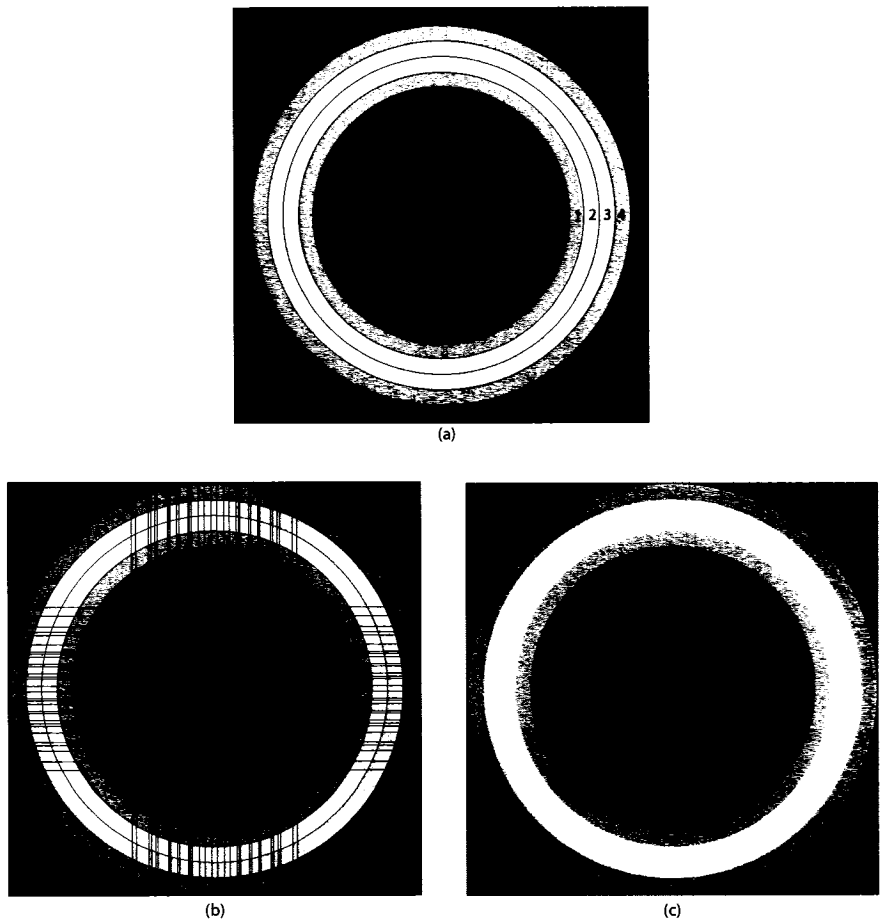

Figure 2.16 Reduced lattice pitch and increase calandria tube diameter with five annular regions in moderator (a), SPM fine mesh (b) and SPM coarse mesh (c).

2.5.4 Direct Cell Simulation for Increase Calandria Tube Diameter

As explained earlier, DCS involves generation of cross section libraries in one step (see section 2.4). The SPH procedure is performed between standard geometry (Figure 2.16(a)) and SPM in the coarse mesh form (Figure 2.16(c)) and generate a library. This step is repeated for different coolant density conditions and a series of coolant density dependent cross section libraries are generated. CVR estimation under homogeneous draining conditions was only considered. Here we will present our validation results by comparing the multiplication factor k_{eff} and the change in reactivity $\Delta\rho$ resulting from total coolant voiding (see Section 1.3). A comparison of k_{eff} in Table 2.4 indicates that the results using coarse mesh match well with the results obtained for exact geometry. The value of CVR also remains unchanged.

Table 2.4 Comparison of k_{eff} and $\Delta\rho$ for CANDU-6 with reduced lattice pitch and increase calandria tube diameter using DCS.

Coolant Density → (g/cm^3)	0.81212	0.60909	0.40606	0.20303	0.00100	$\Delta\rho$ (mk)
k_{eff} ↓	%100 Cooled	%25 Voided	%50 Voided	%75 Voided	%100 Voided	CVR
Exact Figure 2.16 (a)	1.0606	1.0643	1.0683	1.0726	1.0772	+14.5
SPM (coarse mesh) Figure 2.16 (c)	1.0606	1.0643	1.0682	1.0725	1.0772	+14.5
SPM (corners) Figure 2.17	1.0593	1.0630	1.0669	1.0712	1.0759	+14.5

The geometry with corner discretization was created using MATLAB in the same lines as mentioned earlier. We had 42 levels along Y-axis and in each level there were 46

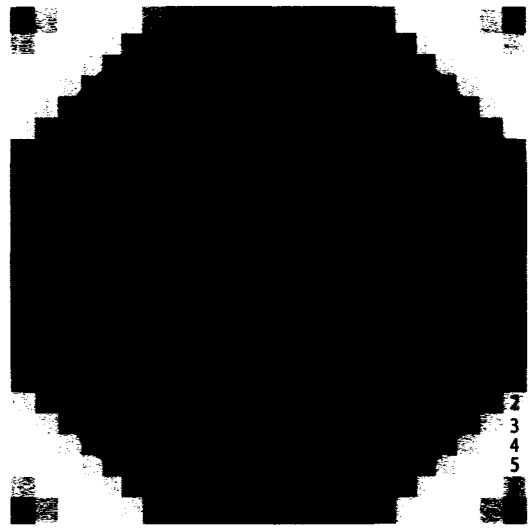

Figure 2.17 Cartesian corner discretization in reduced lattice pitch plus increase calandria tube diameter.

distinct regions. The number of regions and outer surfaces increased to 3557 and 180, respectively. Using MRG: module, we obtained five annular regions in the moderator, seven regions of annular-rectangular form in each corner and three regions in the coolant. A total of 23 calculation regions were thus generated (Figure 2.17).

We observed that when one considers corner discretization, there is an offset of about 1.3 mk for all the coolant states (see Table 2.4). This clearly shows that by discretizing the corner, there is a reduction in k_{eff}. This lattice being less moderated, leads to the situation where the flux shape will change quite drastically close to the corners. The reason can be explained in terms of the change in production and destruction rate of neutrons as mentioned in Section 2.4.3. Here for fully cooled state, the relative production rate was found to increase by 0.0002%, while the relative destruction rate increased by 0.3804%. When compared to that of CANDU-6, the relative destruction rate was found to be increased by almost six times. As a result, the eigenvalue is reduced by 1.3 mk against that

of 0.2 mk for CANDU-6 lattice. This behavior can be noticed only when one dicretizes the corners, which is made possible using this model. However, as mentioned earlier, since the offset is observed to be identical in fully cooled and voided states, the CVR estimated does not change with the use of fine mesh discretization in the corner. So it is concluded that in order to estimate CVR for assembly calculation in a 2×2 pattern, a coarse mesh calculation would suffice.

It can be seen in Figures 2.18 and 2.19, that the flux shapes for fast and thermal neutrons are similar to those which were observed for the case of reduced pitch. It was however noted that the attenuation of fast neutrons, which is the difference in number of fast neutrons close to fuel to that in the corner, decreases. It means that lower number of fast neutrons have been moderated and the spectrum is even harder than before.

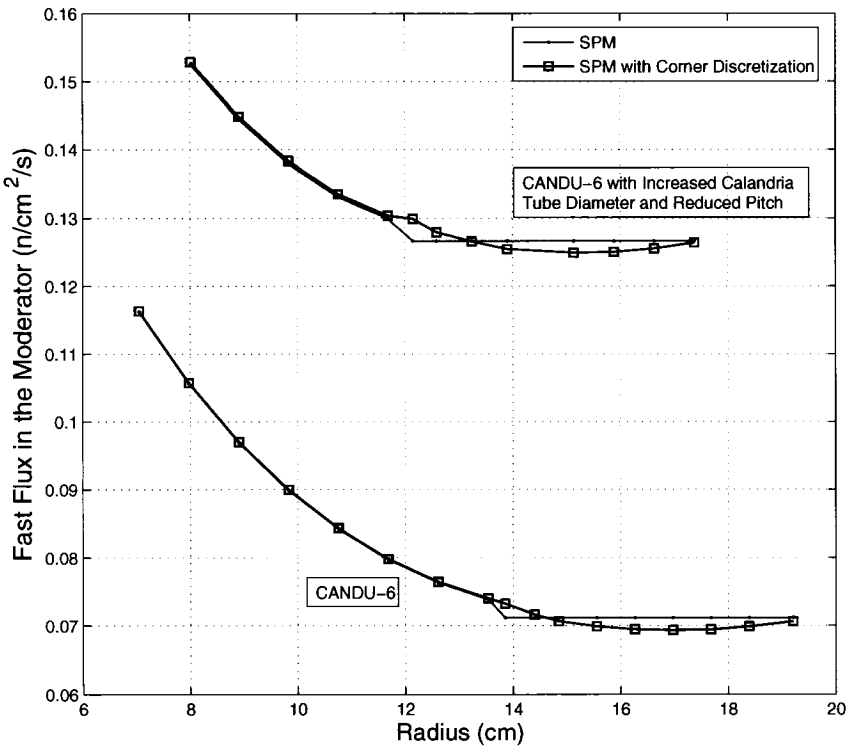

Figure 2.18 Fast flux in the moderator regions of CANDU-6 and CANDU-6 with increased calandria tube diameter and reduced pitch.

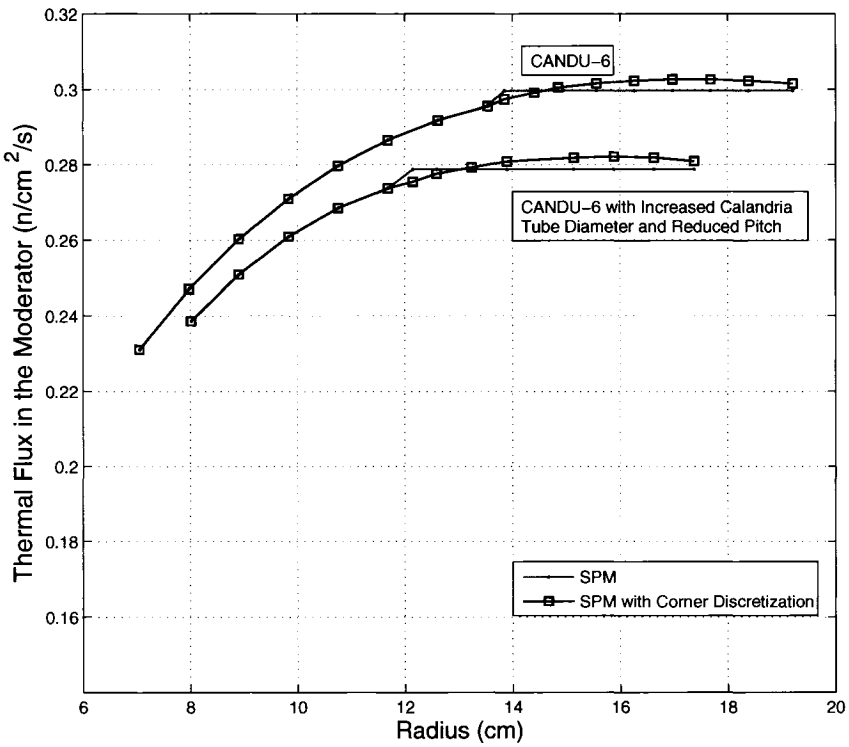

Figure 2.19 Thermal flux in the moderator regions of CANDU-6 and CANDU-6 with increased calandria tube diameter and reduced pitch.

2.6 ACR-700 Design

In the previous sections, we had mentioned the two major steps in evolution of CANDU-6 fuel into ACR-700 type fuel [Ovanes, 2002, Love, 2002]. The third step would be the increase of fuel pins from 37 to 43 and the use of enriched uranium instead of natural uranium. Another important aspect is the use of light water as coolant instead of heavy water. The following will describe the next generation CANDU reactor fuel. Appendix-II gives the physics aspects taken into consideration for the design of fuel for next generation reactors. There is also a comparison of salient engineering details of the two CANDU reactor systems, CANDU-6 and ACR-700.

2.6.1 Standard ACR-700 Geometry

The typical ACR-700 cell (Figure 2.20 (a)) is a 43 element rod cluster fuelled with slightly enriched uranium oxide (2%) and cladded with zircalloy. The central pin alone is made of natural uranium and is mixed with Dysprosium (4.6%). The fuel assemblies are located inside a pressure tube made of zirconium containing light water coolant. This pressure tube is separated by a cover gas from the zircalloy calandria tube which is immersed in a heavy water moderator. The square lattice pitch in a typical ACR-700 core is 22 cm. In this standard geometry, four fuel rings, containing respectively 1, 7, 14 and 21 fuel pins, are considered. The pitch circle radius of each ring are 0.0 cm, 1.734 cm, 3.075 cm and 4.384 cm respectively. The fuel pellet radius in the first and second ring are 0.627 cm and the thickness of its sheathing is 0.048 cm and for third and fourth ring are 0.533 cm and thickness of its sheathing is 0.042 cm. The effective density of the fuel is 10.12 g/cm^3 for the first and second ring while a value of 9.825 g/cm^3 is used for the third and fourth ring. The pressure tube radius is 5.168878 cm and its thickness is 0.50 cm. The calandria tube radius is 7.5 cm and its thickness is 0.3 cm. The gap

between pressure tube and calandria tube is filled with a carbon dioxide cover gas and the thickness of gap is 1.7311 cm. Heavy water moderator fills the region exterior to the calandria tube and within the square lattice pitch of 22 cm.

The coolant region was divided into four annular rings. The first ring contains the central fuel pin, while the second, third and fourth rings contain 7, 14 and 21 fuel pins respectively. The moderator region was divided into 4 regions, including 3 annular rings (with 1.0 cm thickness) and a final annular/Cartesian region. The ACR-700 lattice calculations were found to be very sensitive on the number of discretization per ring. A parametric study was performed in the cooled and voided case with different coolant and moderator discretization. For the transport calculation in order to ensure spatial convergence of the flux, each ring of the coolant was divided into 6 and 12 fine regions. For each fine coolant discretization, the moderator ring was divided into 1, 3 and 6 fine regions. For each coolant and moderator discretization, we studied the effect of two different track densities, i.e. 75 and 150 per cm. Subsequently for each coolant, moderator and track density, we varied the angular quadrature parameter between 11, 41, 81 and 111. The k_{eff} results are shown in the Tables 2.5 and 2.6.

We concluded that for 12 fine regions in each ring of coolant, three fine regions in each ring of moderator, track density of 75 per cm and an angular quadrature of 41 would be optimum for CVR studies in an ACR-700 cell (Figure 2.20 (b)). Each fuel pin also was subdivided into three regions. As a result, the total number of regions and outer surfaces in the reference ACR-700 geometry were 66 and 4 respectively.

Fuel temperature in all rings is 960.0 $^{\circ}K$ and for its sheathing is 573.6 $^{\circ}K$. The temperatures of coolant and pressure tube are 573.6 $^{\circ}K$ and 573.0 $^{\circ}K$ while the temperature of carbon dioxide cover gas and calandria tube is 353.0 $^{\circ}K$. The temperature of moderator is 323.6 $^{\circ}K$.

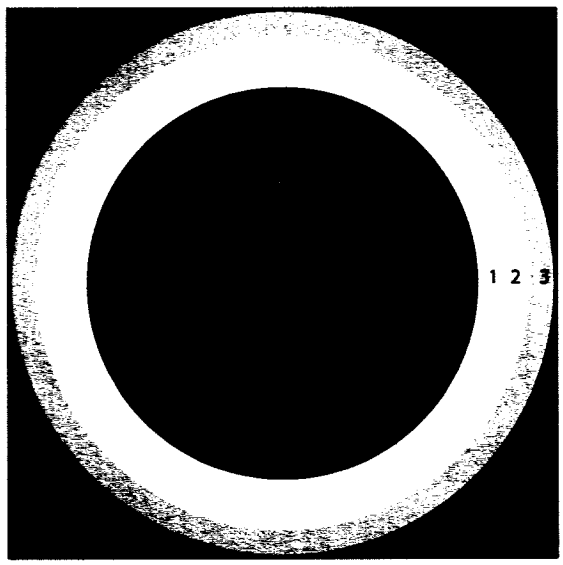

(a)

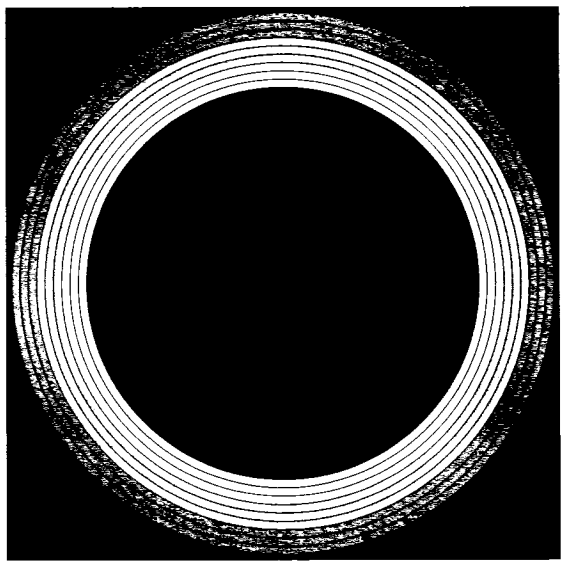

(b)

Figure 2.20 Standard ACR-700 geometry (a) and with chosen discretization (b).

Table 2.5 Comparison of the eigenvalues for ACR-700 with 6 discretized region in each coolant ring and different discretization in each moderator ring along with different track densities and angles.

Coolant splitting	Moderator splitting	Density of track	Number of angle	100% Cooled $k_{eff} \downarrow$	100% Voided $k_{eff} \downarrow$	CVR $\Delta\rho$ (mk)
6	1	75	11	1.234807	1.238774	2.5934
6	1	75	41	1.234817	1.238823	2.6188
6	1	75	81	1.234823	1.238824	2.6155
6	1	75	111	1.234822	1.238823	2.6155
6	1	150	11	1.234807	1.238796	2.6077
6	1	150	41	1.234821	1.238832	2.6220
6	1	150	81	1.234824	1.238834	2.6214
6	1	150	111	1.234823	1.238834	2.6220
6	3	75	11	1.234893	1.238894	2.6152
6	3	75	41	1.234903	1.238944	2.6412
6	3	75	81	1.234908	1.238945	2.6386
6	3	75	111	1.234908	1.238943	2.6373
6	3	150	11	1.234893	1.238916	2.6295
6	3	150	41	1.234907	1.238952	2.6438
6	3	150	81	1.234909	1.238954	2.6438
6	3	150	111	1.234908	1.238954	2.6445
6	6	75	11	1.234904	1.238909	2.6178
6	6	75	41	1.234914	1.238959	2.6438
6	6	75	81	1.234920	1.238960	2.6405
6	6	75	111	1.234919	1.238958	2.6398
6	6	150	11	1.234904	1.238931	2.6321
6	6	150	41	1.234918	1.238967	2.6464
6	6	150	81	1.234921	1.238969	2.6457
6	6	150	111	1.234920	1.238969	2.6464

Table 2.6 Comparison of the eigenvalues for ACR-700 with 12 discretized region in each coolant ring and different discretization in each moderator ring along with different track densities and angles.

Coolant splitting	Moderator splitting	Density of track	Number of angle	100% Cooled $k_{eff} \downarrow$	100% Voided $k_{eff} \downarrow$	CVR $\Delta\rho$ (mk)
12	1	75	11	1.234021	1.238774	3.1092
12	1	75	41	1.234031	1.238823	3.1346
12	1	75	81	1.234037	1.238825	3.1320
12	1	75	111	1.234036	1.238823	3.1313
12	1	150	11	1.234022	1.238795	3.1223
12	1	150	41	1.234036	1.238832	3.1372
12	1	150	81	1.234039	1.238834	3.1365
12	1	150	111	1.234038	1.238834	3.1372
12	3	75	11	1.234109	1.238894	3.1296
12	**3**	**75**	**41**	**1.234118**	**1.238944**	**3.1563**
12	3	75	81	1.234124	1.238945	3.1530
12	3	75	111	1.234124	1.238943	3.1517
12	3	150	11	1.234110	1.238916	3.1433
12	3	150	41	1.234124	1.238952	3.1576
12	3	150	81	1.234126	1.238954	3.1576
12	3	150	111	1.234125	1.238955	3.1589
12	6	75	11	1.234121	1.238909	3.1315
12	6	75	41	1.234130	1.238959	3.1582
12	6	75	81	1.234136	1.238960	3.1549
12	6	75	111	1.234135	1.238958	3.1543
12	6	150	11	1.234121	1.238931	3.1459
12	6	150	41	1.234136	1.238967	3.1595
12	6	150	81	1.234138	1.238969	3.1595
12	6	150	111	1.234137	1.238969	3.1601

2.6.2 Square Pin Model for ACR-700

In this section, an approximate geometry for a ACR-700 cell will be designed. By creation of such model, a 2×2 assembly of ACR-700 cell can be generated. This model has also the ability to discretize Cartesian corner of lattice, finely. The Square Pin Model (SPM) that was considered for our simulations consists of replacing each annular fuel pin and its sheathing by a homogenized square pin (see Figure 2.21 (b)). In this model, the total volume of each square pin (fuel plus sheathing) is selected to be identical to the volume of the original annular pins and subsequently conserving the reaction rates between the two geometries by SPH technique. The location of the center of each of the pins in the SPM, except two pins in the second ring, is identical to that found in the exact geometry (see Figure 2.21 (a)).

In fact after creating the squares in the SPM, two pins in the top and bottom of second ring were found to be overlapping with the other pins. In order to avoid these overlaps, the central location of these two pins were shifted by 2 mm towards the center of the fuel assembly, as shown in Figure 2.21 (a). As in the case of CANDU-6, the SPM was designed using MATLAB for the ACR-700 cell with square pins.

The intersections along the X-axis and Y-axis are now different from that of CANDU-6 lattice, as the number of fuel pins have increased from 37 to 43. Using the same procedure as (see Section 2.2) we obtained 58 levels on Y-axis and in each level there were 45 distinct regions. We obtained fine mesh with 4464 regions and 210 outer surfaces. Each region that has been created for the SPM, is subsequently associated with its corresponding mixture. The numbering of mixture is done from left hand side to right hand side of each level and from inner circle to outer circle. This procedure is followed for each level from bottom to top. The mixtures considered for each region, other than the fuel, of SPM is the same as the ACR-700 cell. The mixtures in the square fuel pins are made by merging the fuel and sheathing of the original ACR-700 cell. Hence, four different mix-

tures were considered for each square fuel pin in each ring respectively. Using the above procedure, one obtains 4464 spatial regions and 210 outer surfaces respectively for the SPM. Afterwards, all the information corresponding to each region were converted from MATLAB to a form that is subsequently utilized by the GEO: module of DRAGON.

Because of the large number of regions involved, analyzing the square pin model is expensive from a computer resources point of view; therefore, we used half cell symmetry along the Y-axis for this approximate geometry and the number of regions and outer surfaces was thus reduced to 2265 and 106 respectively. It was attempted to perform the MSCS for ACR-700 lattice in 69 energy groups for half symmetry. We however found that the CP matrix was too huge to be handled. Therefore we decided to perform only the DCS of SPM for ACR-700 lattice. The coarse mesh model produced in this work is presented in Figure 2.22(a) and contains 15 flux regions. The regions were combined in such a way as to reproduce the four moderator and four coolant regions considered in the exact model. A single pressure tube, calandria tube and gap region was also generated in addition to four different square fuel regions.

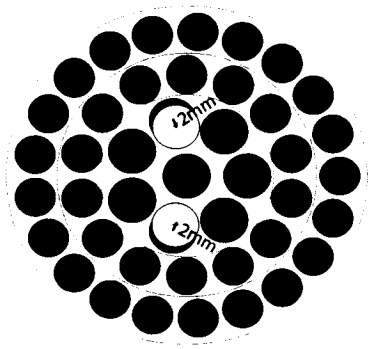

(a)

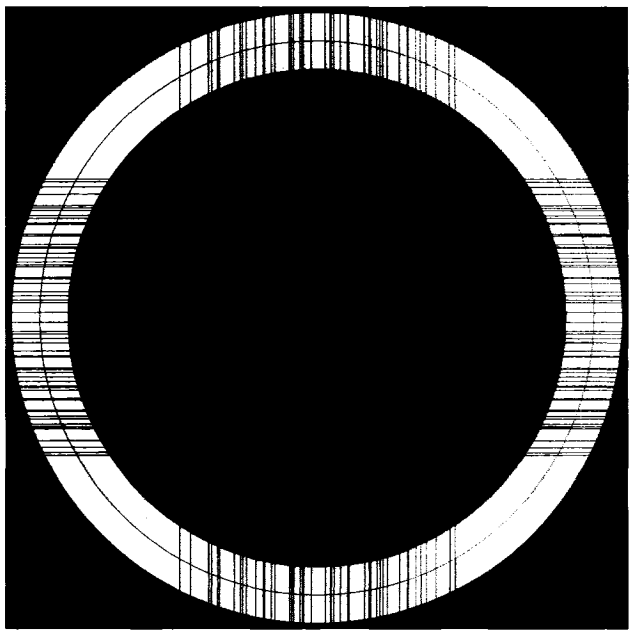

(b)

Figure 2.21 Pins displacement in the pressure tube (a) and SPM fine mesh (b).

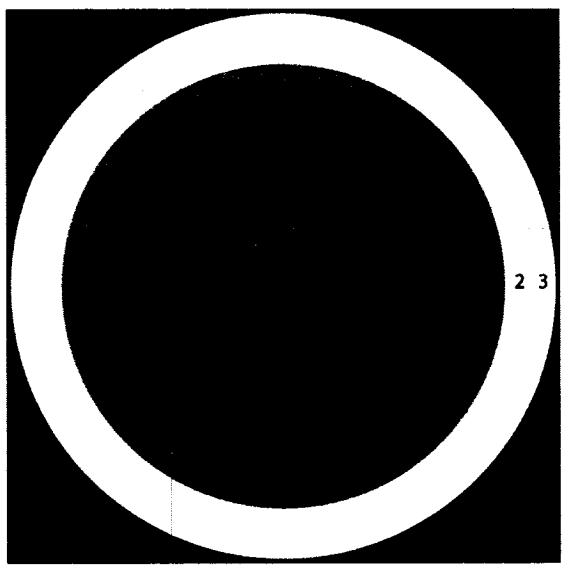

(a)

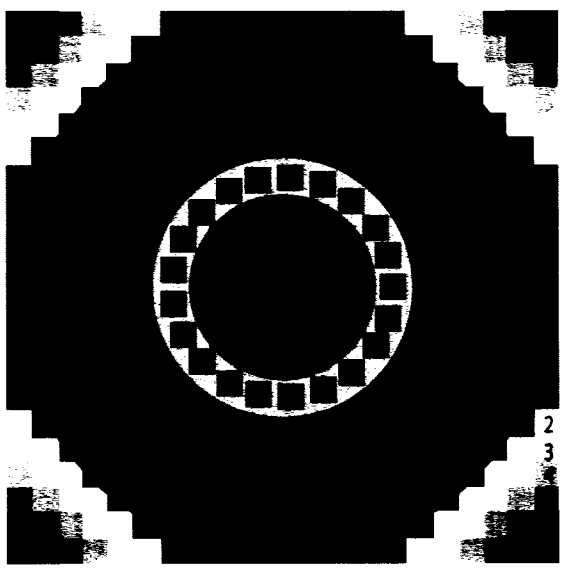

(b)

Figure 2.22 SPM coarse mesh (a) and with corner discretization (b).

2.6.3 Direct Cell Simulation for ACR-700

Direct Cell Simulation (DCS) involves one step to generate the cross section library for SPM (see section 2.4). The SPH procedure is performed between standard geometry and SPM in the coarse mesh form. One solves the transport equation in the exact ACR-700 geometry with annular fuel pins (Figure 2.20(b)) using a 2-D collision probability technique and evaluates the fluxes in various regions of the lattice and the cell eigenvalue for various coolant conditions. Consequently, one uses the SPH technique to convert the annular fuel and clad region into a single square pin region (Figure 2.22(a)) and generate a library. This step is repeated for different coolant density conditions and a series of coolant density dependent cross section libraries are generated. Only the homogeneous draining conditions were simulated for ACR-700 lattice. It was done by reducing the heavy water density uniformly for all the four rings in the coolant region. The reference coolant density was chosen to be 0.8 g/cm^3. The density of the coolant is subsequently reduced uniformly in four discrete steps, i.e. 25% void (0.6 g/cm^3), 50% void (0.4 g/cm^3), 75% void (0.2 g/cm^3) and 100% void (0.001 g/cm^3). These libraries will be used for further simulation associated with corner discretization on the single cell as well as for all the cases in the assembly calculations. The CPU time needed to perform calculation for each voided state is about 110 minutes.

2.6.4 Improvement in Convergence of SPH Iteration Process

An important observation was made during the SPH iteration process which plays an important role in the SPM under development. The SPH factors are calculated for a particular mixture and at a particular group at each iteration. The relative error in SPH factors for each mixture and group, between two successive iterations, is found using the Formula (2.4). Of these errors, the maximum is found using Equation (2.5). This is compared with the convergence criteria. If the criteria is not met, next iteration process is

carried out. It was however noticed that the error reduced initially, but began to increase, as the iteration process proceeded, as shown in Figure 2.23. After a certain number of iterations, the error began to decrease. It was thus found that if convergence is based on Equation (2.5), it would need at least 145 iterations before which we could consider that the process has converged. Also, it was consuming a lot of time (200 minute). So an alternate equation was considered for convergence. Equation 2.6, is essentially the root mean square value of error in all mixtures and all groups. The error thus estimated was compared with that of the convergence criteria, instead of Equation (2.5). It was found that this modification made the iteration process converge more quickly, i.e., after 87 iterations as shown in Figure 2.23. We thus recommend that this error estimation procedure be followed for SPH iteration process.

$$\Delta\mu_g^i(k) = \left[\frac{\mu_g^i(k) - \mu_g^i(k-1)}{\mu_g^i(k)}\right] \tag{2.4}$$

$$\Delta\mu_m(k) = \max \mid \Delta\mu_g^i(k) \mid \tag{2.5}$$

$$\Delta\mu_a(k) = \sqrt{\frac{\sum_i \sum_g \left[\Delta\mu_g^i(k)\right]^2}{N_i N_g}} \tag{2.6}$$

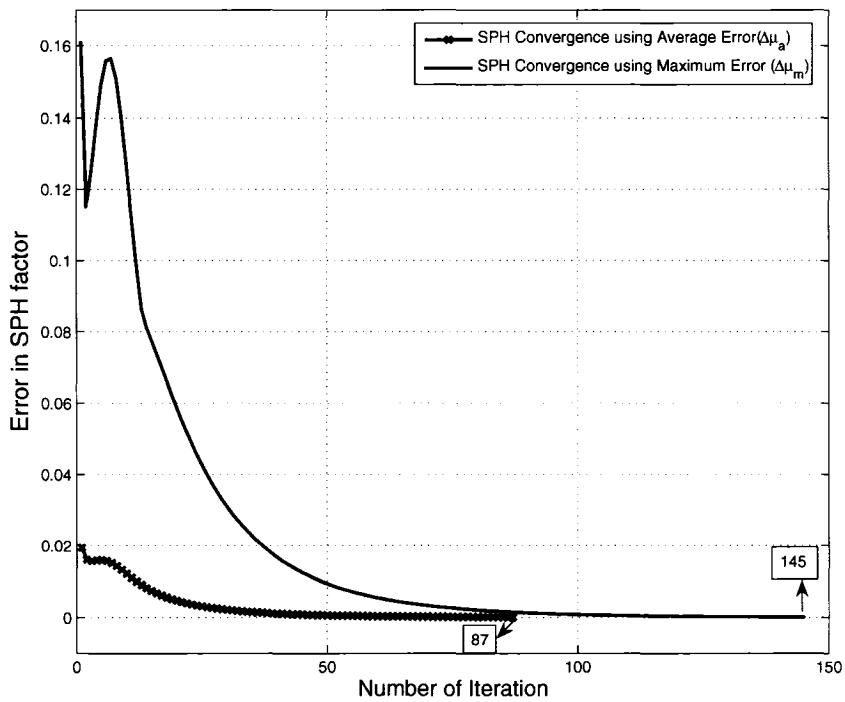

Figure 2.23 Error in SPH Convergence.

2.6.5 Validation of Direct Cell Simulation for ACR-700

In this section we will present the validation of DCS results, by comparing the multiplication factor k_{eff} and the change in reactivity $\Delta\rho$ resulting from total coolant voiding, with the exact modelling of ACR-700 (see Section 1.3). It was observed that the CVR estimated using the exact model was +3.1 mk. The comparison of k_{eff} and CVR using SPM with respect to exact model is provided in Table 2.7. It can be observed that when DCS is performed between exact geometry and SPM coarse mesh, the k_{eff} matches exactly for all the coolant states. Hence the CVR estimated using the SPM also remains unchanged in comparison to the exact model.

Table 2.7 Comparison of k_{eff} and $\Delta\rho$ for ACR-700 using DCS.

Coolant Density → (g/cm^3)	0.800	0.600	0.400	0.200	0.001	$\Delta\rho$ (mk)
k_{eff} ↓	%100 Cooled	%25 Voided	%50 Voided	%75 Voided	%100 Voided	CVR
Exact Figure 2.20 (b)	1.2341	1.2347	1.2348	1.2353	1.2389	+3.1
SPM (coarse mesh) Figure 2.22 (a)	1.2341	1.2347	1.2348	1.2353	1.2389	+3.1
SPM (corners) Figure 2.22 (b)	1.2340	1.2346	1.2348	1.2352	1.2388	+3.1

As mentioned earlier (see Appendix-I), Dysprosium plays a crucial role in affecting the magnitude of CVR when there is complete coolant voiding. In order to study the effect of removal of dysprosium, and to test the validity of SPM, we performed a calculation where the central pin does not have any burnable absorber. It was thus replaced with pure natural uranium pin. It was observed that the CVR increases by 10 mk, which substantiates the earlier claim (see Table 2.8).

2.6.6 Effect of Corners in ACR-700

MATLAB was used to create the geometry with corner discretization, in the same lines as mentioned in section 2.3.3. There were a total of 68 levels in the Y-axis and in each level, 55 distinct regions were obtained. The number of regions and outer surfaces increased to 5742 and 259, respectively. Finally, fine mesh regions that are assumed to possess identical fluxes were combined to obtain three annular regions in the moderator, seven regions of annular-rectangular form in each corner and four regions in the coolant. A

Table 2.8 Comparison of k_{eff} and $\Delta\rho$ for ACR-700 without Dysprosium and using DCS.

Coolant Density → (g/cm^3)	0.800	0.600	0.400	0.200	0.001	$\Delta\rho$ (mk)
k_{eff} ↓	%100 Cooled	%25 Voided	%50 Voided	%75 Voided	%100 Voided	CVR
Exact Figure 2.20 (b)	1.2847	1.2875	1.2901	1.2946	1.3066	+13.0
SPM (coarse mesh) Figure 2.22 (a)	1.2847	1.2874	1.2900	1.2946	1.3066	+13.0
SPM (corners) Figure 2.22 (b)	1.2846	1.2874	1.2900	1.2945	1.3065	+13.0

total of 21 calculation regions were generated (see Figure 2.22 (b)). Afterwards, all the information corresponding to each region were converted from MATLAB to a format that is subsequently used by the GEO: module of DRAGON.

We observed that when one considers corner discretization, the reduction in eigenvalue is of the order of 0.1 mk and the CVR remains unchanged, as shown in Table 2.7. It is interesting to note that the results obtained using the fine mesh discretization in the Cartesian corners is similar to that obtained using a coarse mesh discretization. Similar such observation was made for the lattice without dysprosium in the central pin, as shown in Table 2.8.

As explained in Section 2.4.3, the effect of corner discretization can be explained in terms of the change in production and destruction rate. In the fully cooled state, the relative production rate remained almost the same, while the relative destruction rate increased by 0.0097%, when one considered corner discretization. Since the change in relative production and destruction rate is small, the eigenvalue is affected by only 0.1

mk. Hence, we can conclude that for ACR-700 (with or without Dysprosium), SPM calculation without corner discretization is adequate.

It can be seen in Figure 2.24 that the magnitude of fast flux is lower than that of CANDU-6 with reduced lattice pitch and increased calandria tube. It is however higher than that of exact CANDU-6 lattice. The flux shape is almost flat, which means that the change in fast neutron flux is minimal in comparison to other two cases. It can be seen in Figure 2.25, that the magnitude of the thermal flux is the lowest when compared to the other two cases. The thermal and fast fluxes however show a parabolic shape when the corner is discretized.

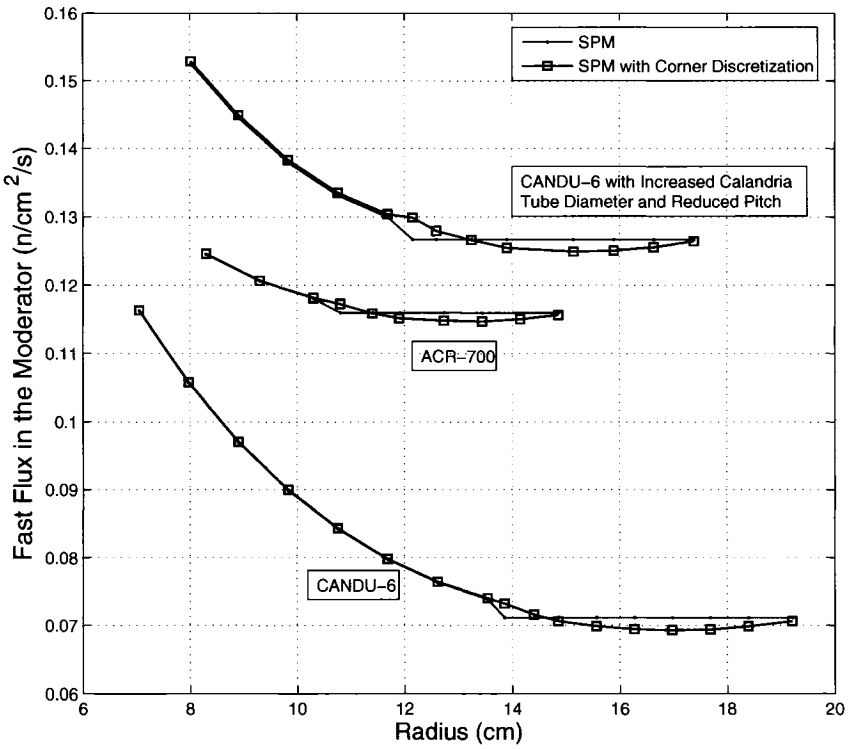

Figure 2.24 Fast flux in the moderator regions of ACR-700, CANDU-6 and CANDU-6 with increased calandria tube diameter and reduced pitch.

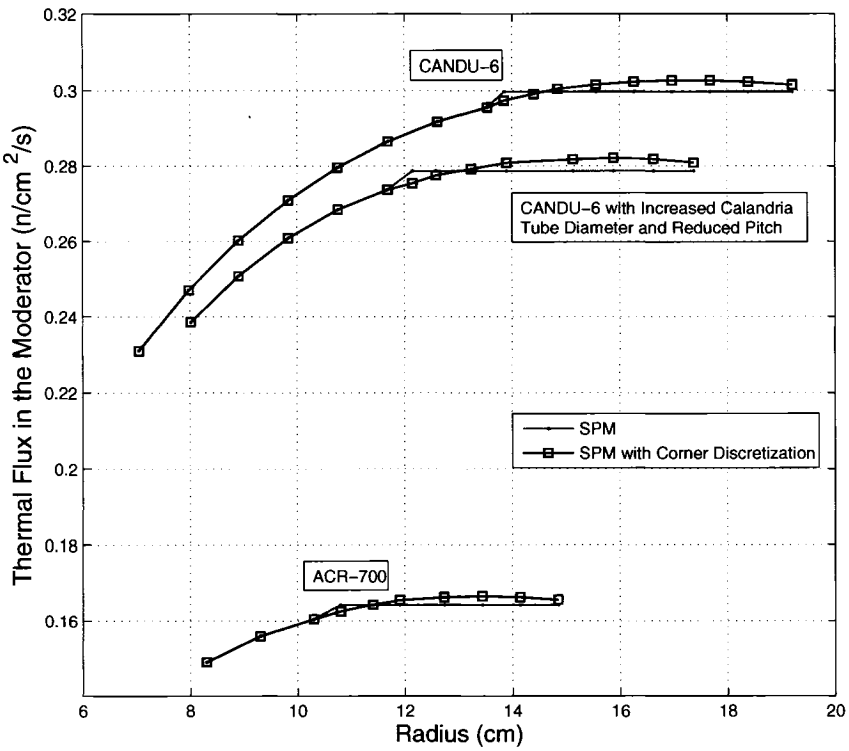

Figure 2.25 Thermal flux in the moderator regions of ACR-700, CANDU-6 and CANDU-6 with increased calandria tube diameter and reduced pitch.

In order to closely examine the effect of corner discretization on the flux shape, an alternative procedure to that mentioned in section 2.4.3 is presented here (see Figure 2.26). It can be seen in Figures 2.27 and 2.28, that the flux is presented as a function of width of regions in the corner. A total of nine regions were identified for CANDU-6 lattice and fluxes were plotted. Similarly eight regions were identified for CANDU-6 with reduced lattice pitch and increased calandria tube, and seven regions for ACR-700 lattice. The plots are in histogram format and a clear change in shape for fast and thermal flux with corner discretization can be observed. As we can see in Figures 2.27 and 2.28, corner discretization helps to determine the correct shape of neutron flux which is essentially the slowing down of neutrons as a function of distance in the moderator.

It can be seen in Figure 2.27, that there is an increase of fast flux in the regions near to the corner (X, Y and Z) and a decrease of thermal fluxes in the same regions (see Figure 2.28). This is mainly due to the use of approximate boundary conditions at the external surfaces, as we explained in section 2.4.3. This effect will vanish when one considers a specular boundary condition or when one considers a 2×2 assembly of cells where there is no boundary condition applied on inner surfaces between lattices (we will see in section 3.3.1).

It can be observed from Figure 2.27, when corner discretization is considered, the shape of fast flux in the regions near to the fuel (see regions R, S in in Figures 2.26 and 2.27) increases, while the thermal flux decreases in the same regions, as shown in Figure 2.28. The effect of corner discretization for both fast and thermal flux for the case of CANDU-6 with increased calandria tube diameter and reduced pitch is higher than that obtained in other cases (see Section 2.5.4).

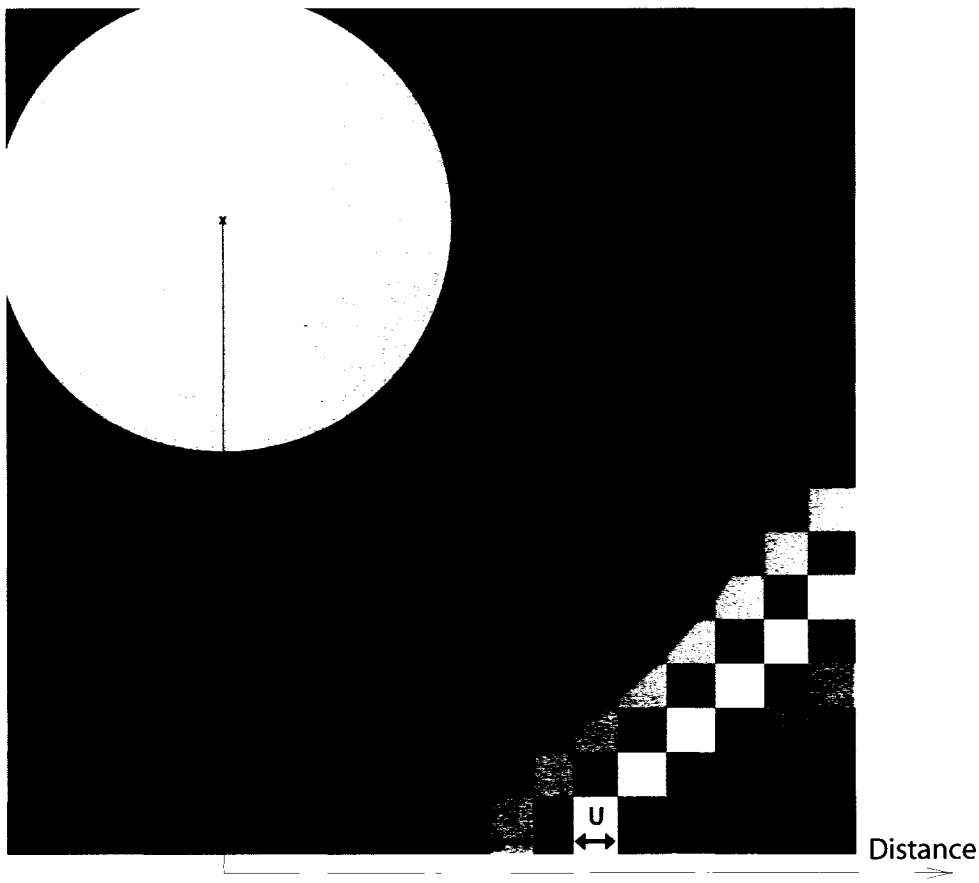

Figure 2.26 Annular-rectangular flux regions in the corner of moderator.

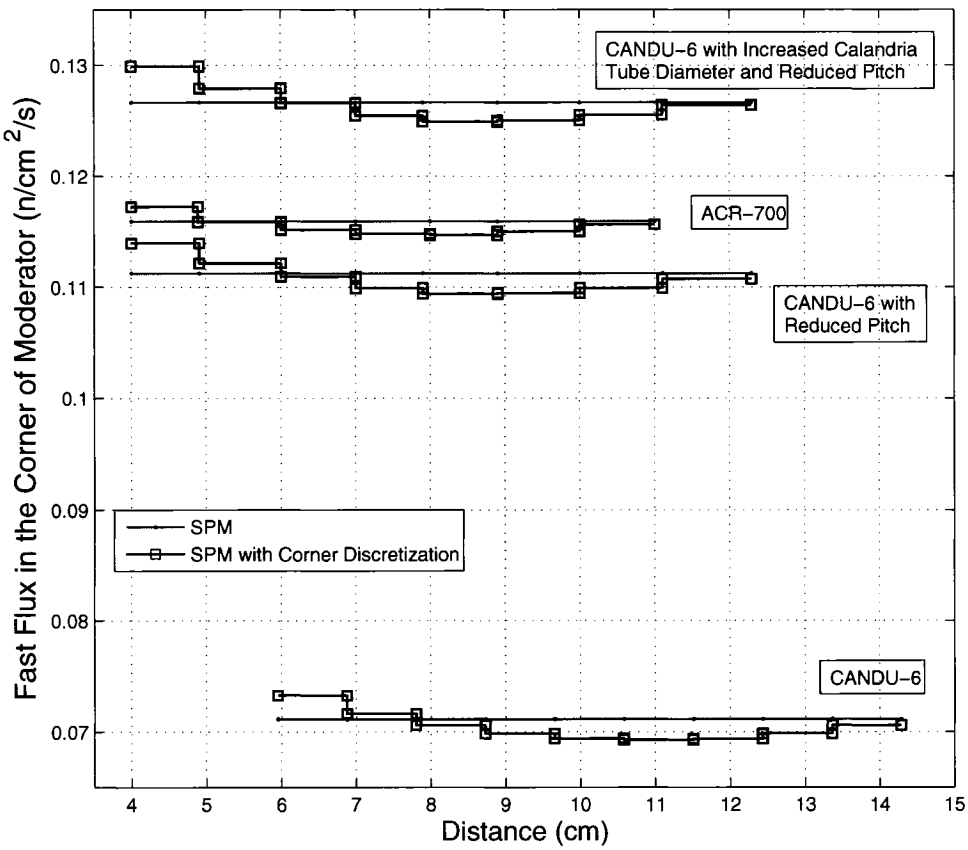

Figure 2.27 Effect of corner discretization in fast flux for all the lattices.

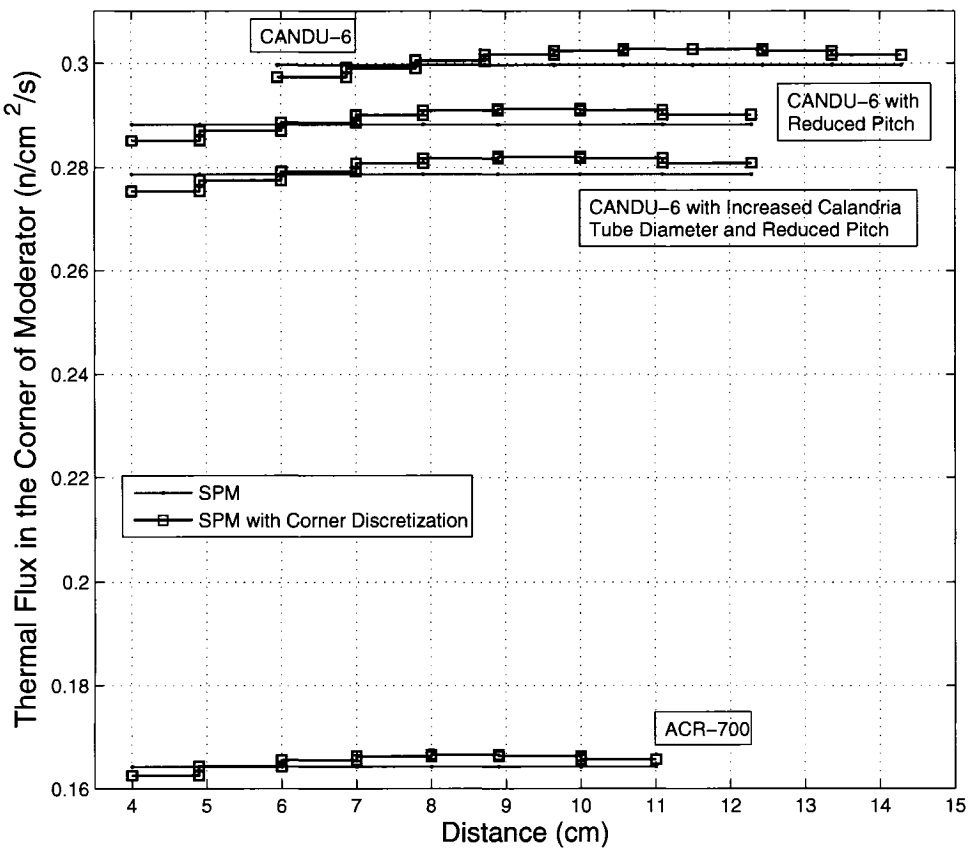

Figure 2.28 Effect of corner discretization in thermal flux for all the lattices.

CHAPTER 3

ASSEMBLY SIMULATIONS IN CANDU

Assembly calculations in a 2×2 pattern offer more options for calculating the reactivity feedback in the reactor due to coolant voiding. In case of single lattice repeating to infinity, using reflective boundary condition, one can only perform eigenvalue calculations for either cooled or voided state. The difference between these two states will give the CVR corresponding to full voiding, and is representative of infinitely similar lattices. This would however represent uniform voiding of the full core. But there is a possibility that coolant is not lost uniformly from all the pressure tubes. When there is a single pump failure or break in only one header pipe, it leads to a situation corresponding to loss of coolant only in certain tubes. In these cases, it may be important to use a model that reflects more accurately the actual voiding situation being studied. Therefore an assembly calculation in a 2×2 black and white pattern (called checkerboard) with translational (periodic) boundary condition must be modelled. This would help in assessing the effect due to coupling of neutrons born in one lattice to those in neighboring lattices.

The main objective of this chapter is to establish a model to evaluate the CVR for a 2×2 heterogeneous assembly of CANDU lattices (CANDU-6 and ACR-700 type lattices) using DRAGON. As mentioned earlier, the existing version of DRAGON has inherent geometry limitations, and CANDU assembly calculations cannot be performed for the exact geometry (see Figure 3.1). It was seen in the case of cell calculations that when the outermost boundary was considered as square, SPM could effectively simulate the CANDU lattice by discretizing the corner. Therefore, in order to perform assembly calculations in a 2×2 pattern with corner discretization using the present version of DRAGON, one has to resort to SPM.

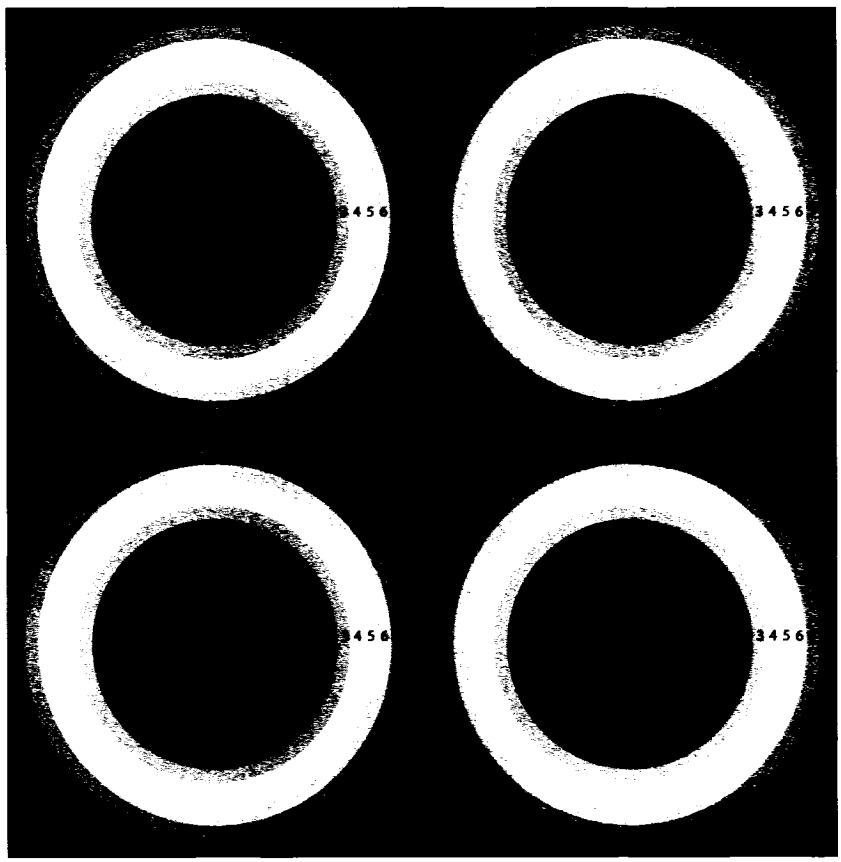

Figure 3.1 A 2 × 2 assembly pattern of exact CANDU-6 geometry.

Using the proposed SPM, DRAGON code can now perform assembly calculation in a 2×2 pattern for different combinations of voiding and fuel state. One can consider, for example, fuel assemblies with different exposures, which would represent equilibrium core pattern in a typical CANDU reactor. In the present study we have considered only fresh fuel and coolant state corresponding to 25% void, 50% void, 75% void and 100% void. The 2×2 pattern can also include reflector cells along with fuel cells. This would give the effect of reflector on neutron flux distribution during coolant voiding. Another interesting possibility of using this model is to estimate the reactivity effect due to heterogeneous draining which is the loss of coolant from top to bottom of the lattice. When such a calculation is performed at the single lattice level, it would represent the loss of coolant uniformly in all the pressure tubes, while in a 2×2 pattern it would represent a situation which might arise when the break in a single feeder pipe takes place. However, such a calculation is not possible by considering annular regions in the coolant. This can be taken up for future studies.

Here we will concentrate our efforts on fuel assembly calculation in a 2×2 pattern for various cell configurations, which are the CANDU-6 cell, CANDU-6 cell with reduced lattice pitch, CANDU-6 cell with reduced lattice pitch and increased calandria tube diameter, and finally the ACR-700 cell.

3.1 CANDU-6 Assembly

The approximate CANDU-6 cell constructed using SPM was used to perform the transport calculation in the 2×2 assembly pattern. The cross section libraries used here are those generated using the cell models described earlier, i.e. the MSCS (section 2.3) and DCS and (section 2.4). It was discussed in the section on CANDU-6 cell simulation (section 2.2), that the number of regions and outer surfaces for fine mesh calculation was 3223 and 132, respectively. Therefore for a 2×2 assembly pattern the number of

fine regions and outer surfaces becomes 12892 and 264 respectively. Even though by use of diagonal symmetry, one could reduce the number of regions and outer surfaces by half, the generation of CP matrix for such a large number of regions would be impossible with the current computer architecture. But there exists only Cartesian symmetry and no diagonal symmetry for the 2×2 assembly pattern of CANDU-6. Therefore one needs to perform calculation for the complete 2×2 assembly pattern, without any geometric simplification. However, the computational efforts can be reduced by using the MRG: module (see section 1.4) incorporated in the code DRAGON, which merges the fine mesh regions having the same mixture, into a coarse mesh region, without altering the cross section. We can now reduce the size of the problem to 76 regions and 8 outer surfaces by using the MRG: module (see Figure 3.2 (a)).

Note that, a 2×2 assembly calculations with fine mesh discretization in the Cartesian corners would involve 17780 regions and 392 outer surfaces in the original format. By using MRG: module and combining the fine mesh regions that are assumed to possess identical fluxes, we obtain nine regions of annular-rectangular form in each corner of each lattices. Finally 108 calculation regions were generated (see Figure 3.2 (b)) and in each assembly case, 19 different mixtures are considered.

In case of single cell calculations, isotropic boundary conditions are uniformly applied on all the external surfaces. When one considers a 2×2 assembly pattern, isotropic boundary conditions are also applied on all external surfaces but there is no boundary condition applied on the inner surfaces. Therefore, within a cell of 2×2 pattern, a flux region near corner 1 is no longer the same as that near corner 2, 3 or 4 (see Figure 3.3). Hence, it would be incorrect to use MRG: module to merge the flux regions in the same way as was done for single cell coarse mesh calculation. Therefore, each lattice has to be divided at least into four parts as shown in Figure 3.3. Identical regions in the lattice are now differentiated for each part of the lattice. Therefore the number of calculation regions increase four times to that of the original SPM. Earlier in a single

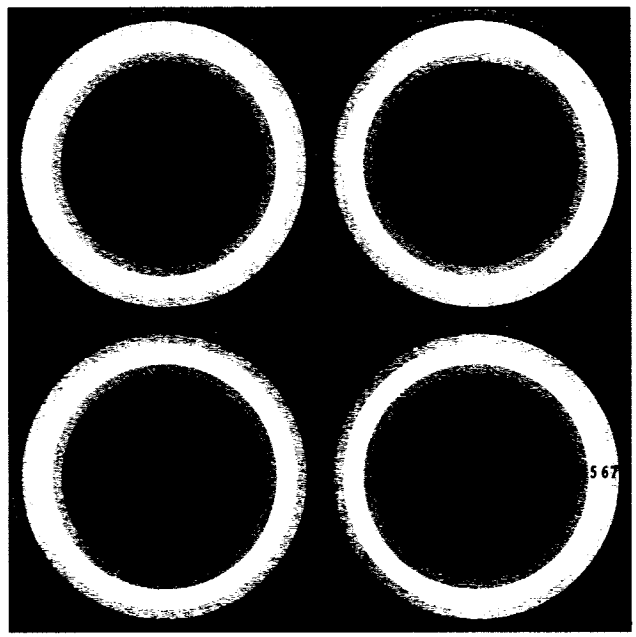

(a)

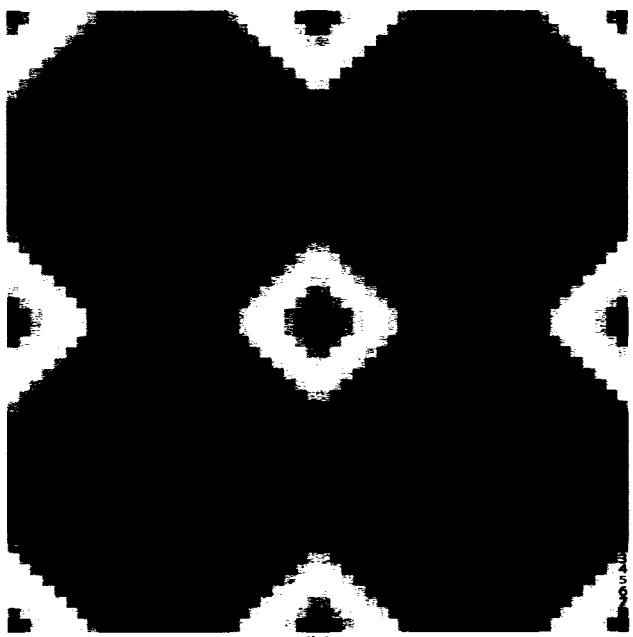

(b)

Figure 3.2 CANDU-6 assembly (coarse mesh) (a) and with corner discretization (b).

cell with discretized corners, the number of regions was 27 and now becomes 108 after division of cell into four parts. Further, the number of regions for a 2×2 assembly pattern becomes 432 (see Figure 3.4). Therefore for all the assembly calculations, each lattice cell was divided into four parts and reflective or translational boundary conditions are applied on the external surfaces.

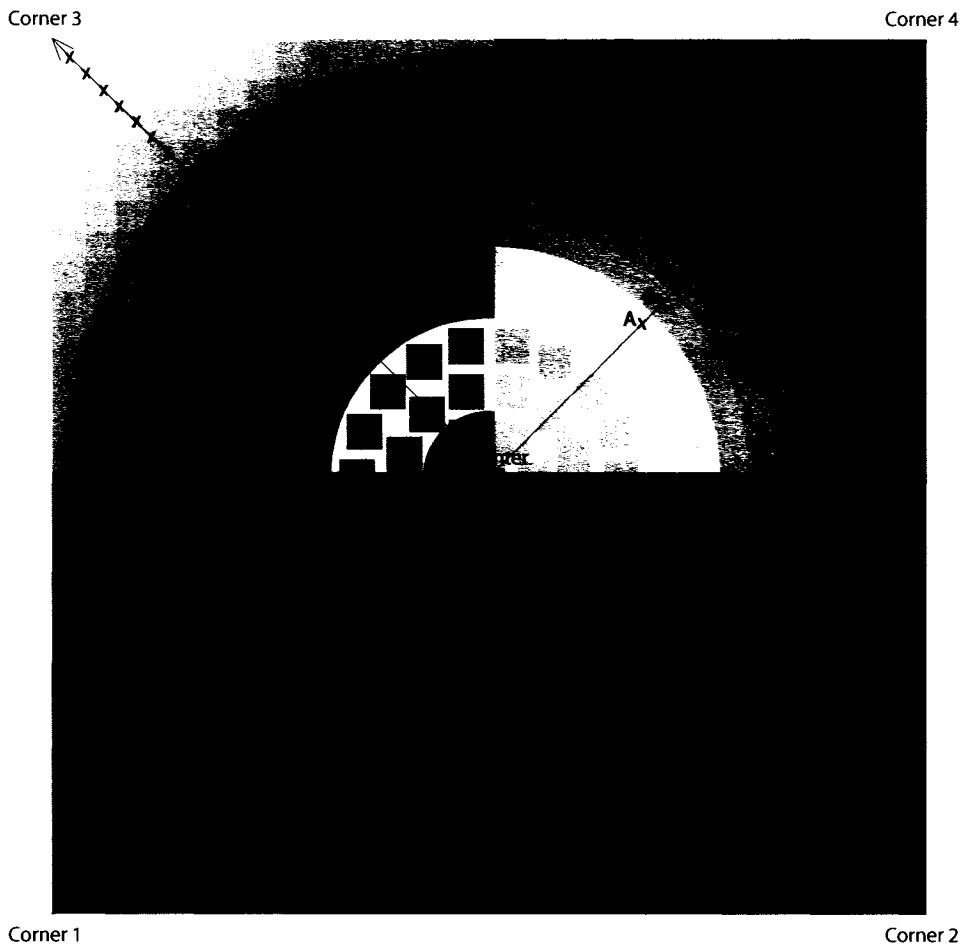

Figure 3.3 Single CANDU-6 cell with different flux regions in each corner.

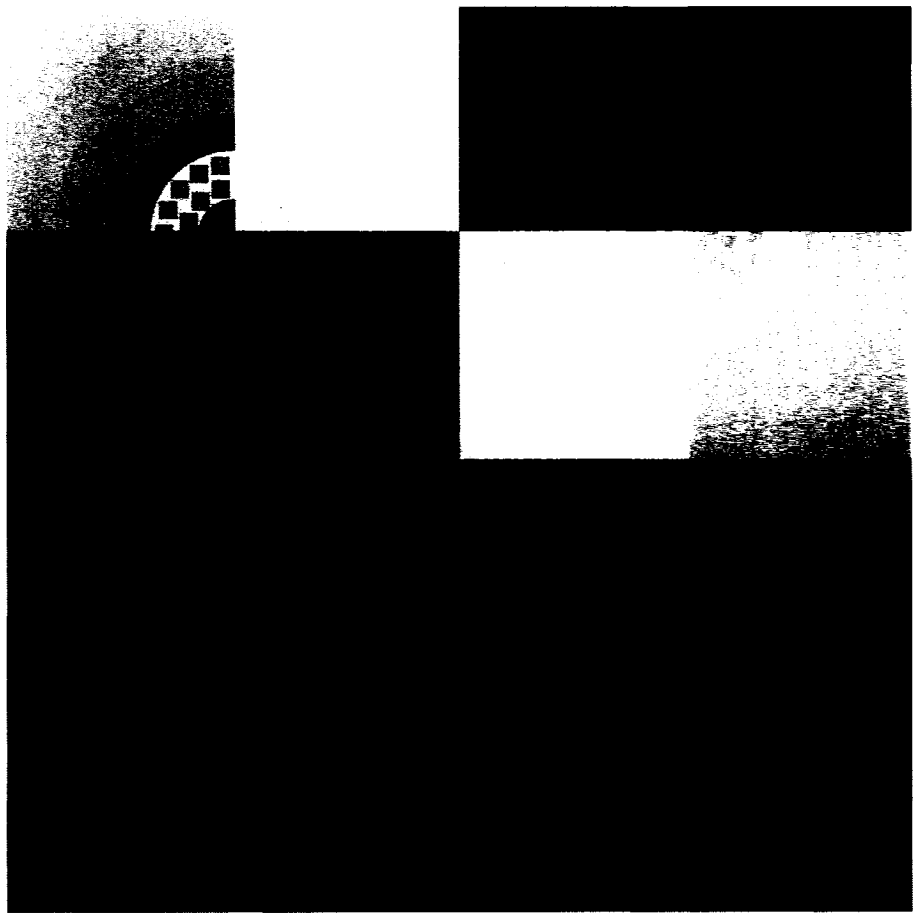

Figure 3.4 A 2×2 CANDU-6 assembly with different flux regions in each corner.

3.1.1 CANDU-6 Assembly Calculation with XS Libraries Generated Using MSCS

In this section we describe the assembly calculations performed using the cross section libraries generated by MSCS (see section 2.3). The first step in the 2×2 assembly calculations consists of validating our model. The case of a 2×2 assembly of identical cells should in principle yield exactly the same results as that of an isolated cell. It can be seen from the first and second line of Table 3.1 that there is a maximum offset of 0.3 mk in the eigenvalue, and the value of CVR remains practically unchanged. This difference, which is small, can be attributed to the boundary condition. As mentioned earlier, for a single cell, isotropic reflective boundary conditions are applied on all the surfaces. But in the case of assembly calculation in a 2×2 pattern, there is no boundary condition that is applied on the inner surfaces and isotropic reflective boundary condition is applied on all the external surfaces.

The second observation is that when the Cartesian corners are discretized in assembly, it results in a 0.3 mk offset in the eigenvalue for almost all the coolant states (see the second and fourth line of the Table 3.1). This is similar to the effect that was observed in single cell calculations using SPM (see the first and third line of the Table 3.1). However, when we compare single cell calculations with corner discretization with that of 2×2 pattern with corner discretization, a constant offset of 0.4 mk is observed, which can be attributed to the difference in boundary conditions, as mentioned earlier. Since the change in eigenvalue is uniform for all the coolant states, the use of corner discretization does not seem to affect the CVR.

Table 3.1 Comparison of k_{eff} and $\Delta\rho$ between single cell and 2×2 assembly of CANDU-6 lattices using MSCS.

Coolant Density $\rightarrow$ (g/cm^3) $k_{eff}\downarrow$	0.81212 %100 Cooled	0.60909 %25 Voided	0.40606 %50 Voided	0.20303 %75 Voided	0.00100 %100 Voided	$\Delta\rho$ (mk) CVR
Single cell (coarse mesh) Figure 2.5 (d)	1.1142	1.1186	1.1232	1.1280	1.1332	+15.1
A 2 × 2 assembly (coarse mesh) Figure 3.2 (a)	1.1139	1.1184	1.1230	1.1278	1.1330	+15.1
Single cell (corners) Figure 2.8	1.1140	1.1185	1.1231	1.1279	1.1330	+15.1
A 2 × 2 assembly (corners) Figure 3.4	1.1136	1.1181	1.1227	1.1275	1.1326	+15.1

In the remaining assembly simulations, a 2×2 checkerboard voiding pattern with discretized corners will be considered (see Figure 3.5). For checkerboard voiding pattern, one cannot apply reflective boundary condition as it will not represent the actual physical situation. Therefore one has to apply translational boundary condition. We will simulate two sets of checkerboard calculations. First, we evaluate the effect of voiding a CANDU-6 assembly in a checkerboard pattern. Then, we study the effect of using the homogenized cross section library associated with a cooled cell to simulate the properties of a voided cell.

In the first set, we considered macroscopic cross section libraries generated with coolant density of 0.81212 g/cm^3 for lattices 1 and 4 and 0.001 g/cm^3 for lattices 2 and 3. The result we obtained for the CVR is 7.7 mk, which is about half of the change (7.55 mk) observed for the case where the full assembly is voided. This means that the cells in the assembly are almost completely decoupled for this CANDU-6 model. This can be explained in the following way. The moderation of the neutrons is near optimal both in the case of a cooled or a voided cell; therefore, the neutron flux in the periphery of one lattice does not affect any other lattice. Accordingly, independent cell calculations can be used to estimate with a very good accuracy the CVR associated with checkerboard voiding.

In the second set, we used the macroscopic cross section library generated with coolant density of 0.81212 g/cm^3 for all the mixtures except for the coolant in lattices 2 and 3 where we use the coolant cross sections that were generated using the fully voided (0.001 g/cm^3) cell calculations. The CVR in this case is two mk less than that obtained using the correctly homogenized cross section. This is because the library of cross sections that is generated by SPH procedure is conditioned by the reference cell calculations and the homogenized cross sections associated with all mixtures are modified by the SPH procedure. Since the cross sections associated with each mixture are indirectly coupled, we cannot partially use the cross sections for the mixtures of the cooled state in the

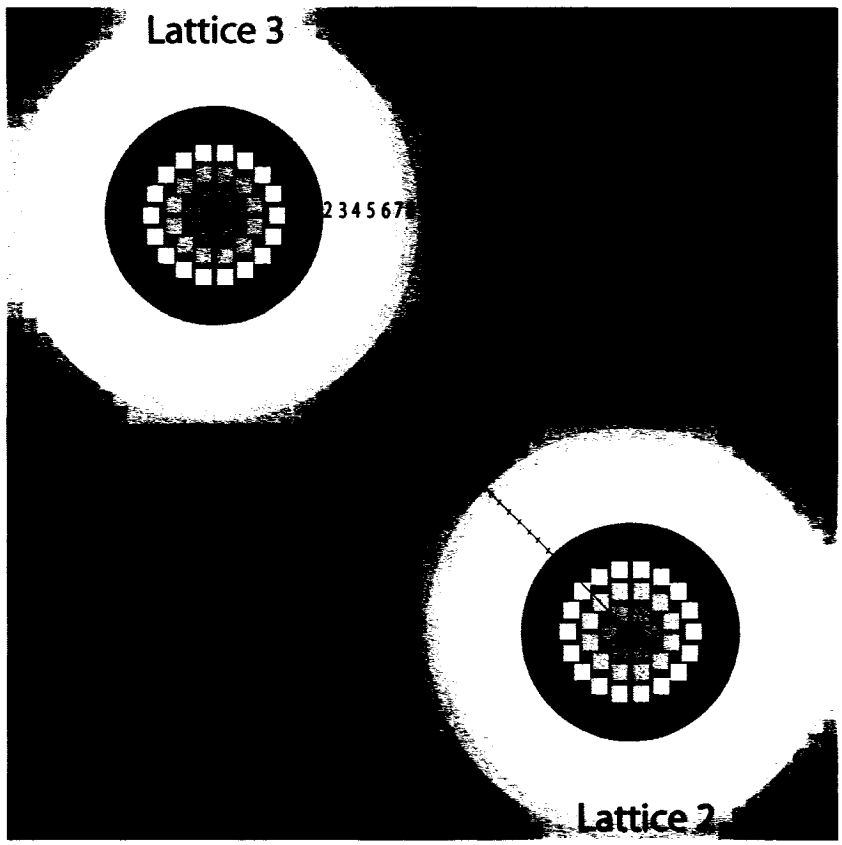

Figure 3.5 A 2 × 2 checkerboard voiding pattern of CANDU-6.

voided lattice and vice versa. Thus, two mk reduction in CVR in the second set of calculations can be interpreted as the effect of interchangeable use of cross sections of the two states.

3.1.2 CANDU-6 Assembly Calculation with XS Libraries Generated Using DCS

In this section we will describe the assembly calculations performed using the cross section libraries generated by DCS (see section 2.4). As mentioned in earlier section, the first step involves validating our model for a 2×2 assembly pattern, by comparing the results with that obtained for an isolated cell. It can be seen from the Table 3.2 that there is a maximum deviation reaching 0.3 mk in the eigenvalue in coarse mesh calculation, and the value of CVR remains almost unchanged. This small difference is related to the use of approximate boundary condition in DRAGON for external surfaces, as mentioned earlier. The results thus obtained confirm that the cross section libraries generated by single step DCS are better than MSCS also in assembly calculation.

As observed in the case of MSCS, discretizing the corner in assembly results in an additional 0.3 mk offset in the eigenvalue with respect to that of coarse mesh calculations (see Table 3.2). This is similar to the offset observed when corner discretization is performed on single cell (see Table 3.2). However, when we compare single cell calculations with corner discretization with that of 2×2 pattern with corner discretization, a constant deviation of 0.4 mk is observed, which can be attributed again to the difference in boundary conditions. As in case of MSCS, the CVR remains mainly unaffected due to the uniform offset for all the coolant states.

As explained in Section 2.4.3, the offset in eigenvalue due to corner discretization in a 2×2 assembly pattern can be explained in terms of the change in production and destruction rate. For fully cooled state, the relative production rate was found to be reduced by 0.0009%, while the relative destruction rate increased by 0.1553%, when one considered corner discretization. This results in the reduction in eigenvalue about 0.3 mk (see the second and fourth line of Table 3.2).

Table 3.2 Comparison of k_{eff} and $\Delta\rho$ between single cell and 2×2 assembly of CANDU-6 lattices using DCS.

Coolant Density $\rightarrow$ (g/cm^3) $k_{eff}\downarrow$	0.81212 %100 Cooled	0.60909 %25 Voided	0.40606 %50 Voided	0.20303 %75 Voided	0.00100 %100 Voided	$\Delta\rho$ (mk) CVR
Single cell (coarse mesh) Figure 2.5 (d)	1.1133	1.1181	1.1230	1.1281	1.1335	+16.0
A 2 $\times$ 2 assembly (coarse mesh) Figure 3.2 (a)	1.1130	1.1178	1.1228	1.1279	1.1333	+16.1
Single cell (corners) Figure 2.8	1.1131	1.1179	1.1229	1.1280	1.1334	+16.0
A 2 $\times$ 2 assembly (corners) Figure 3.4	1.1127	1.1175	1.1225	1.1276	1.1330	+16.1

The CANDU-6 checkerboard calculation was also performed with these set of cross section libraries for a 2×2 pattern (see Figure 3.5). By considering the macroscopic cross section generated with coolant density of 0.81212 g/cm^3 for lattices 1 and 4 and 0.001 g/cm^3 for lattices 2 and 3. In this calculation, the Cartesian corners are also discretized. The obtained result for the CVR is 8.2 mk, which is slightly more than half of the change (8.05 mk) observed for the case where the full assembly is voided. As we mentioned in the previous section, the slowing down of the neutrons at the periphery of a cooled or a voided cell is almost optimum. Hence, the neutron flux in one cell does not influence any other cell. The behavior is linear as expected, because the CANDU-6 is a well moderated system.

It can be observed, for the eigenvalue and CVR estimation in a 2×2 assembly pattern, using the coarse mesh cross section libraries generated by single step DCS are better than the coarse mesh calculation using the fine mesh MSCS library. Hence, we recommend to use the cross section libraries generated by single step DCS that would lead to the estimation of CVR for a 2×2 pattern of ACR-700 lattice.

A discussion on fast and thermal flux shape for a single cell was presented earlier in section 2.4.2. We will now present the variation of flux shape in the moderator region, in the context of assembly calculation in a 2×2 pattern. The fluxes will be represented as a function of radius of each of the 17 regions in the moderator, as shown in Figure 3.3. It can be seen in Figure 3.4 that these radius locations are named A to Q, from inside to the corner 4 of a cell within a 2×2 assembly pattern. The plots of the fast and thermal flux with respect to the radius of each region are shown in Figures 3.6 and 3.7. It can be seen in Figure 3.6 that the fast flux reduces from inside to corner. When one discretizes the corner, it is interesting to note that the flux shape becomes parabolic for the radius I to Q, in comparison to that of a straight line which was obtained when there was no corner discretization. A similar trend is observed for thermal flux, albeit it increases from center to outside, which is shown in Figure 3.7.

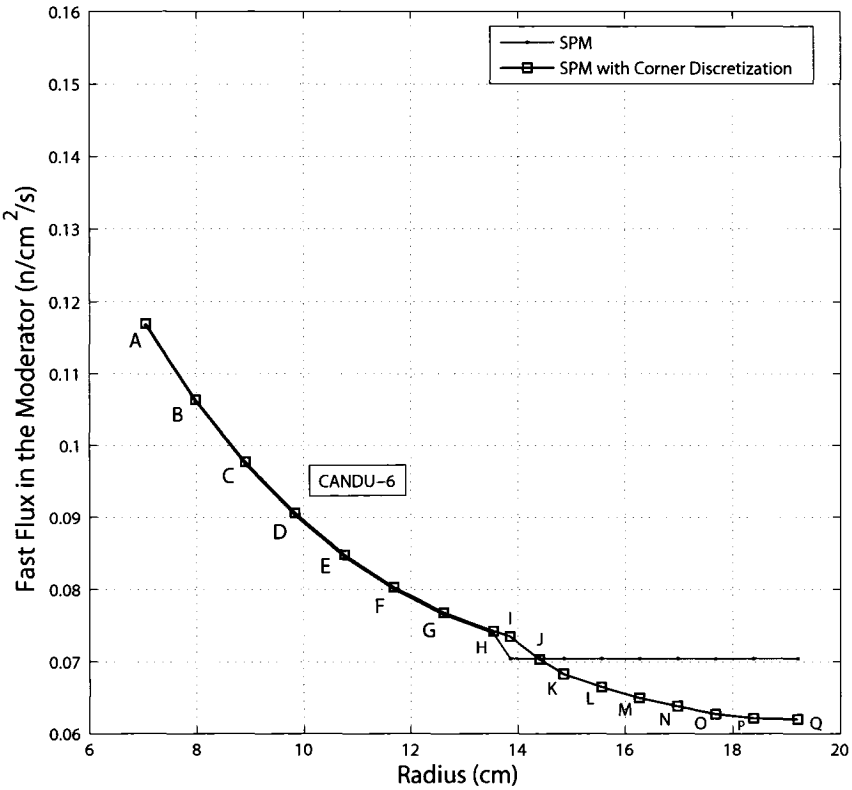

Figure 3.6 Fast flux in the moderator region of CANDU-6 assembly.

It was discussed in section 2.4.3, that there is a positive slope in fast flux and a negative slope in thermal flux close to the corner of the lattice. It was argued that approximate boundary condition was responsible for the same. We can see here that this effect vanishes when one considers a 2×2 assembly of cells, because there is no boundary condition applied on inner surfaces between lattices, as shown in Figures 3.6 and 3.7.

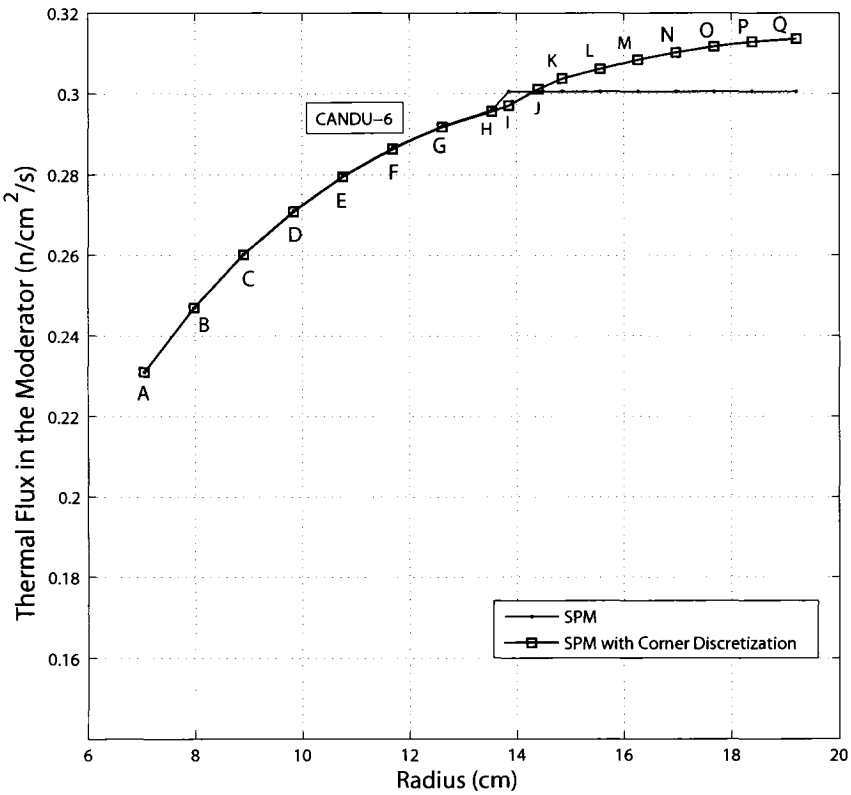

Figure 3.7 Thermal flux in the moderator region of CANDU-6 assembly.

In the present context, another interesting observation is to show the flux shape in the moderator region of a 2×2 checkerboard voiding pattern. As mentioned earlier, lattice 1 is fully cooled and lattice 2 is totaly voided (see Figure 3.5). The moderator of each lattice is split into 17 regions including eight annular rings and nine annular-rectangular regions. In order to present the fluxes, the 34 regions are considered i.e., 17 regions in lattice 1 (from inside to corner 4) and 17 regions in lattice 2 (from corner 3 to inside).

The plots of the fast and thermal fluxes with respect to the radius of each moderator region are shown in Figures 3.8 and 3.9. It can be seen in Figure 3.8 that when assembly is completely voided, the magnitude of fast flux increases. A similar tendency is seen for the thermal flux, although the magnitude decreases when assembly is drained, as observed in Figure 3.9.

It is interesting to note that, there is a clear change in the flux shape due to the checkerboard voiding. It can be seen in Figure 3.8, the fast flux in the cooled lattice (lattice 1) affects very slightly than the flux found when the assembly is fully cooled. But in the voided lattice (lattice 2), it overlaps with that obtained when the assembly is completely voided. The same behavior is observed for the thermal flux, that is the flux in the lattice 1 and 2 are very close to that obtained when the assembly is fully cooled and totaly voided. In the regions near to the corners (corner 3 and 4), the fast and thermal fluxes are the average the cooled and voided state. We will compare these flux shapes with those obtained for ACR-700 pattern is section 3.3.1.

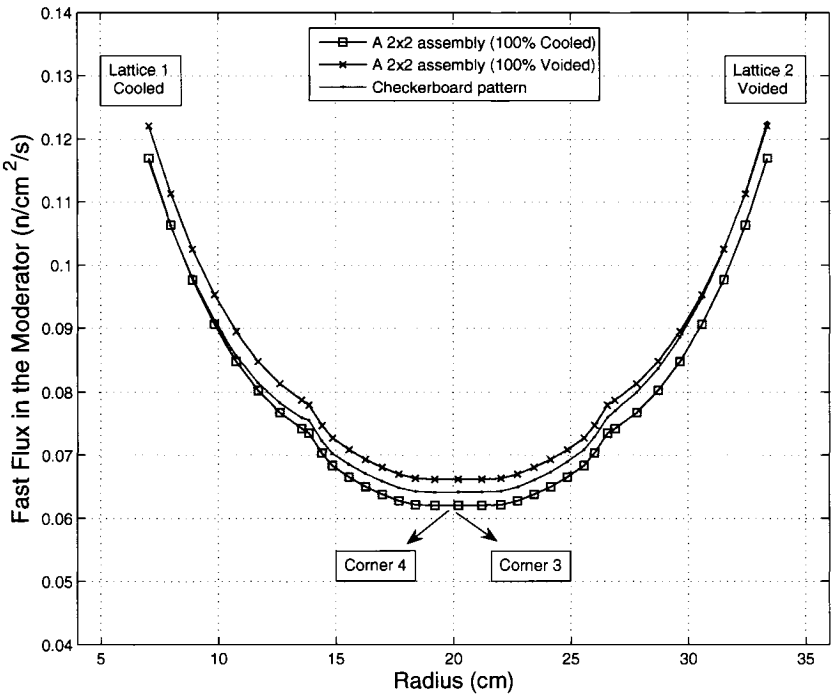

Figure 3.8 Comparison of fast fluxes in a 2×2 CANDU-6 assembly and checkerboard pattern.

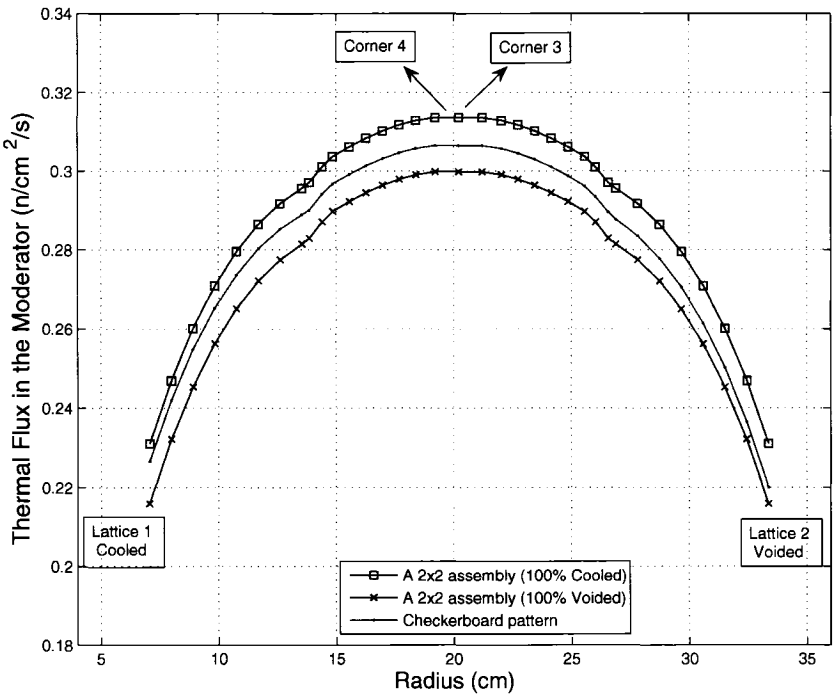

Figure 3.9 Comparison of thermal fluxes in a 2 × 2 CANDU-6 assembly and checkerboard pattern.

3.2 Evolution of CANDU-6 Assembly Towards ACR-700

As mentioned in the previous section, the following studies will focus on evaluation of CVR for a 2×2 ACR-700 pattern using SPM. In order to achieve this goal, we will perform the evolution of a 2×2 CANDU-6 pattern, to a 2×2 ACR-700 pattern in three steps, similar to that performed for single cell calculation. In the first step the lattice pitch will be reduced, maintaining the same configuration of pressure tube and calandria tube as that of CANDU-6. In the second step the calandria tube diameter will be increased. In the third step, the number of pins will be increased from 37 to 43, changing natural uranium to enriched uranium and changing the coolant from heavy water to light water, thereby obtaining a 2×2 ACR-700 pattern. For all the three steps, we have estimated the CVR. All these calculations were performed with and without corner discretization and with different boundary conditions (translational and reflective).

3.2.1 The Effect of Reduction in Lattice Pitch

This section deals with the effect of reduction in the pitch of a 2×2 CANDU-6 pattern on the eigenvalues and CVR. As discussed in Section 2.5.1, the pitch of the lattice was changed from 28.575 cm to 24.575 cm. It was observed that (see the second line of Table 3.3 and Table 3.2) there is a reduction in k_{eff} of 38.7 mk from the 2×2 pattern of original CANDU-6 lattice in the presence of coolant and a reduction of 40.1 mk in the absence of coolant. The CVR was estimated to +15 mk which is still positive but lower than the CVR for original assembly pattern of CANDU-6.

SPM analysis for a 2×2 assembly pattern with reduced pitch was performed along the same lines as was done for original CANDU-6. It was mentioned in section 2.5.1, that for CANDU-6 with reduced lattice pitch, the number of regions and outer surfaces for fine mesh calculation was 2967 and 132, respectively. Therefore, for a 2×2 assembly

Table 3.3 Comparison of k_{eff} and $\Delta\rho$ between single cell and 2×2 assembly of CANDU-6 lattices with reduced pitch.

Coolant Density $\rightarrow$ (g/cm^3) $k_{eff}\downarrow$	0.81212 %100 Cooled	0.60909 %25 Voided	0.40606 %50 Voided	0.20303 %75 Voided	0.00100 %100 Voided	$\Delta\rho$ (mk) CVR
Single cell (coarse mesh) Figure 2.12 (c)	1.0753	1.0793	1.0835	1.0881	1.0929	+15.0
A 2 $\times$ 2 assembly (coarse mesh) Figure 3.10 (a)	1.0752	1.0792	1.0835	1.0880	1.0929	+15.0
Single cell (corners) Figure 2.13	1.0752	1.0792	1.0835	1.0880	1.0929	+15.0
A 2 $\times$ 2 assembly (corners) Figure 3.11 (b)	1.0750	1.0791	1.0833	1.0879	1.0928	+15.0

pattern the number of fine regions and outer surfaces becomes 11868 and 264, respectively.

The calculation for the complete 2×2 assembly pattern is made possible by the use of MRG: module (explained in section 1.4). Using the MRG: module, the number of regions and outer surfaces can be reduced from 11868 and 264 to 68 and 8, respectively (see Figure 3.10 (a)). Also, a 2×2 assembly calculations with fine mesh discretization in the Cartesian corners would involve 14740 regions and 360 outer surfaces. By using MRG: module we obtain seven regions of annular-rectangular form in each corner of each of the lattices and 96 calculation regions were generated (see Figure 3.10 (b)). Finally in each assembly case, 17 different mixtures are considered.

As explained before in section 3.1, for assembly calculation each cell has to be divided into four parts. Identical regions in the lattice are differentiated in each part of the lattice. Therefore, the number of flux regions increases four times with respect to the original lattice. Earlier in a single cell the number of regions was 24 and it now becomes 96 after division of cell into four parts. Furthermore the number of regions for a 2×2 assembly pattern (Figure 3.11 (b)) becomes 384.

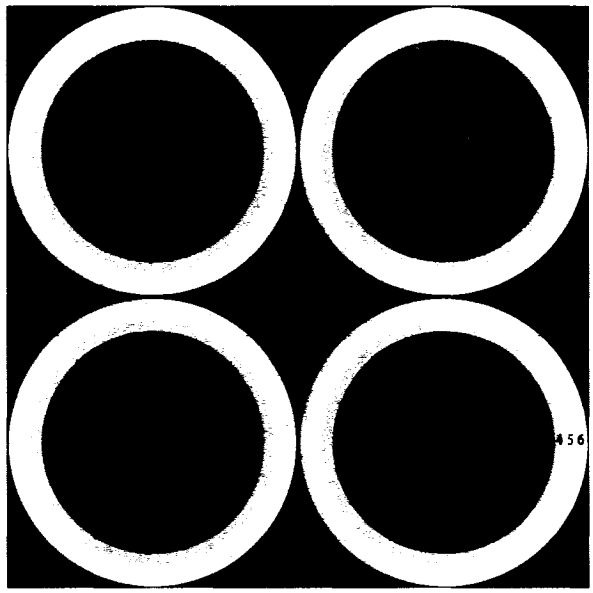

(a)

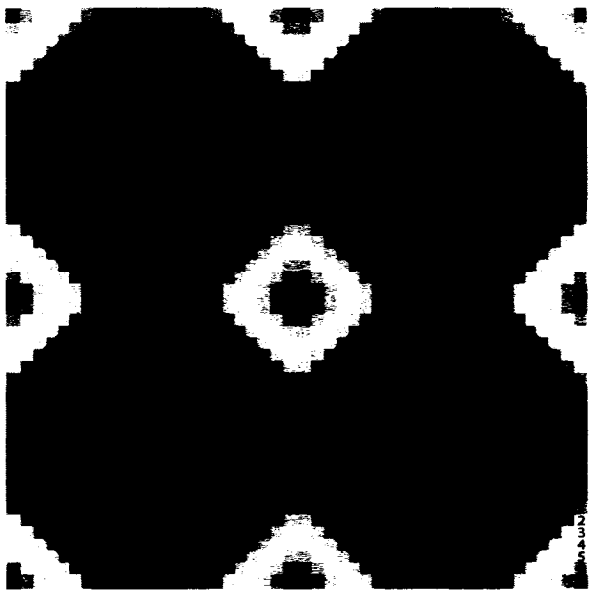

(b)

Figure 3.10 CANDU-6 assembly with reduced pitch (coarse mesh) (a) and with corner discretization (b).

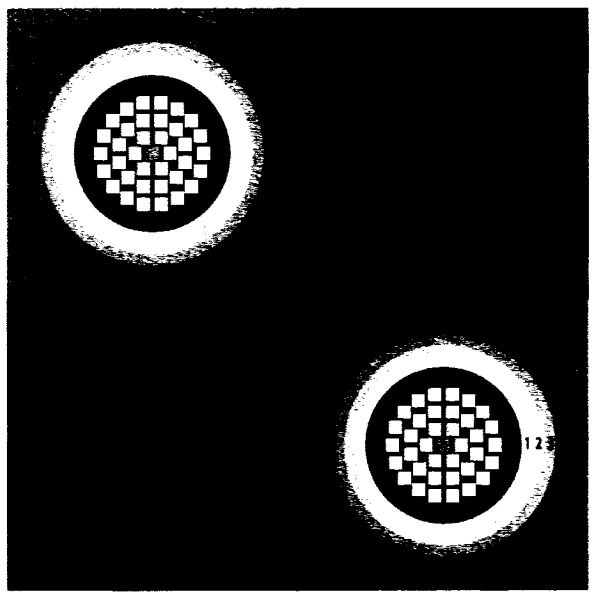

(a)

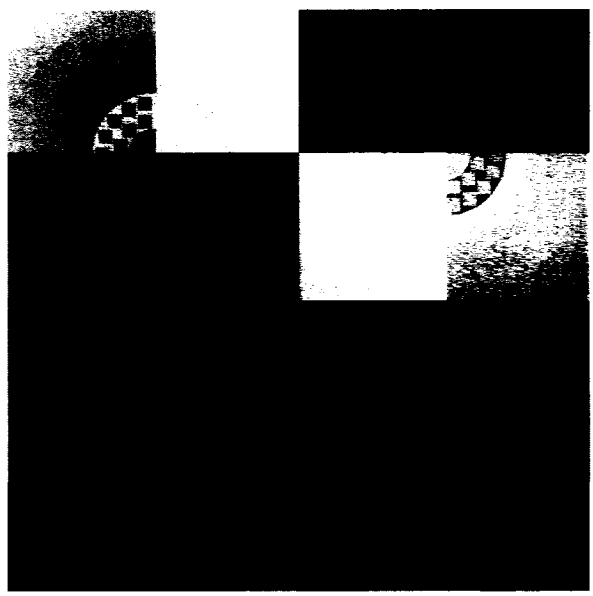

(b)

Figure 3.11 CANDU-6 assembly with reduced pitch (24.575 cm), checkerboard voiding pattern (a) and with four different corners (b).

3.2.2 Assembly Calculation for Reduced Pitch

As we have seen in the section 3.1.1, we will compare the results in a 2×2 assembly of cells with that of an isolated cell. In this section, we describe the assembly calculations performed with the cross section libraries generated using DCS (see section 2.5.2).

It can be observed from the first and second line of the Table 3.3 that there is an offset of 0.1 mk in the eigenvalue, and the value of CVR remains practically unchanged. As we have seen in the case of original CANDU-6 assembly, this small difference can be associated with the use of approximate boundary condition on all the external surfaces for single cell, while there is no boundary condition applied on the inner surfaces of the lattice within an assembly.

The second observation is that the effect of Cartesian corner discretization in assembly results in 0.2 mk deviation in the eigenvalue (see Table 3.3). This difference is identical to that observed in cell calculation with corner discretization (see Table 3.3). A comparison between corner discretization in single cell and 2×2 assembly pattern shows an maximum offset of 0.2 mk which is related to the difference in boundary conditions, as mentioned in the first step. However, the CVR does not change for this case, as observed for the original CANDU-6 assembly.

The effect of corner discretization can be explained in terms of the change in production and destruction rate (see Section 2.4.3). In the fully cooled state, the relative production rate reduced by 0.0009%, while the relative destruction rate increased by 0.0836%, when one considered corner discretization. When compared to that of CANDU-6 assembly, the relative destruction rate was found to be reduced almost by half. As a result, the eigenvalue is affected only with 0.2 mk against that of 0.3 mk for CANDU-6 assembly.

Checkerboard calculation for the CANDU-6 with reduced pitch was also performed with libraries generated by DCS for a 2×2 pattern (see Figure 3.11 (a)). The checkerboard calculation is done with a coolant density of 0.81212 g/cm^3 for lattices 1 and 4 and 0.001 g/cm^3 for lattices 2 and 3. In this calculation, a 2×2 pattern with discretized corners was considered. The CVR is 7.6 mk, which is almost half of the change (7.5 mk) observed for the case where the full assembly is voided. As we have seen earlier for CANDU-6 assembly, checkerboard calculation for a reduced lattice pitch remains linear.

In this 2×2 pattern we also plot the neutron fluxes (fast and thermal) in the moderator region from inside to corner 4 (see Figure 3.11 (b)). It can be seen in Figures 3.12 and 3.13, that the fast and thermal fluxes have a similar shape as those observed in CANDU-6 assembly. The magnitude of fast flux is seen to increase, but the magnitude of thermal flux is almost the same as CANDU-6 assembly. The thermal flux is slightly higher initially, but decreases towards the corner. As we mentioned earlier in section 2.5.2, the main effect on the multiplication of the system is due to the small change in the thermal flux. As we have seen in CANDU-6 assembly, it can be observed the positive and negative slope in the fast and thermal flux close to the corner of the lattice have disappeared.

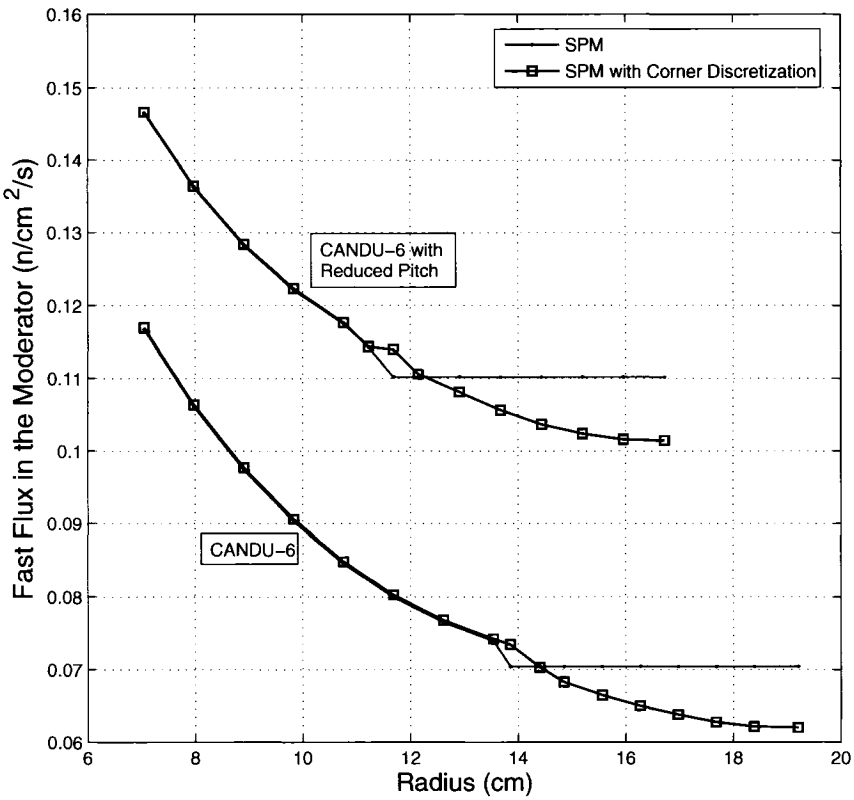

Figure 3.12 Fast flux in the moderator region for assemblies of CANDU-6 and CANDU-6 with reduced pitch assemblies.

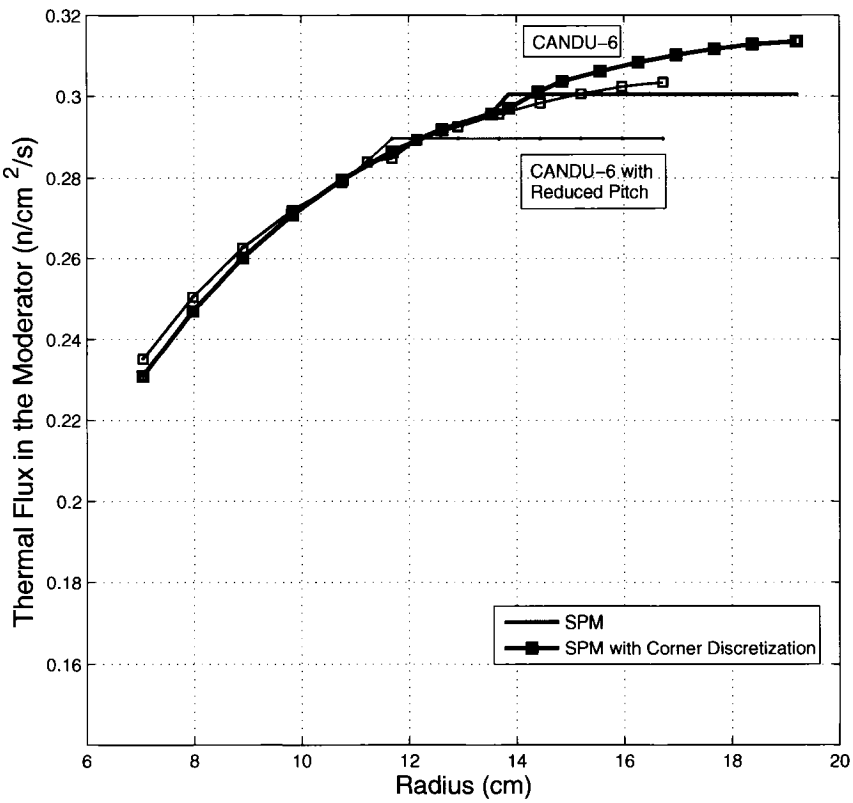

Figure 3.13 Thermal flux in the moderator region for assemblies of CANDU-6 and CANDU-6 with reduced pitch assemblies.

3.2.3 Effect of Increase in Calandria Tube Diameter

In this section for a 2 × 2 CANDU-6 pattern, the effect on eigenvalue and CVR resulting from an increase of the calandria tube diameter and a reduce of the lattice pitch is studied. The calandria tube inner/outer diameter is increased from 12.8956/13.175 to 14.8956/15.195 cm to almost match with that of ACR-700 lattice and the pitch was 24.575 cm. The CANDU-6 configuration, including the fuel assembly and the pressure tube, remains unchanged. It was observed that (see the second line of Table 3.4 and Table 3.2) there is a reduction in k_{eff} of 53 mk from the 2 × 2 pattern of original CANDU-6 lattice in fully cooled state and a reduction of 56 mk for totally voided state. In this case also, the CVR was computed as +14.5 mk which is still positive but lower than the CVR for the original pattern.

The assembly calculation in a 2 × 2 pattern was performed along the same lines as for the original CANDU-6 assembly. It was discussed in section 2.5.3, for CANDU-6 cell with increased calandria tube diameter and reduced pitch, the number of regions and outer surfaces for fine mesh calculation was 2839 and 132, respectively. Hence, the number of fine regions and outer surfaces for a 2 × 2 assembly pattern becomes 11356 and 264, respectively.

In this case also, assembly calculations must be performed in the complete 2 × 2 pattern, as mentioned earlier. Therefore using the `MRG:` module (see section 1.4), one can obtain 64 regions and 8 outer surfaces (see Figure 3.14 (a)). For fine mesh discretization in the Cartesian corners of a 2 × 2 assembly, there are 14228 regions and 360 outer surfaces. Using `MRG:` module once again, we obtain seven regions of annular-rectangular form in each corner of each lattice and 92 calculation regions were generated (see Figure 3.14 (b)). Finally in each assembly case, 16 different mixtures are considered.

As explained before in section 3.1, for assembly calculation, each cell has to be divided

Table 3.4 Comparison of k_{eff} and $\Delta\rho$ between single cell and 2×2 assembly of CANDU-6 lattices with increased calandria tube diameter and reduced pitch.

Coolant Density → (g/cm^3)	0.81212	0.60909	0.40606	0.20303	0.00100	$\Delta\rho$ (mk)
k_{eff} ↓	%100 Cooled	%25 Voided	%50 Voided	%75 Voided	%100 Voided	CVR
Single cell (coarse mesh) Figure 2.16 (c)	1.0606	1.0643	1.0682	1.0725	1.0772	+14.5
A 2×2 assembly (coarse mesh) Figure 3.14 (a)	1.0604	1.0641	1.0680	1.0723	1.0770	+14.5
Single cell (corners) Figure 2.17	1.0593	1.0630	1.0669	1.0712	1.0759	+14.5
A 2×2 assembly (corners) Figure 3.15 (b)	1.0592	1.0629	1.0668	1.0711	1.0758	+14.5

into four parts and in each part of the cell, identical regions are differentiated. Therefore, the number of calculation regions increase four times with respect to the original lattice. Earlier in a single cell the number of regions was 23 and now becomes 92 after division of cell into four parts. Further the number of regions for a 2×2 assembly pattern (Figure 3.15 (b)) becomes 368.

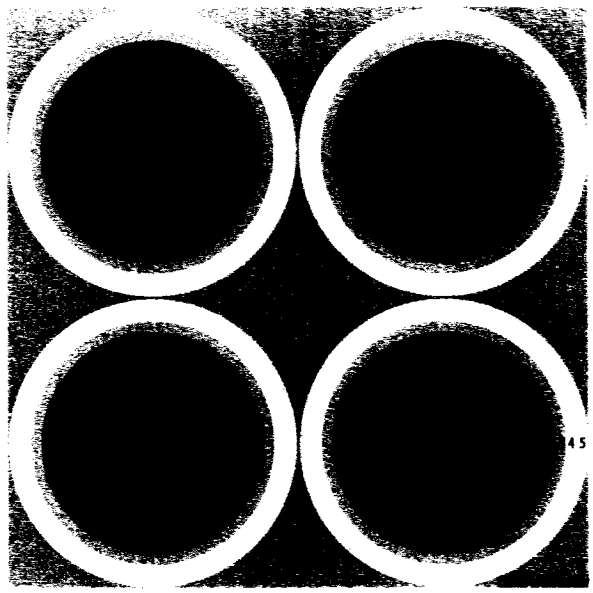

(a)

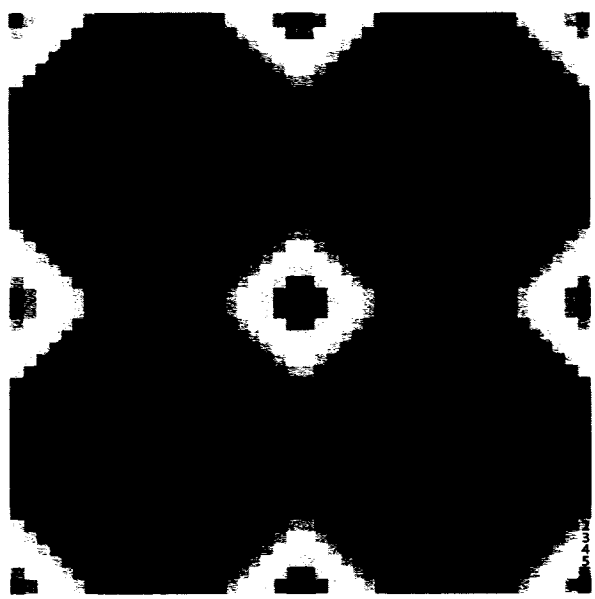

(b)

Figure 3.14 CANDU-6 assembly with reduced pitch and increased calandria tube diameter (coarse mesh) (a) and with corner discretization (b).

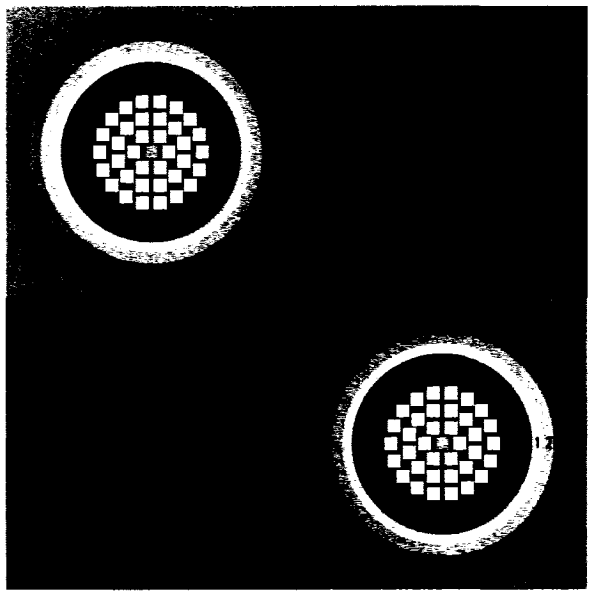

(a)

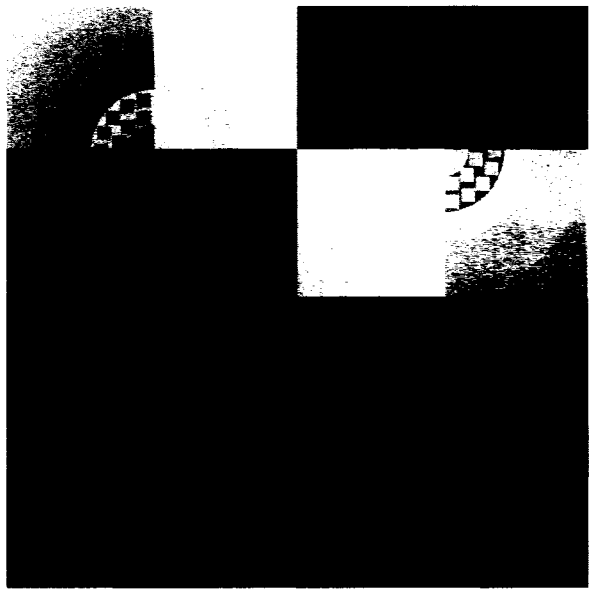

(b)

Figure 3.15 A 2 × 2 CANDU-6 pattern with increased calandria tube diameter and reduced pitch, checkerboard (a) and with different corners (b).

3.2.4 Assembly Calculation for Increased Calandria Tube Diameter

In this section, we describe the assembly calculations (with and without corner discretization) performed with the cross section libraries generated using DCS (see section 2.5.4). We will now describe the various steps involved in assembly calculations.

In the first step, the validation of results obtained for a 2×2 assembly of cells is done against an isolated cell (as mentioned in section 3.1.1). A constant offset of 0.2 mk in the eigenvalue can be seen from the first and second line of the Table 3.4. The value of CVR remains unchanged. As we explained in section 3.1.2 this small difference is due to the use of approximate boundary condition.

There is a constant deviation of 1.2 mk in the eigenvalue when one considers an assembly with corner discretization (see Table 3.4). The same effect can be seen in the cell calculation with corner discretization (see the first and third line of the Table 3.4). Subsequently, corner discretization effect between a single cell and a 2×2 assembly pattern results in an additional 0.1 mk offset in the eigenvalue which is due to the difference in boundary conditions. As observed in the original pattern of CANDU-6 assembly, the CVR remains unaffected even in this case.

As mentioned earlier, the effect in eigenvalue due to the corner discretization in a 2×2 assembly pattern can be explained in terms of the change in production and destruction rate (see Section 2.4.3). In the fully cooled state, the relative production rate was found to be reduced by 0.0002%, while the relative destruction rate increased by 0.5072%. When compared to that of original CANDU-6 assembly, the relative destruction rate was found to be increased by more than three times. As a result, the eigenvalue is reduced by 1.2 mk against that of 0.3 mk for the original case. Therefore, Cartesian corner discretization has a large effect in this case. Since the offset in fully cooled and voided states does not change, a 2×2 coarse mesh pattern yields the same value of CVR and can thus be

concluded that a coarse mesh calculation would be enough for the CVR estimation.

The checkerboard calculation in this case was also performed with libraries generated by DCS for a 2×2 pattern (see Figure 3.15 (a)). As it was explained before, the macroscopic cross section libraries generated with coolant density of 0.81212 g/cm^3 is considered for lattices 1 and 4 and 0.001 g/cm^3 for lattices 2 and 3. The corner discretization was considered in a 2×2 voiding pattern. The obtained result for the CVR is 7.4 mk, which is almost half of the change (7.3 mk) observed for the case where the full assembly is voided. The same linear behavior of CANDU-6 assembly can also be observed for checkerboard calculation.

In order to obtain the fast and thermal flux in a 2×2 pattern, the corner 4 of the moderator region of the cell within a assembly is considered (see Figure 3.11 (b)). It can be seen in Figures 3.16 and 3.17, that the flux shapes for fast and thermal neutrons are similar to that which was observed for the case of assembly with reduced pitch. The attenuation of fast neutrons, which is the difference in number of fast neutrons close to fuel to that in the corner, decreases due to the reduction in moderator volume. It means that fewer fast neutrons have been moderated and the spectrum is even harder than the case with reduced pitch.

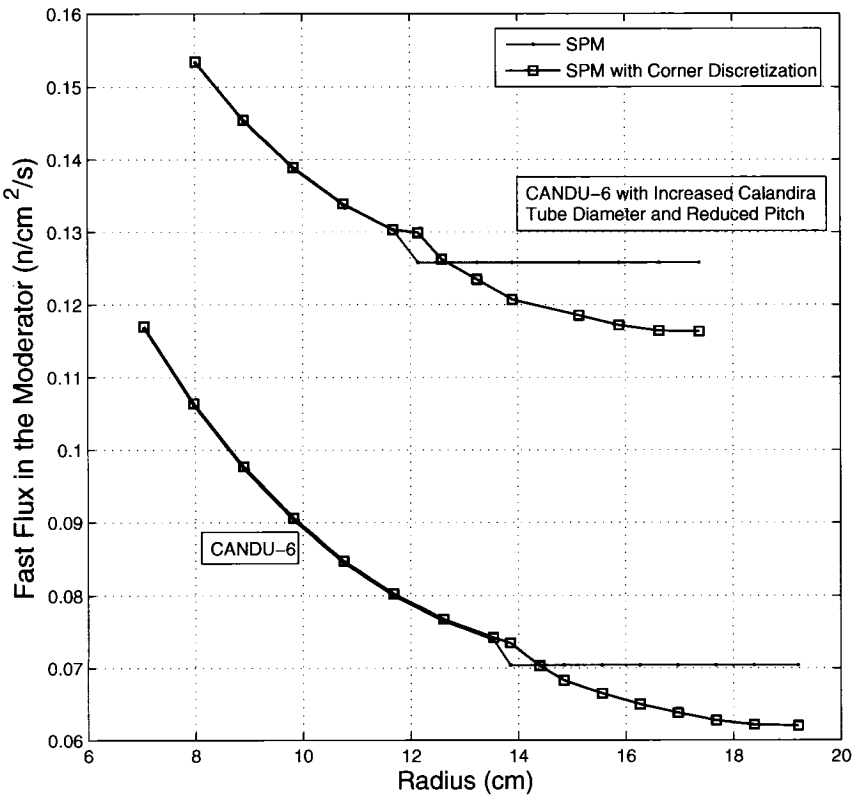

Figure 3.16 Fast flux in the moderator region for assemblies of CANDU-6 and CANDU-6 with increased calandria tube diameter and reduced pitch.

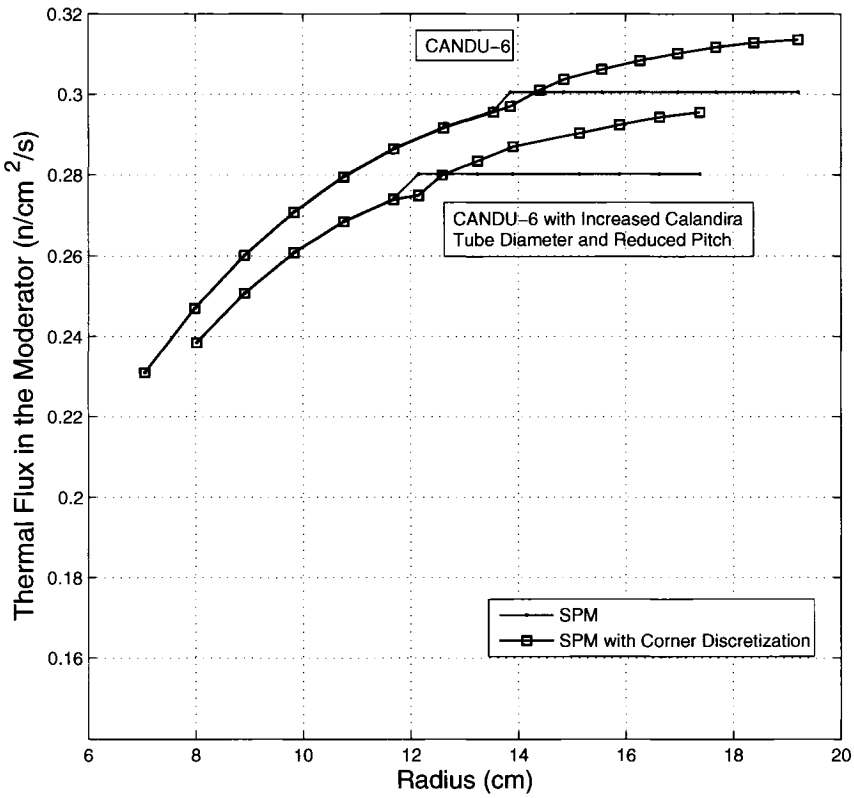

Figure 3.17 Thermal flux in the moderator region for assemblies of CANDU-6 and CANDU-6 with increased calandria tube diameter and reduced pitch.

3.3 ACR-700 Assembly

In the previous sections, we had mentioned the two major steps in evolution of a 2×2 CANDU-6 fuel assembly into ACR-700 type fuel assembly using SPM. The third step would be the increase of fuel pins from 37 to 43 and use of enriched uranium instead of natural uranium. Another important aspect is the use of light water instead of heavy water as coolant. The approximate ACR-700 cell constructed using SPM was used to perform the transport calculation in the 2×2 assembly pattern. The cross section libraries used here are those generated using DCS. It was discussed in the section on cell simulation for ACR-700 cell (Section 2.6.2), that the number of regions and outer surfaces for fine mesh calculation was 4464 and 210, respectively. Therefore, in a 2×2 assembly pattern the number of fine regions and outer surfaces becomes 17856 and 420, respectively.

As we mentioned earlier, using diagonal symmetry one could reduce the number of regions and surfaces by half. But, only Cartesian symmetry exists along Y-axis and there is no diagonal symmetry for the 2×2 assembly pattern of ACR-700. Therefore one needs to perform calculation for the complete 2×2 assembly pattern, without any geometric simplification. Generation of collision probability matrix for such a large number of regions would be impossible with the current computer architecture. However, the computational efforts can be reduced by using the `MRG:` module incorporated in the code DRAGON (see section 1.4) and is now reduced to 60 regions and 8 outer surfaces (see Figure 3.18 (a)). Also, a 2×2 assembly calculation with fine mesh discretization in the Cartesian corners would involve 22968 regions and 518 outer surfaces. By using `MRG:` module and combining the fine mesh regions, we obtain seven regions of annular-rectangular form in each corner of each lattice and 84 flux regions were generated (see Figure 3.18 (b)). In each assembly case, 15 different mixtures are considered.

As explained before in section 3.1, for the assembly calculation in a 2×2 pattern of ACR-700, each lattice must be divided into four parts. Identical regions in the lattice are differentiated in each part of the lattice. Therefore, the number of flux regions increases four times the fine mesh lattice. Earlier in a single cell the number of regions was 21 and it now becomes 84 after division of cell into four parts. Further the number of regions for a 2×2 assembly pattern (Figure 3.19 (b)) becomes 336.

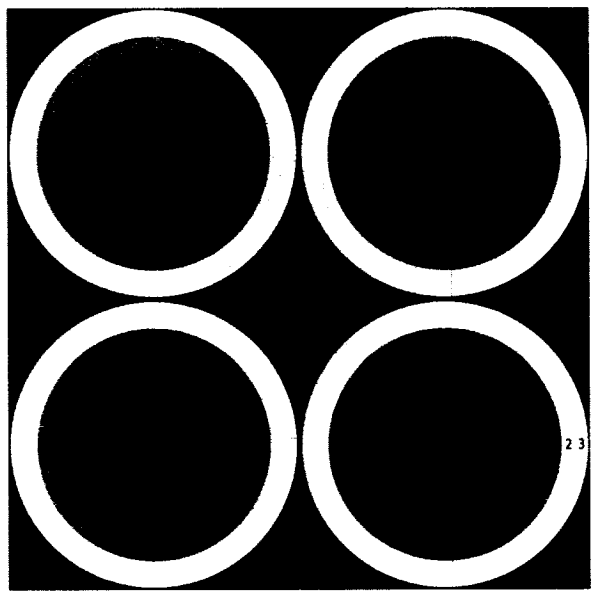

(a)

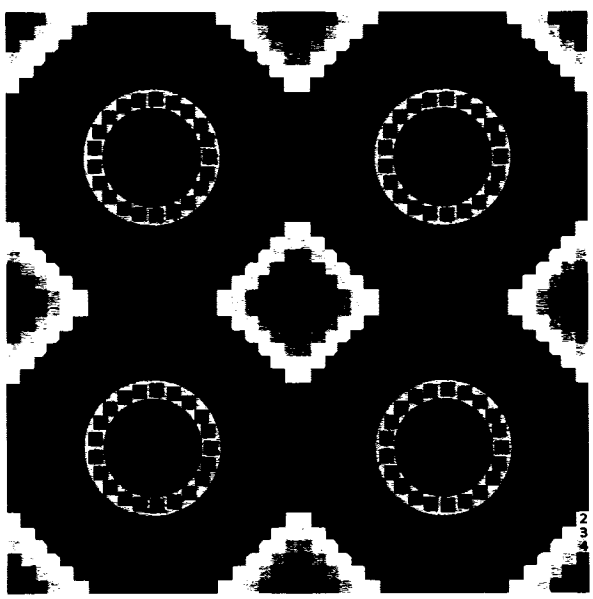

(b)

Figure 3.18 ACR-700 assembly in a coarse mesh (a) and with corner discretization (b).

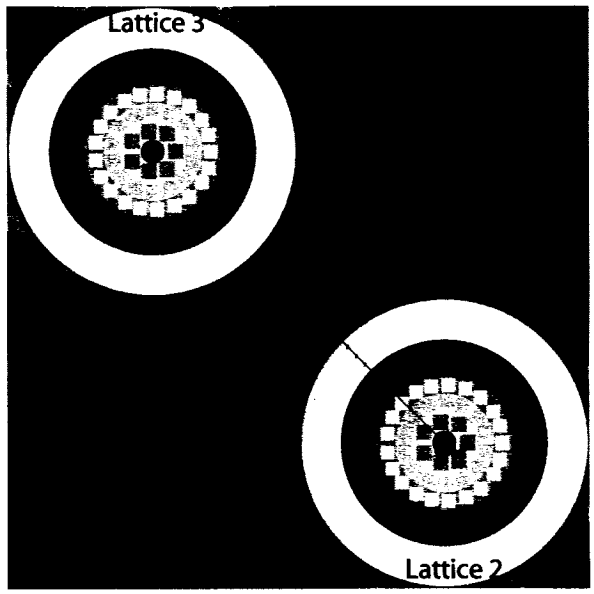

(a)

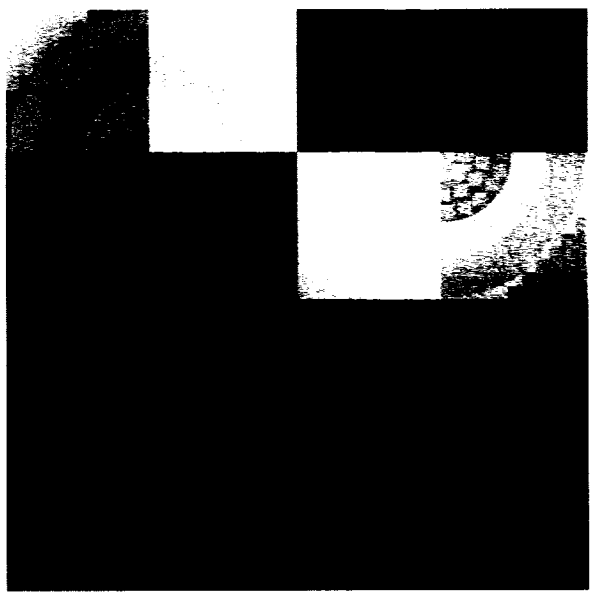

(b)

Figure 3.19 A 2 × 2 ACR-700 pattern, checkerboard (a) and with different corners (b).

3.3.1 ACR-700 Assembly Calculation

In this section, we explain the assembly calculations performed with the cross section libraries generated using DCS (see section 2.6.3). As we have seen in the section 3.1.1, we will compare the results in a 2×2 assembly of cells with that of an isolated cell.

It can be seen from the first and second line of the Table 3.5, that there is a steady increase in the deviation of k_{eff} as a function of void and reaches to a maximum of 0.7 mk for fully voided condition. This can be attributed to the difference in boundary conditions, as mentioned earlier. Since the density of coolant is reduced, the neutrons become more energetic due to reduction in moderation. Therefore, the spectrum become more harder and the neutrons are strongly coupled to the neighboring lattices. The CVR estimated for a 2×2 assembly of ACR-700 increases by 0.4 mk in comparison to single ACR-700 lattice cell.

The effect of Cartesian corner discretization in assembly results in 0.1 mk deviation in the eigenvalue (see Table 3.5). This difference is the same as that seen in cell calculation with corner discretization (see Table 3.5). A comparison between corner discretization in a single cell and a 2×2 assembly pattern shows a maximum offset of 0.7 mk which can be related to the difference in boundary conditions and neutron coupling in the assembly case. As mentioned earlier, in a 2×2 pattern, the neutrons born in one cell are coupled to the surrounding cells, especially when there is no coolant in the system. The 0.4 mk change in CVR is the same, as observed before.

The effect of corner discretization can be explained in terms of the change in production and destruction rate (see Section 2.4.3). In the fully cooled state, the relative production rate increased by 0.0010% and the relative destruction rate increased by 0.0650%, when one considered corner discretization. When compared to that of CANDU-6 assembly, the relative destruction rate was found to be reduced almost by half. As a result, the

Table 3.5 Comparison of k_{eff} and $\Delta\rho$ between single cell and 2×2 assembly of ACR-700 lattices.

Coolant Density $\rightarrow$ (g/cm^3)	0.81212	0.60909	0.40606	0.20303	0.00100	$\Delta\rho$ (mk)
$k_{eff}\downarrow$	%100 Cooled	%25 Voided	%50 Voided	%75 Voided	%100 Voided	CVR
Single Cell (coarse mesh) Figure 2.22 (a)	1.2341	1.2347	1.2348	1.2353	1.2389	+3.1
A 2 × 2 assembly (coarse mesh) Figure 3.18 (a)	1.2342	1.2349	1.2350	1.2357	1.2396	+3.5
Single Cell (corners) Figure 2.22 (b)	1.2340	1.2346	1.2348	1.2352	1.2388	+3.1
A 2 × 2 assembly (corners) Figure 3.19 (b)	1.2341	1.2348	1.2349	1.2356	1.2395	+3.5

eigenvalue is affected only with 0.1 mk against that of 0.3 mk for CANDU-6 assembly. We can conclude that, the use of corner discretization does not affect the CVR in a 2×2 assembly pattern of ACR-700.

The 2×2 checkerboard voiding pattern with discretized corners for ACR-700 lattice (see Figure 3.19 (a)) was analyzed. As explained before, calculation was performed with the libraries generated by DCS. The macroscopic cross section libraries generated with coolant density of 0.8 g/cm^3 is considered for lattices 1 and 4 and 0.001 g/cm^3 for lattices 2 and 3. The obtained result for the CVR is 7.8 mk, which is more than double the change (3.5 mk) observed for the case where the full assembly is voided. In fact, these results reveal the importance of checkerboard calculations especially when light water is used in the system. This non-linear behavior is mainly due to coupling of neutrons born in one lattice to those in neighboring lattices, and due to high absorptive behavior of light water coolant as compared to heavy water coolant. Accordingly, independent cell calculations **can not** be used to estimate the CVR with a very good accuracy for ACR-700.

The plots of fast and thermal flux with respect to the radius of each region located in corner 4, are shown in Figures 3.20 and 3.21. It can be seen in Figure 3.20 that the magnitude of fast flux is lower than that of CANDU-6 assembly with reduced lattice pitch and increased calandria tube diameter. However, it is higher than that of exact CANDU-6 assembly. The flux shape is almost flat, which means that the change in fast neutron flux is minimal in comparison to other two cases. A similar trend is observed for thermal flux, even though it increases from center to corner 4, which is shown in Figure 3.21. When one discretizes the corner, it is interesting to note that both flux shapes become parabolic in comparison to that of straight lines which were obtained when there was no corner discretization. Due to the fact that, there is no boundary condition between the cells within a assembly, positive and negative slope in fast and thermal flux vanish.

Figure 2.26 shows an alternative way to present the variation of flux shape as a function of distance when one considers corner discretization (located in corner 4 of lattice 1). It can be seen in Figures 3.22 and 3.23, that the fast and thermal flux, in histogram format, shows a clear change in shape with corner discretization, which is essentially the slowing down of neutrons as a function of distance in the moderator.

When corner discretization is considered, it can be seen from Figure 3.22, the shape of fast flux in the regions near to the fuel (see regions R, S in Figures 2.26 and 3.22) increases, while the thermal flux decreases in the same regions, as shown in Figure 3.23. The effect of corner discretization for both fast and thermal flux for the case of CANDU-6 assembly with increased calandria tube diameter and reduced pitch is higher than that obtained in two other cases.

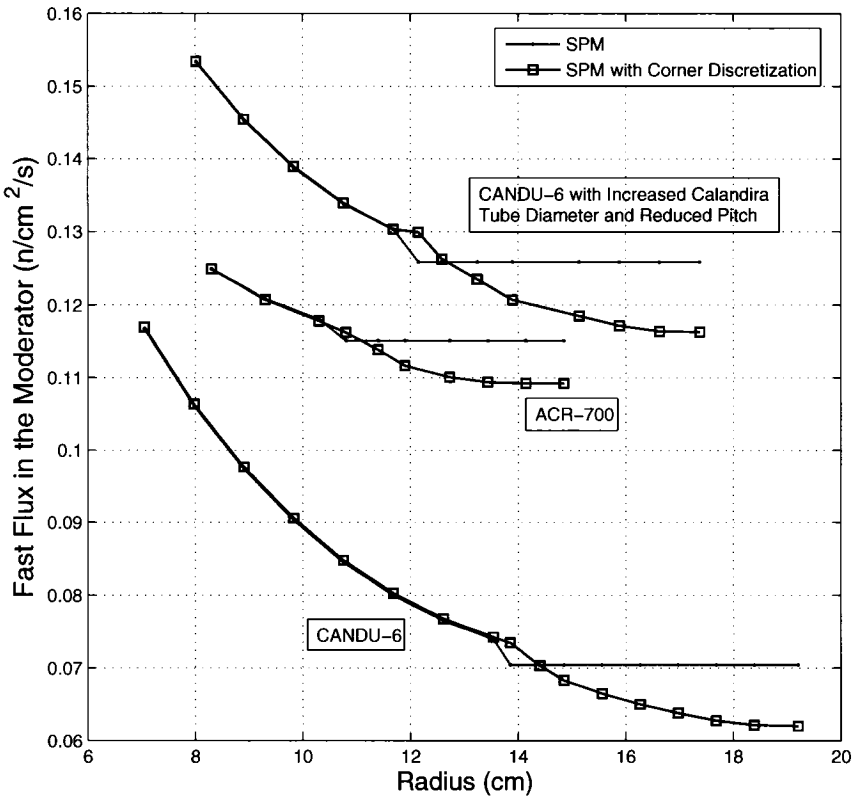

Figure 3.20 Fast flux in the moderator region for assemblies of ACR-700, CANDU-6 and CANDU-6 with increased calandria tube diameter and reduced pitch.

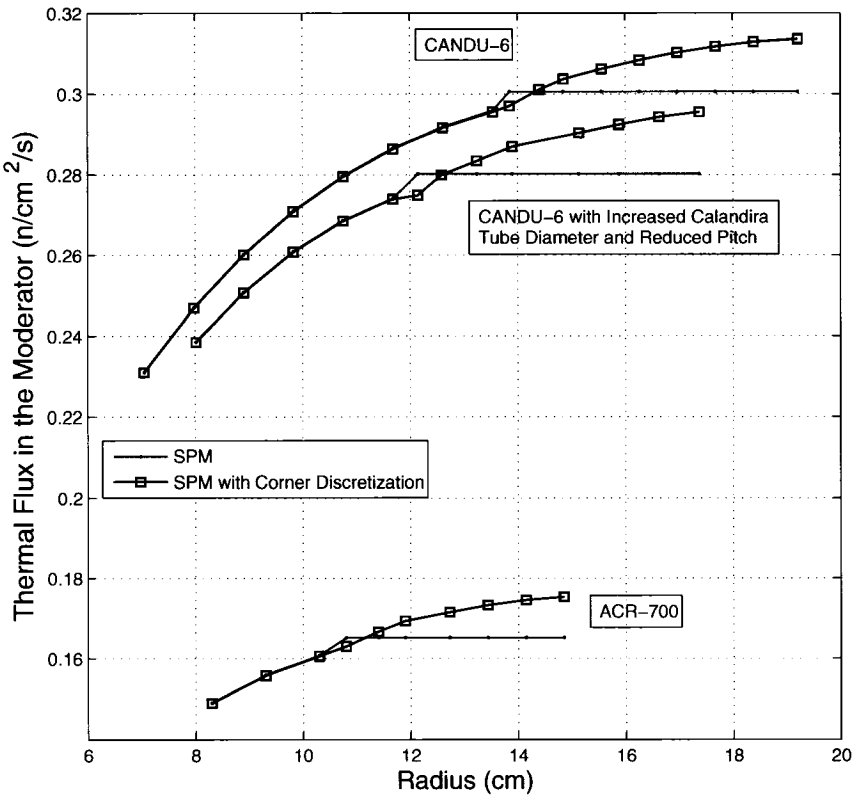

Figure 3.21 Thermal flux in the moderator region for assemblies of ACR-700, CANDU-6 and CANDU-6 with increased calandria tube diameter and reduced pitch.

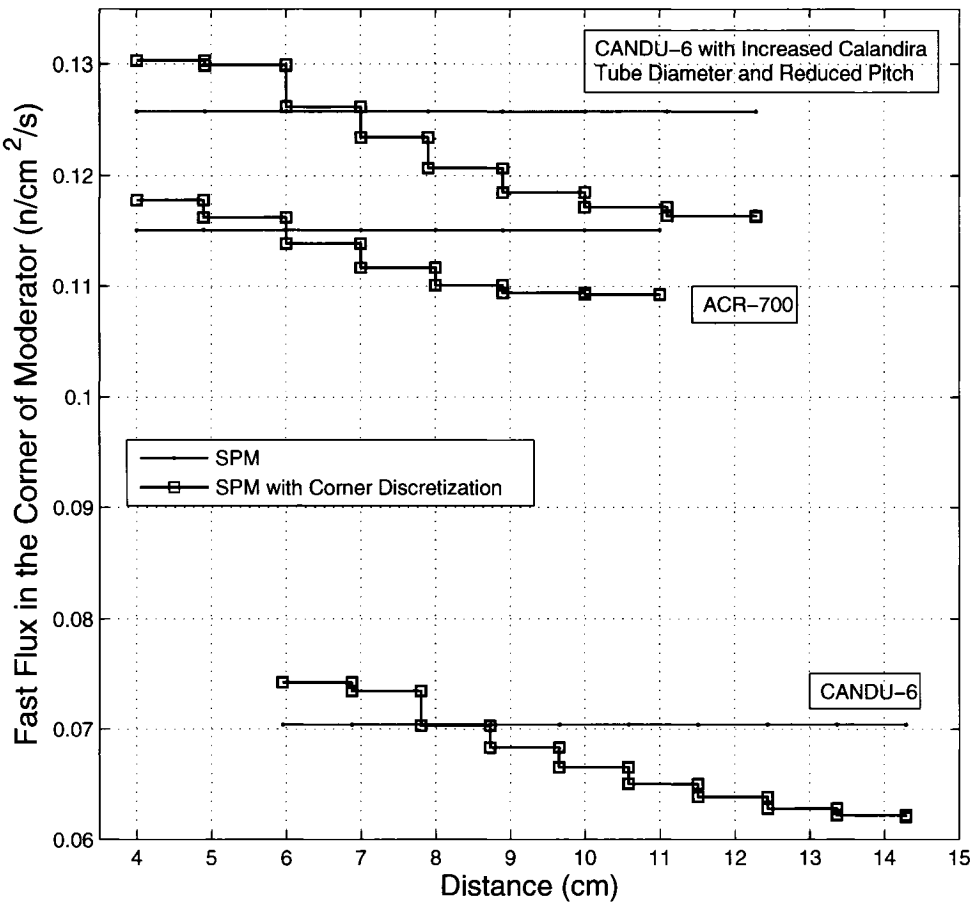

Figure 3.22 Effect of corner discretization in fast flux for the three assemblies.

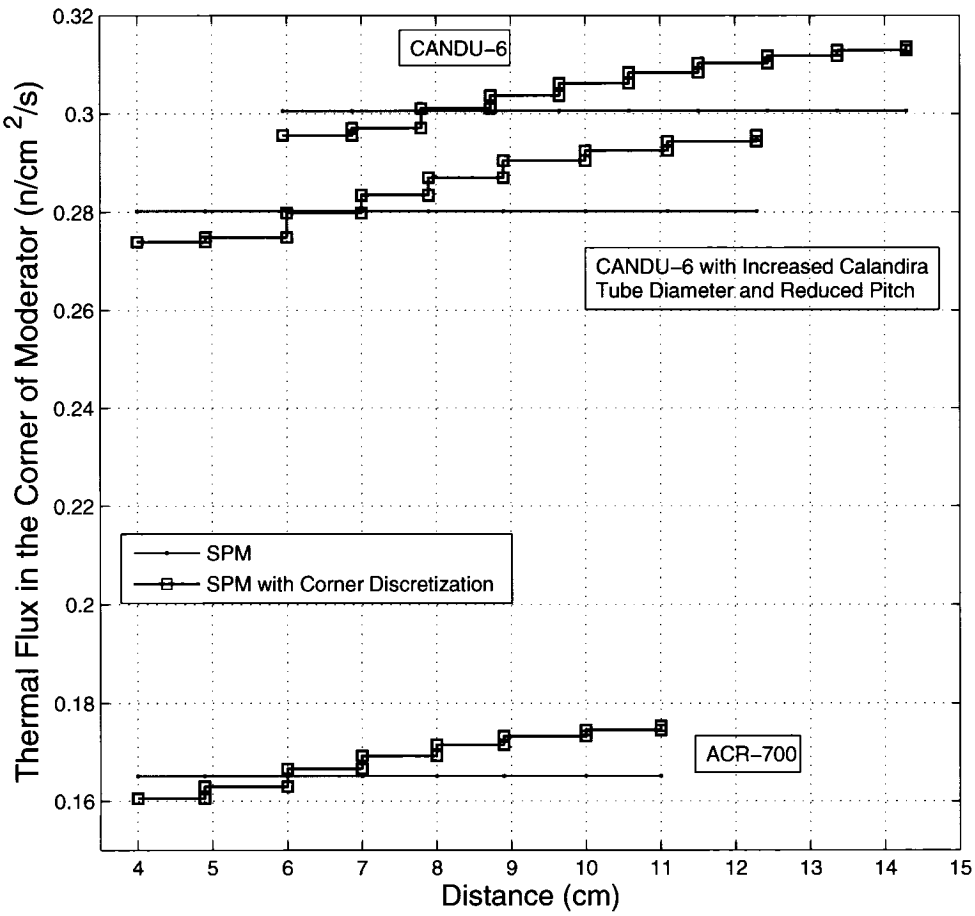

Figure 3.23 Effect of corner discretization in thermal flux for the three assemblies.

As mentioned earlier (see section 3.1.2), it is important to present the flux shape in a 2×2 checkerboard voiding pattern where lattice 1 is fully cooled and lattice 2 is totally voided (see Figure 3.19 (a)). The moderator of each lattice is split into 10 regions including three annular rings and seven annular-rectangular regions. In this case the pressure tube, carbon dioxide cover gap and calandria tube were also considered. Therefore we had 13 regions from inside to corner 4 of lattice 1 and the same 13 regions, in lattice 2 (from corner 3 to inside).

The plots of the fast and thermal flux with respect to the radius of each region, are shown in Figures 3.24 and 3.25. It can be seen in Figure 3.24 that when assembly is completely voided, the fast flux has a similar shape as that observed in CANDU-6. However the magnitude of fast flux significantly increases while the thermal flux decreases, as shown in Figure 3.25.

Interestingly, the change in the flux shape due to the checkerboard voiding is different from those obtained in CANDU-6. It can be seen in Figure 3.24, the fast flux in the cooled lattice (lattice 1) is not close with the flux found when the assembly is fully cooled. The same trend is observed in voided lattice (lattice 2). In the regions near to the corners (corner 3 and 4), the fast flux is averaged with that obtained for fully cooled and totaly voided case. The behavior of thermal flux is almost the same as that observed in CANDU-6, unless the flux in the regions near to the corners toward the voided lattice, is even harder than obtained for totally voided case. We can conclude that the flux in a 2×2 checkerboard voiding pattern of ACR-700 system has a non-linear behavior.

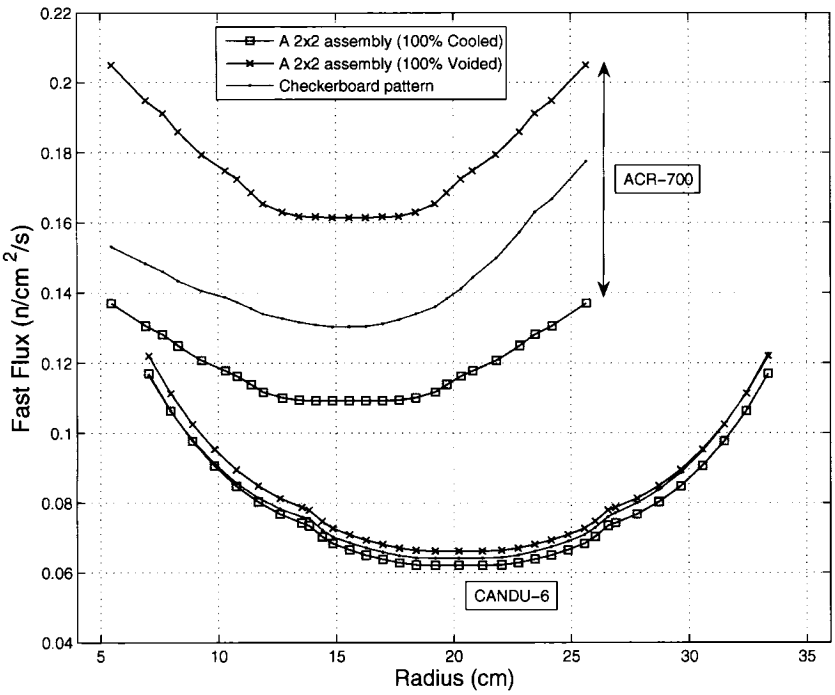

Figure 3.24 Comparison of fast fluxes for assemblies and checkerboard patterns.

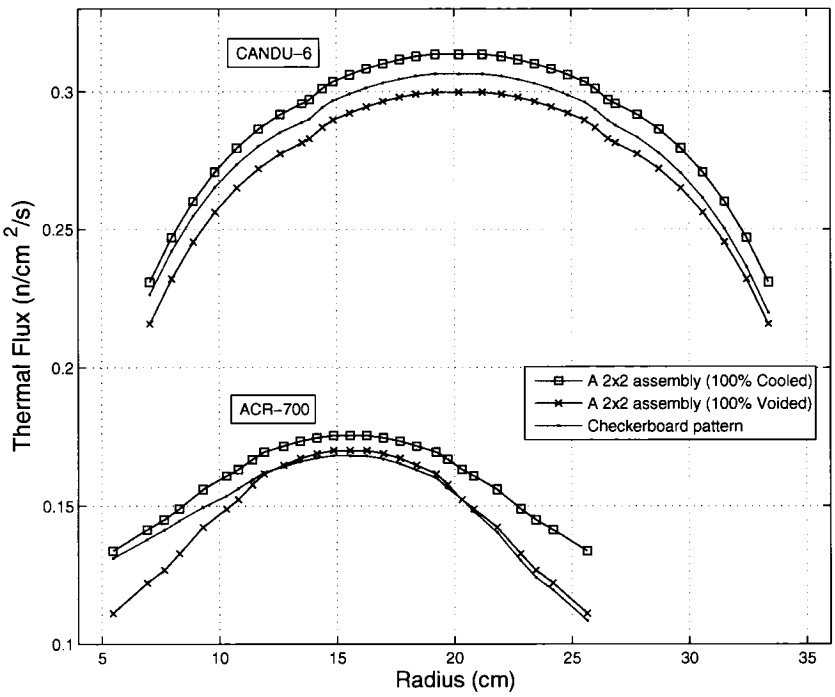

Figure 3.25 Comparison of thermal fluxes for assemblies and checkerboard patterns.

CONCLUSION

We have attempted to estimate the CVR of CANDU cells (CANDU-6 and ACR-700 type lattices), using the code DRAGON. It is well known that when LOCA happens, assembly calculation in a 2×2 pattern can predict the reactivity feedback in the reactor better than single lattice calculation. Because the current version of DRAGON has inherent geometry limitations, CANDU assembly calculations cannot be performed in the exact geometry. Accordingly, an approximate model - the Square Pin Model (SPM) - for each geometry has been developed.

We found that this model gives a good estimation of CVR for all the 2×2 patterns which include CANDU-6, CANDU-6 with reduced lattice pitch, CANDU-6 with reduced lattice pitch and increased calandria tube diameter, and finally the ACR-700 lattices. An interesting simulation of a 2×2 pattern, which is the checkerboard voiding was made possible using the SPM. It was observed that for CANDU-6 lattices the CVR estimated for checkerboard pattern was about half of the value obtained for total coolant voiding. This behavior was maintained for CANDU-6 lattice when the pitch was reduced and also along with an increase in calandria tube diameter.

But a very interesting behavior was observed for ACR-700 lattice when light water was used as coolant. The CVR estimated for checkerboard pattern was more than double the value obtained for total coolant voiding. It thus showed a non-linear behavior. With the proposed model, we could analyze the effect of corner discretization. It was noted that corner discretization does not affect the estimation of CVR. Two ways of cell simulation were performed - Multi Step Cell Simulation (MSCS) and Direct Cell Simulation (DCS). It was observed from all the analysis that cross sections generated using DCS is sufficient for estimation of CVR using SPM. It is important to note that this model is approximate, and to calculate CVR more precisely, it would be necessary to perform

the calculations using exact geometry. The module to track assembly of CANDU cells in the checkerboard pattern is still under development in the code DRAGON. The CVR in checkerboard pattern has been estimated for the first time using code DRAGON. The model proposed in this thesis is ad-hoc, but effective.

As a part of future studies, one could use the proposed model in DRAGON to perform assembly calculation in a 2×2 pattern for different combinations of voiding and fuel state. One can consider fuel assemblies with different burnups, which would represent equilibrium core pattern in a typical CANDU reactor. The 2×2 pattern can also include reflector cells along with fuel cells. This would give the effect of reflector on neutron flux distribution during coolant voiding. Another interesting possibility of using this model is to estimate the reactivity effect due to heterogeneous draining of the coolant. It is essentially the loss of coolant from top to bottom of the pressure tube. Such a calculation is not possible by considering annular regions in the lattice, but is possible with the proposed SPM.

REFERENCES

ALDAMA LOPEZ, D., LESZCZYNSKI, F., TRKOV, A., 2003. Final report of a co-ordinated research project on WIMS-D Library Update. International Atomic Energy Agency, Vienna, Austria.

ASAHI, Y., WATANABE, T., 1989. "Analysis of Spectral Shift Effect on Reactor Dynamics and its Application to RBMK-1000 and Light Water Reactors ". *Nucl. Sci. Eng.*, **101**, 226.

BRIESMEISTER, J. F., 1986. MCNP: A General Monte Carlo Code for N-Particle Transport Code, Version 3A. LA-7396-M, Rev. 2, Los Alamos National Laboratory, New Mexico, USA.

BRIESMEISTER, J. F., 1997. MCNP: A General Monte Carlo Code for N-Particle Transport Code, Version 4B. LA-12625-M, Los Alamos National Laboratory, New Mexico, USA.

BRIESMEISTER, J. F., 2000. MCNP: A General Monte Carlo Code for N-Particle Transport Code, Version 4B. LA-13709-M, Los Alamos National Laboratory, New Mexico, USA.

CHAN, P.S.W., TSANG, K.T., BUSS, D.B., 2001. "Reactor Physics of NG CANDU ". 22^{th} Annual Conference of the Canadian Nuclear Society, Toronto.

CONSTANTIN, M., BALACEANU, V., 2002. "Void Reactivity and Pin Power Calculation for a Typical CANDU Cell Using CPs and a Two-Stratified Coolant Model ". *Ann. Nucl. Energy*, **29**, 791.

CONSTANTIN, M., GUGIU, D., BALACEANU, V., 2003. "Void Reactivity and Pin Power Calculation for a CANDU Cell Using the SEU-43 Fuel Bundles ". *Ann. Nucl. Energy*, **30**, 301.

COTTON, C.A., LEE, D., and DOWNAR, T., 2004. "Coolant Void Reactivity Analysis of CANDU and ACR-700 Lattices ". *Trans. Am. Nucl. Soc.*, Pittsburgh, USA.

COTTON, C.A., LEE, D., KOZLOWSKI, T., DOWNAR, T., YANG, W.S., CARLSON, D.E., 2005. "Physics Analysis of Coolant Voiding in the ACR-700 Lattices ". *Trans. Am. Nucl. Soc.*, USA.

DONNELLY, J. V., 1986. WIMS-CRNL: A User's Manual for the Chalk River Version of WIMS. AECL-8955, AECL Research Group.

GLASSTONE, S., SESONSKE, A., 1981. Nuclear Reactor Engineering. MALABAR, FLORIDA : KRIEGER PUBLISHING COMPANY.

HÉBERT, A., 1993. "A Consistent Technique for the Pin-by-Pin Homogenization of a Pressurized Water Reactor Assembly ". *Nucl. Sci. Eng.*, **113**, 227.

HÉBERT, A., and MATHONNIÈRE, G., 1993. "Development of a Third-Generation Superhomogénéisation Method for the Homogenization of a Pressurized Water Reactor Assembly ". *Nucl. Sci. Eng.*, **115**, 129.

HÉBERT, A., MARLEAU, G., and ROY, R., 1995. "Application of the Lattice Code DRAGON to CANDU Analysis ". *Trans. Am. Nucl. Soc.*, **72**, 335.

HÉBERT, A., 1997. "Application of Transport Methods to Lattice Calculations ". Frédérick Joliot Summer School. Cadarache.

KAVENOKY, A., 1978. "The SPH Homogenization Method ". Proc. Specialist' Mtg. Homogenization Methods in Reactor Physics. Lugano (Switzerland).

LEWIS, E. E., MILLER, W. F., 1984. Computational Methods of Neutron Transport. New York : John Wiley and Sons.

LOVE, J.W., HAU K.F., and MAHENDRALINGAM, T., 2002. "Design Characteristics of ACR-700 ". 23^{th} Annual Conference of the Canadian Nuclear Society, Toronto.

MACFARLANE, R.E., MUIR, D.W., 2000. NJOY99.0 Code System for Producind Pointwise and Multigroup Neutron and Photon Cross sections from ENDF/B Data. Los Alamos National Laboratory, New Mexico, USA.

MARLEAU, G., HÉBERT, A., and ROY, R., 1992. "New Computational Methods Used in the Lattice Code DRAGON ". *Topical Meeting on Advances in Reactor Physics*, pp 1.177, Charleston, South Carolina.

MARLEAU, G., HÉBERT, A., and ROY, R., 2000. *A User Guide for DRAGON. Version DRAGON-000331 Release 3.04*, Report IGE-174 Rev.5, Institut de Génie Nuc1éaire, École Polytechnique de Montréal, Montréal, Québec.

MARLEAU, G., 2001. Dragon Theory Manual Part1: Collision Probability Calculations. Montréal : Institut de Génie Nucléaire. IGE-236 Rev. 1.

NUREG, 1990. SCALE-4: A Modular Code System for Performing Standardized Computer Analyses for Licensing Evaluation, NUREG/CR-0200 Rev.4. ORNL/NUREG/CSD-2/R4, RSIC/CCC-545.

OVANES, M., CHAN, P.S.W., MAO, J., 2002. "Reactor Physics Innovations in ACR-700 Design for Next CANDU Generation ". 23^{th} Annual Conference of the Canadian Nuclear Society, Toronto.

RAHNEMA, F., MOSHER, S., PARVAIZ, A., SERGHIUTA, D., 1998. "Void Reactivity Calculations in a Typical CANDU Cell Using MCNP and HELIOS ". *International Conference on the Physics of Nuclear Science and Technology*, Long Island, USA.

ROUBEN, B., 1995. "Overview of Current RFSP-Code Capabilities for CANDU Core Analysis ". *Trans. Am. Nucl. Soc.*, TANSAO 72, 339, USA.

ROY, R., MARLEAU, G., TAJMOUATI, J., and ROZON, D., 1994. "Modeling of CANDU Reactivity Control Devices with the Lattice Code DRAGON ". *Ann. Nucl. Energy*, **21**, 115.

ROZON, D., 1992. Introduction to nuclear reactor kinetics. Montréal : Éditions de l'École Polytechnique de Montréal.

STAMMLER, R. J., 2003. HELIOS: A Neutron Transport Code System, Version 1.8. Studsvik Scandpower.

TALEBI, F., MARLEAU, G., 2005. "Evaluation the Coolant Void Reactivity of Assemblies of CANDU-6 Lattices ". 26^{th} Annual Conference of the Canadian Nuclear Society, Toronto.

VALKÓ, J., FEHÉR, S., HOOGENBOOM, J.E., and SLOBBEN, J., 1995. "Calculation of the Void Reactivity of CANDU Lattices Using the SCALE Code System ". *Ann. Nucl. Energy*, **159**, 225.

VARIN, E. HÉBERT, A. ROY, R. KOCLAS, J. 2000. A User Guide for DONJON. Montréal : Institut de Génie Nucléaire. IGE-208 Ver. 2.01.

VILLARINO, E. A., STAMMLER, R. J.J., FERRI, A.A., CASAL, J.J., 1992. "HELIOS: Angularly Dependent Collision Probability ". *Nucl. Sci. Eng.*, **112**, 16.

WHITLOCK, J.J., GARLAND, W.J., and MILGRAM, M.S., 1995. "Effects Contributing to Positive Coolant Void Reactivity in CANDU ". *Trans. Am. Nucl. Soc.*, **72**, 329.

APPENDIX I

LOCA IN CANDU

The coolant, which is heavy water for the CANDU-6 and light water for the ACR-700 essentially removes heat from the core. The coolant is pumped through inlet headers before branching into hundreds of feeders that are connected to the ends of fuel channels. The hot water coming from the channels are routed by feeders to the outlet headers. The thermal energy of the coolant is converted to steam by steam generators and is then used by turbines to generate electricity (see Figure I.1).

The Loss Of Coolant Accident (LOCA) is one of the most serious accident scenarios possible in CANDU reactors. It can occur under a number of circumstances ranging from breaking of headers to the complete failure of pumps. Any of the above-mentioned accidents can result in the improper delivery of coolant to the channels that would overheat the core of the reactor. In the worst case scenario, it can even result in the release of fission products into the coolant circuit.

In the event of an occurrence of LOCA, the system experiences two major failure sequences. To understand the possible sequences, one needs to look at the coolant circulation in the core of the reactor (see Figure I.2). It can be seen in Figure I.2 that the hot coolant goes to the steam generators through headers 1 and 4, is cooled and returned back to the fuel channels through headers 2 and 3. In the case of an accident where all the headers or all the pumps break down, the fuel channels in the calandria are fully voided (see Figure I.3). However, when coolant is not lost uniformly in all coolant tubes, which can happen when there is a single pump failure or if there is a problem with only one header, a checkerboard voiding pattern will first appear. For instance, when header 4 fails, coolant is lost from fuel channel 1 while fuel channel 2 still functions thereby

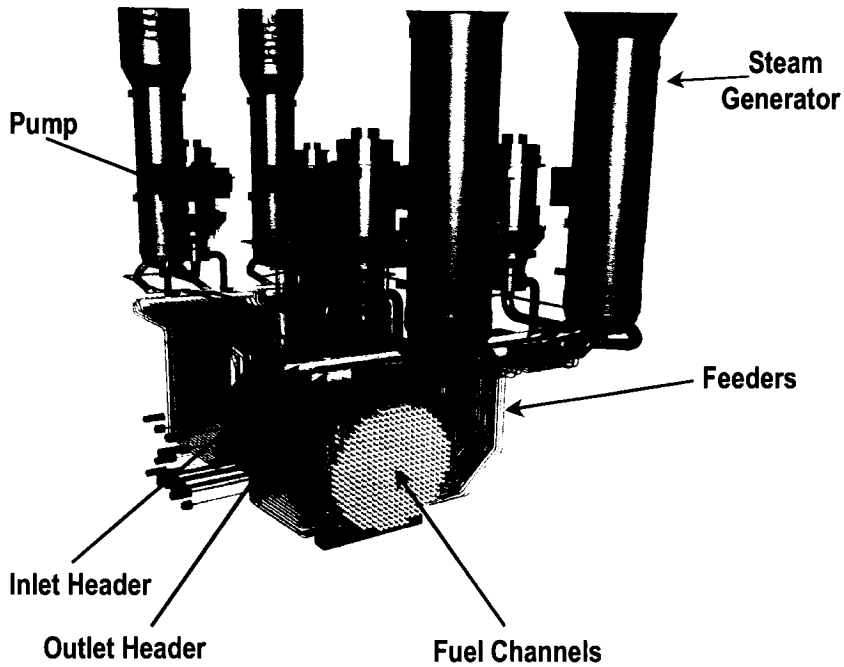

Figure I.1 CANDU-6 reactor.

generating a checkerboard voiding pattern. The checkerboard scenario is however transient and transforms into a fully voided pattern in a time period that is dependent on the size and kind of accident.

It is important to understand how the two failure sequences: transformation from fully cooled to fully voided or from fully cooled to checkerboard voided to fully voided affect the stability of the system.

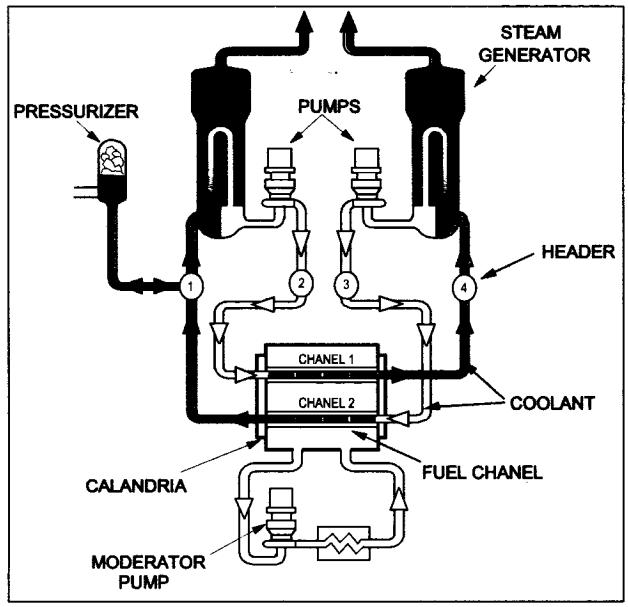

Figure I.2 Coolant circulation in the CANDU reactors.

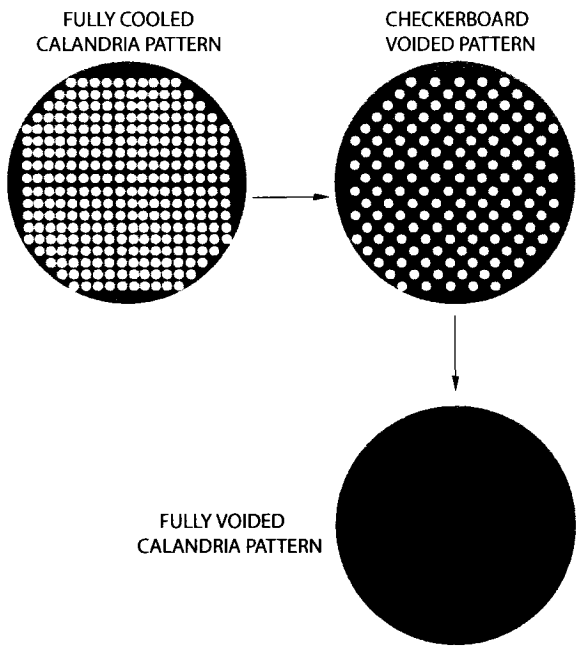

Figure I.3 End-view of calandria in the CANDU reactors.

APPENDIX II

ACR-700 DESIGN

The Next Generation of CANDU design called CANDU-NG or Advanced CANDU Reactor (ACR) is based on the standard proven CANDU-6 design [Chan, 2001]. It is being developed for the market requirements of low cost and reliable energy supplies. Several designs have been worked out, of which ACR-700 is one of the most competitive reactor design. The ACR-700 retains many of the standard CANDU-6 features. Some of the major modifications in the ACR-700 in comparison to CANDU-6 are [Love, 2002]:

- 43 fuel pencils with Dysprosium in the central pin instead of 37.
- Light water coolant instead of heavy water.
- Slightly Enriched Uranium (SEU) fuel, contained in CANFLEX bundles to achieve increased burnup.
- Extended fuel life with reduced volume of irradiated fuel.
- Reduction in heavy water inventory by decreasing the lattice pitch and increasing the calandria tube diameter.

In order to reduce the fuel cost and to increase the residence time of fuel in the reactor, a 43 pin cluster containing SEU has been considered against the usual 37 rod cluster with natural uranium. A higher burnup up to 20500 MWD/T can be achieved as compared to 7500 MWD/T for CANDU-6 reactor. Also the residence time can be increased to about three times thereby reducing the pressure on fuel manufacturing and supply rate. It does however involve the costs of enriching the fuel. Another important feature of ACR-700

is the reduction of heavy water by 72% due to reducing the lattice pitch and increasing the calandria tube diameter and also using the light water as a coolant in heat transport system. This also helps in decreasing the costs in building the reactor.

When one uses heavy water coolant with reduced pitch, there is a loss of reactivity which will affect the life of fuel within the reactor. Therefore, one has to consider light water as coolant, so that it contributes to moderation as much as the heavy water moderator. But light water is not only a good moderator, but also a good absorber of thermal neutrons. So the effect of presence and absence of coolant plays an important role in reactivity feedback in reactor operation.

The design of fuel assembly thus has to take into account the reactivity change due to presence and absence of coolant. Presently, the design considers use of burnable absorber like dysprosium in the center of the fuel assembly along with natural uranium. It was observed that when LOCA happens, the thermal flux in the center increases. Presence of a strong thermal absorber like dysprosium in the center will thus have an effect on reactivity when there is loss of coolant. It is thus important to estimate the CVR as accurately as possible for ACR-700 type of lattice. Table II.1 gives the comparison of salient engineering details of the two reactor systems.

Table II.1 Data Comparison between CANDU-6 and ACR-700 Reactors.

Parameter	**CANDU-6**	**ACR-700**
Number of Fuel Channels	380	284
Number of Bundles per Channel	12	12
Length of Bundle [mm]	495.3	495.3
Bundle Weight [kg]	24.1 (19.2 kg U)	23.1 (18 kg U)
Lattice Pitch (square) [cm]	28.575	22.0
Reactor Diameter [m]	7.6	5.2
Coolant (average temperature)	D2O @ 290 °C	H2O @303 °C
Moderator (average temperature)	D2O @ 68 °C	D2O @ 80 °C
Moderator Systems [Mg D2O]	265	129
Heat Transport Systems [Mg D2O]	192	0.0
Heavy Water Reserve [Mg D2O]	9	2
Reflector Thickness [mm]	655	500
Radial Form Factor	0.83	0.93
Gross Electrical Power Output [MW (e)]	728	731
Thermal Output to-	2064	1982
-Steam Generators [MW (th)]		
Fuel Type	37 CANDU	43 CANFLEX
Fuel Enrichment [wt% 235U]	0.71	2.0
Dysprosium in Central Pin [wt% Dy]	0.0	4.6
Fuel Sheathing	Zr	Zr with 2.5% Nb
Core Average Fuel Burnup [MWd/T]	7,500	20,500
Max Fuel Element Burnup [MWd/T]	17,000	26,000
Fuel Bundles Required per Full Power Day	16	5.8
Channel Visits per Full Power Day	2	2.9
Fuelling Scheme	8-bundle-shift	2-bundle-shift
Max Time-Average Channel Power [MW (th)]	6.7	7.5
Max Time-Average Bundle Power [kW (th)]	800	880
Max Instantaneous Channel Power [MW (th)]	7.0	7.8
Max Instantaneous Bundle Power [kW (th)]	900	900
Max Instantaneous Linear-	57	51
-Element Rating [kW/m]		
Reactor Outlet Header Pressure [MPa (a)]	10	12
Reactor Outlet Header Temperature [°C]	310	325
Reactor Inlet Header Pressure [MPa (a)]	11.3	13.2
Reactor Inlet Header Temperature [°C]	266	278.5
Reactor Core Coolant Flow (total) [Mg/s]	7.7	6.9
Single Channel Flow (maximum) [kg/s]	25.6	26